CHANNEL MODELLING AND ANALYSIS OF WITS MOCK–MINE WITH DIFFERENT ANTENNA PARAMETERS

Intikhab Hussain

A research report submitted to the Faculty of Engineering and Built Environment, University of Witwatersrand, Johannesburg, in partial fulfilment of the requirements for the degree of Masters of Science in Engineering

Johannesburg, 2017

DECLARATION

I declare that this research report is my own unaided work. It is being submitted for the degree of Master of Science in Engineering to the University of the Witwatersrand, Johannesburg. It has not been submitted before for any degree or examination to any other University.

2 February 2017

ABSTRACT

In the mining industry, communication systems are important for ensuring personnel safety and optimizing the mining processes underground. Achieving robust and reliable through-the-air (TTA) communication system has always been a challenge in the underground mining environment due to harsh and dynamic conditions. TTA requires radio channel characterization for efficient designing and deploying of the communication system. The literature covers the statistical radio propagation of a room and pillar coal mine, a longwall coal mine, CANMET Gold mine, Camborne School of Mines hard rock mine tunnel, MÜZ Coal mine, an iron-ore mine and a lead-zinc mine with linearly polarized antennas at different frequencies. To the best of our knowledge, no open literature is available on the radio propagation of 1) deep underground mining tunnels (i.e. steel-supported arch-shaped mining tunnel), 2) mine vertical shaft and 3) underground mining tunnels with circularly polarized antennas. The experimental work on the performance comparison of different antennas in the underground mining tunnels is also sparse. This work presents the statistical radio propagation performance study of steel supported arch-shaped underground mining tunnel with antennas having different polarization, transmission frequency, configuration and directivity at different positions inside the tunnel. Moreover, the statistical radio propagation of WITS vertical shaft is also studied. The wideband measurements are used to obtain path-loss exponent, shadow fading statistics, channel impulse response, power delay profile, mean excess delay, RMS delay spread, maximum delay spread and coherent bandwidth parameters for the performance comparison. The results reveal that the antenna placement, antenna polarization, antenna directivity and transmission frequency have a significant impact on the performance of TTA communication system. The path-loss exponent values of less than free-space show waveguide propagation in underground tunnels. Circularly polarized directional antennas offer higher channel capacity whereas linearly polarized omni-directional antennas offer lower attenuation rate. Furthermore, higher frequency signals show lower attenuation rate and coherent bandwidth than lower frequency signals.

ACKNOWLEDGEMENT

My heartfelt acknowledgements are due to the following spectacular individuals for their guidance, support, encouragement and contributions in making my research work successful:

- My supervisors, Professor Frederick Cawood (Director WITS Mining Institute (WMI), University of Witwatersrand) and Professor Rex van Olst (School of Electrical and Information Engineering, University of Witwatersrand) for their indispensable and crucial academic guidance throughout the research and prompt reading of the draft chapters and draft thesis.

- The University of Witwatersrand's Digital Mine Laboratory and Sibanye Gold for funding this research.

- Professor Alan Clark (School of Electrical and Information Engineering, University of Witwatersrand) for the Electromagnetics Laboratory equipment.

- Benjamin Klein, Steven Chabalala Chabalala and Muhammad Ali Khalid for kind support and help for different research activities.

- All staff members of School of Mining Engineering and School of Electrical and Information Engineering, University of Witwatersrand, for their moral support throughout the stay.

To my dear parents, sisters, brothers,

and to

those who think they can, and do.

Table of Contents **Page No.**

LIST OF FIGURES

LIST OF TABLES

LIST OF ABBREVIATIONS

CH_4	Methane
O_2	Oxygen
AWGN	Additive White Gaussian Noise
BW	Band-Width
CDF	Cumulative Distribution Function
CMPA	Cylindrical-shape Microstrip Patch Array
CSM	Camborne School of Mines
CST	Computer Simulation Software
DSonsole	Dispatch Console Software
DSP	Digital Signal Process
ELF	Extremely Low Frequency
eLTE	Enhanced Long-Term Evolution
EM	ElectroMagnetic
FDTD	Finite-Difference Time Domain
FEM	Finite Element Method
FIT	Finite Integral Technique
GB	GigaByte
GDI	Gas Detection Instrument
GHz	GigaHertz
GTD	Geometric Theory of Diffraction
HGA	High Gain Amplifier

IFFT	Inverse Fast Fourier Transform
IP	Internet Protocol
ISI	Inter-Symbol Interference
KS	Kolmogorov-Smirnov
LF	Low Frequency
LOS	Line-of-Sight
LTE	Long-Term Evolution
MF	Medium Frequency
MHz	MegaHertz
MIMO	Multiple Input Multiple Output
MMS	Multimedia Messaging Service
MoM	Method-of-Moments
MÜZ	Maschinenübungszentrum
NLOS	Non-Line-of-Sight
OFDM	Orthogonal Frequency Division Modulation
PC	Personal Computer
PDP	Power Delay Profile
PMPA	Planar Microstrip Patch Array
PTD	Physical Theory of Diffraction
PTT	Push-to-Talk
RAM	Random-Access Memory
RF	Radio Frequency

RFID	Radio Frequency Identification
RHCP	Right-Hand Circularly Polarized
RMS	Root Mean Square
Rx	Receiver
SHF	Super High Frequency
SISO	Single Input Single Output
SLNA	Super Low Noise Amplifier
SMS	Short Message Service
SNR	Signal-to-Noise Ratio
TTA	Through-The-Air
TTE	Through-The-Earth
TTW	Through-The-Wire
Tx	Transmitter
UE	User Equipment
UHF	Ultra High Frequency
UWB	Ultra-WideBand
VHF	Very High Frequency
VLF	Very Low Frequency
VNA	Vector Network Analyser
WiFi	Wireless Fidelity
WLAN	Wireless Local Area Network
CO	Carbon Monoxide

dB	DeciBel
$nsec$	Nano-Second
μsec	Micro-Second

1. INTRODUCTION

1.1. General

Mining and mineral resources play an important role in the global economy. In the past, many lives have been lost and significant financial losses incurred because of mining accidents, especially in underground mines [1]. Monitoring underground mines becomes important in order to avoid accidents and launching of rescue operations in case of an accident. Communication systems play an important role to improve personnel health and safety and optimize the mining processes underground [2]. The task of reliably and quickly collecting and communicating information in underground mining is very important because losses (i.e. loss of lives, productivity, and deployed infrastructure) due to inefficient or incorrect information can be significant.

The interest in wireless communication systems in underground mines started in the 1920's [3]. The first commercial development took place in the 1970's using VHF radios and leaky feeder distribution systems [4-5]. The modern era of underground mine communication systems began in the early 2000's leveraging on considerable advancement of UHF technologies (e.g. cellular phones), ultra-wideband (UWB), radio frequency identification (RFID) and wireless-local-area-networks (WLAN) [2]. Although, the nature of the mining industry is inherently conservative and sceptical to invest on new unproven technologies, the health and safety issues invoke the mines and regulators to improve conditions by applying reliable underground communication systems [2].

The deployment of a wired communication system is a troublesome task in an underground mine. It requires expensive maintenance and has limited scalability [6]. Wireless communication systems on the other hand can benefit from its ease of deployment with an increased scalability, self-adaptive nature and low maintenance cost. Recent studies and applications of underground wireless communication systems have been stimulated by the potential advantages of next generation mobile communication systems. Underground mining is one of the few fields where the environment has a significant and direct impact on the communication performance [7]. Establishment of a reliable system in an underground mining environment is very difficult because of extreme working conditions [8-10, 11]; e.g. poor line-of-sight (LOS), air quality and temperature, humidity, noise caused by different appliances/ cable lines/ electric motors/mining equipment, in-mine vehicle accidents, waveguide effect, toxic gases, floods, roof-fall and dust. The following sub-sections discuss the research scope and objective, research question, conceptual framework and thesis outline.

1.2 Research Scope and Objective

The research aims at the propagation modelling of WITS mock-mine (i.e. steel supported arch-shaped underground mining tunnel and vertical shaft) to determine the manner in which the propagation environment distorts wireless signals in a form that would be useful in the designing and deploying of a wireless or through-the-air (TTA) communication system. The TTA channel modelling is a function of radio propagation effects of the environment. The literature shows that the TTA propagation is specific to the mining site and poses a challenge to theoretically model the propagation characteristics with high accuracy and low complexity. Available results provide the guidelines to understand the impact of various environment characteristics. The objective of the study includes the following:

- To analyse the effect of antenna placement, polarization, directivity and configuration, and transmission frequency on TTA communication system in underground mining environment for SISO antenna system.

1.3 Research Question

The central issue in this research is to investigate the effect of antenna parameters on the performance of wireless communication system for transferring voice, video and data in underground hard-rock mines (represented by WITS mock-mine). The research aims to answer the following key question:

- What is the effect of antenna placement, polarization, directivity and configuration, and transmission frequency on the performance of TTA communication systems in deep hard-rock mining environment for SISO antenna system?

1.4 Research Conceptual Framework

The work is based on real measurements conducted in the mock-mine at Chamber of Mines Building, the University of Witwatersrand, Johannesburg. It is divided into seven case studies to analyse the effect of antenna placement, polarization, directivity and configuration, and transmission frequency on the performance of TTA communication systems in underground mines. The performance of radio channel is studied by evaluating path-loss exponent, shadow fading statistics, channel impulse response, power delay profile, mean excess delay, RMS delay spread, maximum delay spread and coherent bandwidth for each case study. A conceptual framework of channel modelling is shown in Figure 1.1.

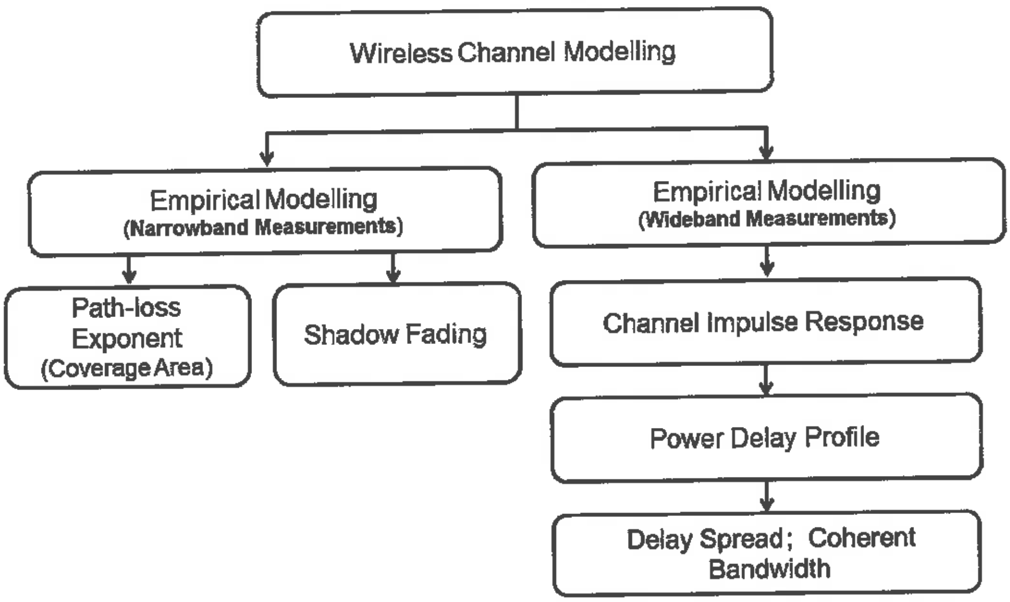

Figure 1.1 Conceptual Framework of Channel Modelling

1.5 Thesis Outline

Chapter one – *Introduction* covers the background, the scope of the research, objective of the research, research question, conceptual framework and organization of the thesis.

Chapter two – *Communication Systems for Underground Mines* discusses the wireless propagation terminologies. This chapter also reviews the three types of mine communication systems, i.e. through-the-earth (TTE), through-the-wire (TTW) and through-the-air (TTA) communication systems.

Chapter three – *Research Challenges in Though-the-Air (TTA) Communication System* discusses the effect of tunnel cross-section geometry, tunnel roughness, obstructions and communication system antenna parameters on the performance of TTA communication systems.

Chapter four – *Current Research in Through-the-Air (TTA) Communication Systems* reviews the statistical radio propagation of Room and Pillar Coal mine, Longwall Coal mine, CANMET Gold mine, Camborne School of Mines hard rock mine tunnel, MÜZ Coal mine, Iron mine and Lead-Zinc mine. This chapter also presents the digital systems installed and tested at the University of Witwatersrand mock-mine. The chapter is concluded with the open research areas in through-the-air (TTA) communication system.

Chapter five – *Research Methodology* explains the test environment description, experimental protocol, channel sounder and data acquisition procedures for measuring the statistical radio channel parameters.

Chapter six – *Case Studies: Results and Analysis* presents and analyses the effect of antenna placement, polarization, directivity and configuration, and transmission frequency on the performance of TTA communication system in WITS mock-tunnel by dividing into different case studies. This chapter also evaluates the statistical radio propagation of WITS vertical shaft.

Chapter seven – *Summary and Conclusion* highlights the findings of the study and conclusions drawn.

2 COMMUNICATION SYSTEMS FOR UNDERGROUND MINES

2.1 General

The wireless signal experiences different propagation phenomena, i.e. diffraction, refraction, reflection and scattering. This multipath fading effect needs to be taken into account when designing or developing a radio communication system. Modelling the radio channel has been the most difficult part of radio communication design and is typically done using statistical approach where the signal characteristics are measured at different points and using statistical models derived to match the measurements of the intended spectrum [12]. The following sub-sections discuss the radio propagation terminologies and classification of underground mine communication systems. The significance of radio channel characterization for the wireless communication system is also highlighted.

2.2 Radio Propagation Terminologies

The wireless channel can be modelled in the following way:-

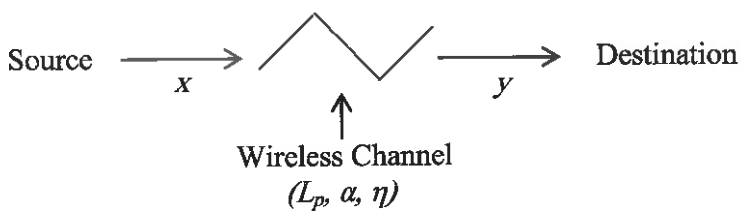

where x and y are the transmitted and received signals respectively, and Lp, α and η are the path loss, attenuation/multipath fading and additive white Gaussian noise (AWGN) due to wireless channel respectively. Equation (1) shows the relationship between transmitted and received signals at a particular distance of a given time [13].

$$y(t) = L_p . \alpha(t). x(t) + \eta(t) \quad (1)$$

Fading can be categorised in two types: large-scale and small-scale fading. Propagation models that predict mean received signal strength at any Tx-Rx distance are useful for estimating the coverage area over large distance and are called large-scale propagation model [12]. Typically, the local average received power is measured at a track of 5λ-40λ for large-scale measurements [12]. Path loss L_p and path-loss exponent n are the terms used in large-scale models at a single frequency [2]. The path loss and its relation with distance is defined as [12]:-

$$L_p\ (dB) = P_{Tx}\ (dBm) + G_{Tx}\ (dBi) + G_{Rx}(dBi) - P_{Rx}\ (dBm) \qquad (2)$$

$$L_p(d) = L_{p_o} + n10log_{10}\frac{d}{d_o} + X_\sigma \quad [\text{dB}] \qquad (3)$$

where P_{Rx} and P_{Tx} are the time-averaged power at the receiver input and transmitter output respectively, G_{Rx} and G_{Tx} are the receiver and transmitter antenna gains. L_{po} is the path-loss, in dB, at the reference distance d_o and X_σ is the standard deviation of shadow fading statistics. The value of L_{po} is based on either close-in measurements or free-space assumption at the reference distance (typically, d_o = 1 meter) [12].

Most path-loss models have several breakpoints that separate the areas where radio waves experience different path loss exponents [2], as shown in Figure 2.1. The breakpoints' r_{bp}[1] location depends on the height or width, i.e. (w, h), of the tunnel and the wavelength (λ) [68]:-

$$r_{bp} = max\left(\frac{w^2}{\lambda}, \frac{h^2}{\lambda}\right) \qquad (4)$$

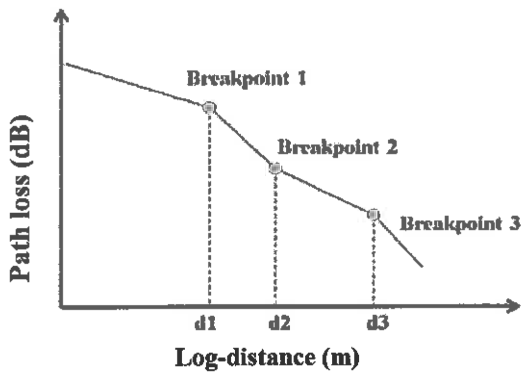

Figure 2.1 A path-loss model with three breakpoints [2]

[1] For a tunnel of (w, h) = (3.026 m, 2.69 m), r_{bp} = 74.81 m at 2.45 GHz and r_{bp} = 178.56 m at 5.85 GHz.

Small-scale fading or fading is the rapid fluctuation of the amplitude of radio signal over short travel distance (i.e. few wavelengths) or interval of time (i.e. of the order of seconds) [12]. Fading is caused by the multiple versions of transmitted signal at the receiver and it depends on the relative propagation time, distribution of intensity and the bandwidth of transmitted wave. The received radio signal in case of small-scale fading is given by [13]:-

$$y(t) = \sum_{k=1}^{N} \rho_k(t) e^{j\theta_k(t)} x(t - \tau_k(t)) + \eta(t) \tag{5}$$

where,

$\rho_k(t)$ = Attenuation of the k^{th} path;

$\theta_k(t)$ = Phase shift of the k^{th} path = $2\pi f_k - 2\pi(f_c + f_k)\tau_k(t)$;

$\tau_k(t)$ = Delay of the k^{th} path;

f_k = Doppler frequency shift of k^{th} path

Multiple components of the transmitted signal combine vectorially at the receiver antenna and can cause deep fading at a particular location in a small period of time [12]. Maintaining good communication is difficult, therefore diminishing the effect of deep fading for a longer period of time is of considerable importance. Different received signal replicas can cause frequency-selective fading as a result of time dispersion (quantified as delay spread). The frequency-selective fading results in inter-symbol interference (ISI). It is the main reason of interference in high data rate systems [14]. Coherent bandwidth that is necessary for optimization of data rate and modulation schemes can be determined from RMS delay spread [2]. When the scatterers or Tx/Rx terminal are in relative motion with constant speed, the received signals experience time-selective fading (also called Doppler spread).

Depending on the relationship between the channel parameters (Doppler spread and RMS-delay spread/coherent bandwidth) and signal parameters (symbol period and bandwidth) the transmitted signal will face different types of fading as [12]:-

Small Scale Fading

(Based on delay spread)

Flat Fading

1. BW of signal less than BW of channel
2. Delay spread less than symbol period

Frequency Selective Fading

1. BW of signal greater than BW of channel
2. Delay spread greater than symbol period

Small Scale Fading

(Based on Doppler spread)

Slow Fading

1. Low Doppler spread
2. Coherence time greater than symbol period
3. Channel variations slower than baseband signal variations

Fast Fading

1. Higher Doppler spread
2. Coherence time less than symbol period
3. Channel variations faster than baseband signal variations

By knowing the mean delay spread (τ_d) or the coherent bandwidth (B_c)[2], the frequency-selective fading can turn into flat fading channel by applying orthogonal frequency division modulation (OFDM) technique. Typically, the flat fading channel cause deep fades and it can be overcome by antenna/time diversity or increasing the transmitting power. However the time-selective fading can be ignored in mining environment due to little relative motion. For frequency-flat channel, the delay spread is small compared to the symbol duration [12]. Therefore,

$$x(t - \tau_k(t)) \approx x(t) \tag{6}$$

In this regard Equation (5) becomes,

$$y(t) = x(t) \sum_{k=1}^{N} \rho_k(t) e^{j\theta_k(t)} + \eta(t) \tag{7}$$

$$\alpha(t) = \sum_{k=1}^{N} \rho_k(t) e^{j\theta_k(t)} \tag{8}$$

[2] τ_d describes the time dispersion and B_C describes the frequency selectivity of the multipath channels.

$$y(t) = \alpha(t).x(t) + \eta(t) \quad (9)$$

Where $\alpha(t)$ describes the time varying nature of the received envelope of a flat fading (both in time and frequency) signal. A constant value of $\alpha(t)$ is desired in bit duration and estimated at the receiver using *channel estimator*. The signal performance can be improved on fading channel by using diversity techniques like frequency, time and space. The space diversity is also known as multiple input multiple output (MIMO) system.

2.3 Classification of Underground Mine Communication Systems

In general, the underground mine communication systems can be classified as through-the-earth (TTE), through-the-wire (TTW) and through-the-air (TTA) communication systems [2, 15]. With the evolution of underground mine communication systems, risk-to-man, man-to-man, man-to-machine and machine-to-machine communication is established for personnel health and safety and to meet efficiency and productivity objectives.

2.3.1 Through-The-Earth (TTE) Communication Systems

TTE communication systems use significant transmitting power and larger antennas to transfer ELF (Extremely Low Frequency)/VLF (Very Low Frequency)/ LF (Low Frequency) signals through solid rocks from the earth's surface into the underground mine [8, 16-17]. These low frequency signals can penetrate to several hundreds of meters through solid rocks in the mining environment [18]. TTE communication is used in case of disaster recovery to locate trapped miners [19]. There is a trade-off between transmission rate and its range. Also these systems are highly dependent on operating frequency, depth and characteristics of the ground [8]. Recent mining regulations have renewed interest in through-the-earth (TTE) communication systems because it offers wide coverage compared to through-the-air (TTA) communication systems [2]. These TTA/ modern wireless communication systems have apparent advantages (i.e. real time-voice, video and data messages) in underground mines but they could be quite vulnerable in case of a major disaster [2]. Figure 2.2 shows the transmission through-the-earth and transmission through-the-mine communication systems.

These systems support real-time voice, voice messages, data messages and beacon signals but there are limitations on transmission rates due to the low operating frequency bands [19]. Digital signal process (DSP) is used to make the voice signal compatible with narrow band carrier frequency [18]. The operational concept envisions mine emergency when no other form of communication is possible [20].

(a)

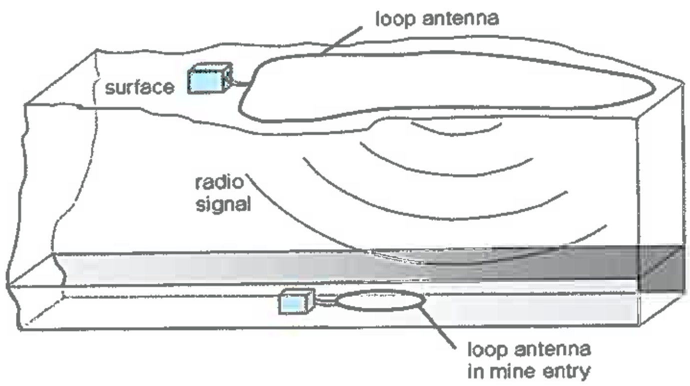

(b)

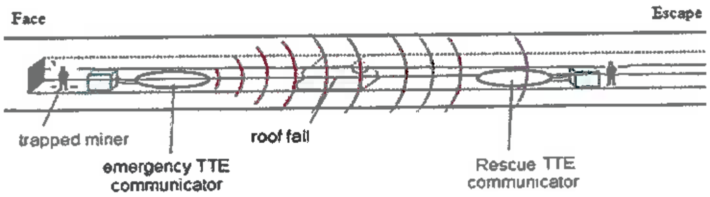

Figure 2.2 Transmission (a) Through-the-Earth (b) Through-the-Mine Communication Systems [19]

2.3.2 Through-The-Wire (TTW) Communication Systems

TTW communication systems have wired connections between different communication nodes, i.e. twisted pair, trolley, coaxial, and fibre optics from the surface or inside the mine. Among these through-the-wire based communication system leaky feeder is the well-known [2], as shown in Figure 2.3. It is also called semi-wireless or hybrid communication system in which one side is wired and the other is wireless. Key disadvantages of leaky feeder are low capacity, low coverage near face, fixed infrastructure, expensive and difficult maintenance [21, 22]. TTW communication systems use MF (Medium Frequency)/ VHF (Very High Frequency)/ lower-UHF (Ultra High Frequency) frequency bands for transferring voice messages, text messages and real-time voice/data messages [17, 23].

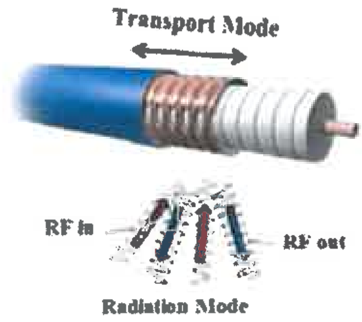

Figure 2.3 Leaky feeder cable [5]

2.3.3 Through-The-Air (TTA) Communication Systems

TTA is a wireless communication system in underground mines that uses upper-UHF (Ultra High Frequency)/ SHF (Super High Frequency) bands for two-way real-time voice, video and data communications, video surveillance, tracking miners and equipment, sensing and remote control etc. [17, 24-25]. It is more flexible and efficient than wired and leaky feeder coaxial cable because of its low-cost, easy to implement, minimal maintenance and scalability [25-26]. Due to the bounding walls of mine tunnels, the propagation characteristics of electromagnetic (EM) signals are very different from the terrestrial wireless signals [27]. Before deploying the wireless communication system, characterization of the channel propagation parameters (such as path-loss, angular spread and delay spread) is required. The channel characterization is required because the underground mining environment wireless propagation is significantly different from outdoor and indoor environments wireless propagation [2, 25]. Therefore, it is necessary to develop channel models that give insight to channel impairments and their dependence on the mining environment. Channel modelling enables efficient system design and deployment by answering [2]: 1) What is the effective frequency, range and antenna configuration/placement? 2) What channel impairments are needed to mitigate? So an accurate channel characterization is essential for addressing the communication system issues [28]. The optimum frequency for through-the-air communication depends on the structure, size, shape and infrastructure of the underground mine [2].

Wireless communication solution needs a reliable channel model. So, the prediction will be as good as the channel model. It is vital pre-requisite for communication system design, for example:-

- Simulation of the system design using the channel model.
- It tells that what kind of equalizer is required.
- It extracts the nature of the receiver design.

It also determines the maximum achievable data rate, coverage area and effective frequency for the communication system. The knowledge of the channel propagation also provides an insight to predict the performance of signal channel coding, multiple access techniques, modulation schemes and antenna configuration/placement [28].

2.4 Conclusion

This Chapter discusses the wireless propagation terminologies and technical details of through-the-earth (TTE), through-the-wire (TTW) and through-the-air (TTA) underground mine communication systems. TTE communication systems offer several hundred of meters signal penetration through solid rocks with limited transmission rates. The operation concept of TTE envisions mine emergency when no other form of communication is possible. However, TTW and TTA communication systems offers higher transmission rates for two-way real-time voice, video and data communication, video surveillance, tracking miners and equipment, sensing and remote control. The low-cost, easy to implement, minimal maintenance and higher scalability of TTA communication systems make it more flexible and efficient. The significance of radio channel characterization for the wireless communication system is also highlighted.

The next chapter covers the research challenges for designing and deploying through-the-air (TTA) communication system in underground mines. This chapter is concluded with a summary of the effect of tunnel geometry, communication system's antenna parameters, tunnel roughness and obstruction on TTA communication systems.

3 RESEARCH CHALLENGES IN THROUGH-THE-AIR (TTA) COMMUNICATION SYSTEMS

3.1 General

There is significant literature on theoretical and experimental work that has been done on high-ways and rail road tunnels where the cross-section dimensions are larger compared to wavelengths. The theory mentioned in [51], predicts the far-zone (where only one mode exist) attenuation of idealized circular and rectangular tunnels (both straight and gently curved) to be inversely proportional to frequency squared. This theory agreed well with the real non-circular and non-rectangular shape with smooth walls and smaller longitudinal non-uniformities. This is in contrast to the cases of caves or mining tunnels, which often have larger wall roughness and significant change of shape in longitudinal direction. As mentioned in [29], far-zone attenuation decreases with frequency in a straight rectangular underground mine tunnel upto 900MHz. The following sub-sections discuss the effect of tunnel geometry, transmission frequency, tunnel roughness, obstructions and antenna parameters on the performance of TTA communication systems.

3.2 Effect of Tunnel Cross-section Shape and size

As mentioned in review paper [2], propagation characteristics of subway tunnels show some similarities to those of underground mines although it lacks rough and tilted walls. Kim et al, in an analysis of radio wave propagation characteristics in rectangular road tunnel at 800 MHz and 2.4 GHz [52], mentioned that radio propagation in tunnels depends on the shape and tunnel cross-section dimensions. Hrovat et al, in a survey of radio propagation modelling for tunnels [53], mentioned that tunnel cross-section greatly impacted on attenuation rate. Figure 3.1 shows the typical cross-sections of tunnels. Underground mining tunnels differ from the subway tunnels, i.e. the permittivity and permeability of roof, floor and side walls are different. However, Changsen et al [54] proposed general radio signal attenuation 'α' (dB/m) for tunnels in Equation (10).

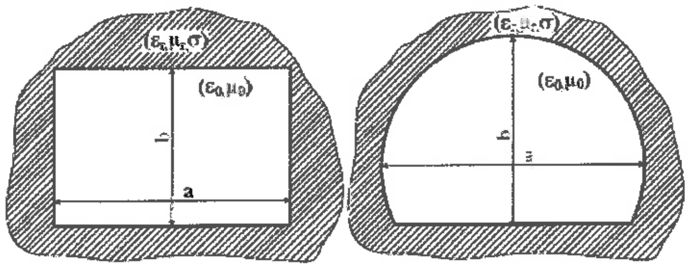

Figure 3.1 Typical tunnels cross-section shapes [53]

$$\alpha = \Bbbk \lambda^2 \left[\frac{\epsilon_r}{a^3\sqrt{\epsilon_{r-1}}} + \frac{1}{b^3\sqrt{\epsilon_{r-1}}}\right] \quad (10)$$

where a, b and ϵ_r are the maximum tunnel width, maximum tunnel height and permittivity of the tunnel. $\Bbbk = [4.343, 4.45, 5.09, 5.13]$ for rectangular, oval, circular and arched tunnels respectively. Conductors such as water pipes, power cables and metallic support system also affect the radio signals propagation [2, 47]. As shown by recent studies [37,49] that radio propagation is less dependent on the tunnel's dimensions when using directional antennas at transmitters and receivers.

3.3 Effect of Antenna Parameters

As mentioned in review paper [2], propagation characteristics of subway tunnels show some similarities to those of underground mines although it lacks rough and tilted walls. Radio propagation in tunnels depends on polarization, placement and radiation pattern of the transmitted and received antennas [26, 55-56]. Extensive measurements for vertically, horizontally, and cross-polarized (i.e. vertical-horizontal and horizontal-vertical) signals in mines and tunnels have been done with different antenna placement, configuration, spacing [37, 39, 43-44, 48, 50, 57-60]. It is evident from literature that horizontally polarized antennas perform better in horizontal aspect-ratio (i.e. width is greater than height) and vertically polarized antennas perform better in vertical aspect ratio. In [61-62], measurements have been done with circular polarized antenna in railway tunnels but there is no performance comparison with linearly polarized antennas.

Linard et al, in an investigation on MIMO channels in subway tunnels [59], found that directional antenna in MIMO system may not be a good solution unless antenna beam-width is equal to angular spread of the subway tunnels. Angular spread is the function of tunnel size and tunnel zone (transmitter-receiver distance) [2]. Figure 3.2 shows the angular spread of two subway tunnels. Underground mines can have different angular spread because of the underground mine infrastructure and wall's roughness [2].

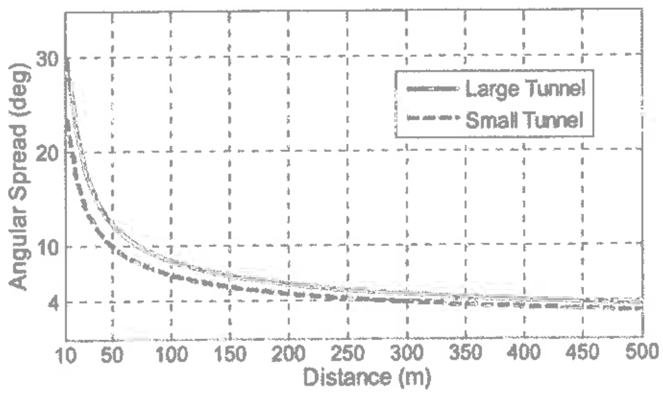

Figure 3.2 Angular spread of subway tunnels (large: 8m x 6.1m; small: 5.1m x 3.8m) [60]

3.4 Other Key Challenges

Table 3.1 shows the significant results that would be useful for wireless system designing and deploying in underground environment at UHF. As mentioned in [2], optimization of antenna parameters that matched to tunnel environment is an open topic for future. Antenna pattern, polarization and placement are important in underground mines because these have significant impact in wireless propagation in the confined environments like underground mines [2]. Antenna placement is important as it impacts the radiation pattern of antenna by introducing additional loss. That means the antenna pattern measured in Anechoic Chamber would not be same as in underground mines.

Table 3.1 Key Effects on Wireless/TTA Communication System in UHF frequency band[3]

		Path Loss	RMS delay spread	References
Tunnel Geometry	**Curvature/corner/branch**	Increase (less significant at lower frequencies)	Increase	[34, 72]
	Cross-Sectional Size (same impact as frequency)	Increases with larger size at fixed frequency in LOS scenario	Decrease with larger size at fixed frequency	[34]
	Wall tilt	Increase (less significant at lower frequencies)	No information available in literature	[29, 34]
Tunnel roughness		Increase (less significant at higher frequencies)	Increase	[29, 34]
Obstructions		Increase	Increase	[72]
Antenna Properties	**Radiation pattern**	Directional Antennas perform better in LOS	Smaller value for directional antenna compared to omni-directional one	[29, 72]
	Polarization	Mine with larger horizontal dimension shows low loss for horizontal polarization	Mine with larger horizontal dimension shows larger value for horizontal polarization	[26, 27, 30, 34, 72]
	Placement	Lower loss at the center of tunnel compared to off-centre	Larger value at the center of tunnel compared to off-centre	[26]

[3] UHF frequency band ranges from 300 MHz to 3 GHz.

3.5 Conclusion

This chapter highlights that the tunnel geometry, communication system's antenna parameters, tunnel roughness and obstruction have significant impact on the performance of through-the-air communication system. The path-loss and RMS delay spread increases with the tunnel curvature. Antenna placed at the center of the tunnel presents lowest path loss. The horizontally polarized antenna offers low attenuation and high RMS delay spread in a wide tunnel as compared to vertically polarized antennas. The directional antenna performs better in terms of path-loss in line-of-sight situation and offers high coherent bandwidth.

The next chapter reviews the statistical radio propagation of through-the-air communication systems in Room and Pillar Coal mine, Longwall Coal mine, CANMET Gold mine, Camborne School of Mines hard rock mine tunnel, MÜZ Coal mine, Iron mine and Lead-Zinc mine. This chapter also discusses the digital systems installed and tested at the University of Witwatersrand mock-mine.

4 CURRENT RESEARCH IN THROUGH-THE-AIR (TTA) COMMUNICATION SYSTEMS

4.1 General

As mentioned in review paper [2], theoretical models give valuable insights of channel propagation that are mostly based on unrealistic assumptions and need to be evaluated through experiments. So, the measurement based approach would be the principle method of characterizing the wireless environment. In literature the measurement based models are not as common as theoretical models because of the difficulties to access underground mines, safety, measurement complexities and expense. In UHF (Ultra High Frequency) band, theoretical studies show that mine tunnels act as relatively low-loss dielectrics and transmission takes place in the form of waveguide propagation [29]. Whereas, practical tests showed that MF (Medium Frequency) band has good coverage/less severe attenuation compared to UHF band both in metal/non-metal and coal mines [16].

The results presented in the review paper of period 1920-2012 [2] show that in underground mines, the path loss and delay spread is dependent on the measurement scenario, size/structure of the tunnel and operating frequency. Nerguizian et al, in a study of radio channel characterization of an underground mine at 2.4GHz [30], also found that the RMS-delay spread distance profile is specific to underground mine gallery. The proposed channel model in [26] showed that attenuation is mostly dependent on the tunnel size and operating frequency and tunnel wall's humidity affects the conductivity so the attenuation of radio signal affected. Whereas, temperature and tunnel walls materials have little effect on the signal propagation. The following sub-sections reviews the performance of different TTA communication systems in different underground mines. Also, the key findings of an analytical model developed for underground tunnels are discussed.

4.2 Room and Pillar Coal Mine

Laliberte, in summary study of underground communications technologies [31], tested communication VHF, UHF, Zig-bee and Wi-Fi radios with omni-directional and directional antennas in room and pillar coal mine (Figure 4.1). The results showed that 2.4 GHz Wi-Fi signal frequency has higher coverage area compared to others at different roof heights as shown in Figure 4.2. Some of the observations at 2.4GHz Wi-Fi signal frequency were made with directional antenna while rest of the observations were with omni-directional antennas. The experimental results showed that Wi-Fi radios at 2.4GHz outperforms at different roof heights. The propagation range of Wi-Fi signals increases significantly with the increase of roof height. It is also observed that no information about the antenna polarization and antenna directivity is provided.

Tao, in technology study of wireless communication system under the coal mine tunnel [32], discussed that tunnel cross-section has great impact on radio propagation as compared to cross-section shape. This study showed that transmission loss becomes small at operating frequency above 2GHz. The radio power of the communication system must be reduced in the coal mines and potential explosive environments for the health and safety issues [31].

Figure 4.1 Room and Pillar Coal Mining in Skyline [31]

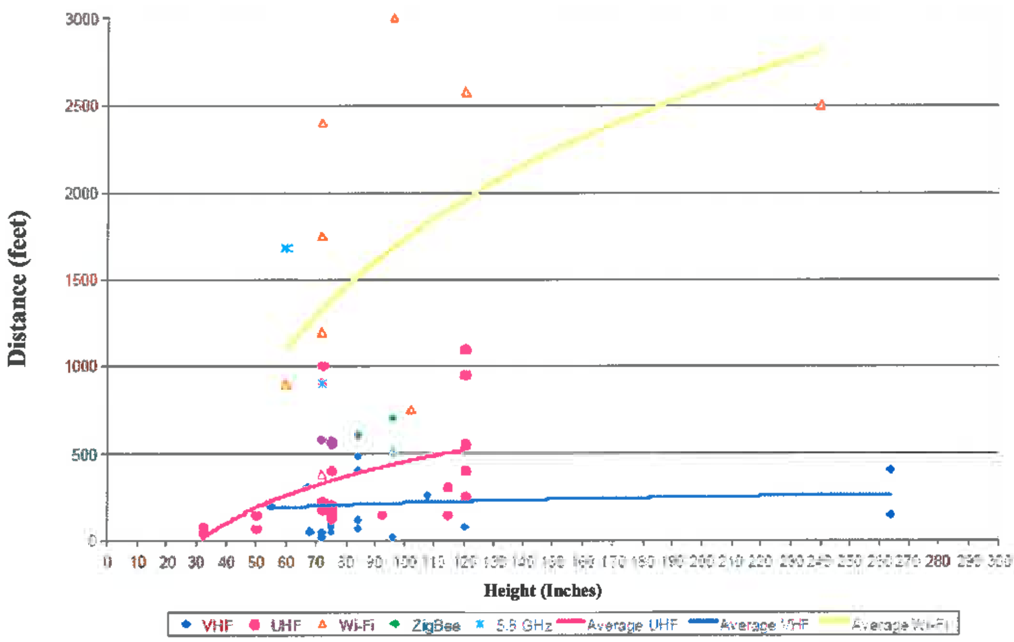

Figure 4.2 Range as a function of roof height and frequency – line-of-sight situation [31]

4.3 Longwall Coal Mine

Zhang et al, in a study of radio propagation at 900MHz in underground coal mines [33], reported experimental radio propagation results in two fully equipped and operational (i.e. passageways and mining areas) longwall coal mines at Shanxi province Northern China. The arch-shaped passageways of 12-15 square meter cross-section area reinforced with concrete were used for transportation and ventilation. The passageways had the trolleys of 1.5m height, 1m width and 3m long, and 30° inclined conveyor belts of 2m width. The coal breaker, stage loader, power substation, extendable belts, metallic support, log support and hydraulic props were installed in the mining area, which comprise of gate entries and longwall face. The cross-section of gate entries was almost 9.0 square meters in cross-section area. The experimental results showed one-slope and two-slope path-loss regression fit models for the mining areas and the passageways, respectively. In addition, the pathloss did not vary largely in different passageways and mining areas. The cross-section ratio of mining equipment to open space and sharpness of bents presented additional propagation losses.

4.4 CANMET Gold Mine

Gold mine measurements have been conducted in the underground gallery of an old gold mine in Canada at different levels [30, 34]. Figure 4.3 (a) shows the underground gallery at level 40 stretched over 75m with height of 5m and width of 4m (on average). Its walls are very rough and are supported with metallic grid and roof bolt, the floor is not flat and it contains some water plaques [30]. The temperature may vary from 6 ° to 15 ° C along the year. Figure 5 in reference [35] that flexible ventilation duct is used. Some of the measurements have also been done at level 70 with height of 4m and width of 2.5m [34], as shown in Figure 4.3 (b). This gallery has very rough surfaces and is very humid. The floor is flatter than the ceiling and side walls, has some water plaques and some areas of level 70m are also supported by metallic grid and roof-bolt [36].

Figure 4.3 CANMET gold mine photograph of underground at (a) 40m level [35], (b) 70m level [34]

The radio propagation parameters of different environments (free space, indoor, underground tunnels and mining tunnels) with antenna configurations are summarized in appendix A for better understanding. This information is quite useful for efficient system designing and deploying. The wideband measurement results with omni-directional antennas performed at 2.4GHz on different levels (i.e. 40m and 70m) were quite different [34]. It is also evident that the path loss and delay spread varies by the operating frequency, tunnel geometry and antenna parameters. The performance of MIMO system (i.e. path-loss exponent, capacity and signal decorrelation) has also been tested in CANMET Mine Laboratory.

In [47], linearly polarized omni-directional and patch antennas were tested in 2.3GHz and 5.8 GHz frequency bands. The high gain patch antenna showed lower attenuation rate in line-of-sight (LOS) and non-line-of-sight (NLOS) situations. However, Rissafi el. al., in an experimental characterization of an UWB propagation channel in CANMET underground mines [48], found that directional antenna performs better in terms of time dispersion parameters for LOS situation and omni-directional antenna performs better in terms of path loss for NLOS situation (shown in table \ref{table3}). Khaled et al, in a Performance Study of Line-of-Sight Millimeter-wave Underground Mine Channel [28], studied omni-horn and horn-horn antenna configuration in different mining environments. The paper concludes that it is better to use omni-directional antennas; horn-omni and omni-horn antenna configurations for higher system capacity.

In [35, 41-43, 47], a performance comparison of SISO and MIMO antenna system is presented with 2x2 linearly polarized omni-directional and patch MIMO antenna systems. The results showed a higher transmission range and channel capacity of MIMO than SISO antenna system. Mabrouk et. al. [43, 45, 46], observed that directional MIMO suppress multipath that reduces rms-delay spread and channel capacity due to the increases in correlation as compared to omni-directional MIMO.

In [37-39], Mabrouk et. al. tested 2x2 MIMO Regular (λ/2 antenna element separation) and 30° Angled Vivaldi antenna of (30°, 30°) element beamwidth in LOS and NLOS situations. NLOS situation took into account the machinery effect and showed a substantial effect on communication system performance. The results demonstrated that MIMO antenna system and a rich scattering environment are necessary for increasing channel capacity. The LOS results indicated an increase of system performance in terms of channel capacity and pathloss exponent as compared to NLOS situation due to higher SNR. MIMO-A showed significant increase of channel capacity in LOS situation due to multipath richness as compared to MIMO-R antenna system. Therefore, it is concluded to be in LOS situation with higher antenna decorrelation configuration.

Ghaddar et. al. [44] presented the low-cost beam space technique with MIMO-patch antenna element beamwidth of (92.4°, 71.3°) for increasing system capacity. The orthogonal beams were generated by 30° conformal cylindrical-shape microstrip patch array (CMPA). The 4x4 MIMO results revealed that CMPA enhances the propagation characteristics and capacity gain compared to conventional planar microstrip patch array (PMPA), especially in NLOS situation. This can be explained by MIMO-antenna sub-channels higher decorrelation relationship. Furthermore, 4x4 MIMO showed almost double the channel capacity over 2x2 MIMO antenna system [44, 46].

In [35, 40], Mabrouk et. al. observed that the human presence induces great amplitude variations to the received signal and time dispersion parameters. Moreover, the presence of mineworker increases channel capacity due to multipath propagation gain and pathloss exponent. Therefore, the effect of human body must be included in the designing and modelling of a reliable underground communication system.

4.5 CSM Hard Rock Mine and MÜZ Coal Mine

Kennedy, in a study of high resilience wireless mesh networking characteristics and safety applications within underground mines [47], did testing in straight railway tunnel, hard-rock mine and coal mine as shown in Figure 4.4. The linearly polarized omni- and patch antennas with different gains were tested at 2.3GHz and 5.8 GHz frequency bands. In hard-rock mine tunnel, higher frequencies showed lower attenuation over long distance beyond the initial sharp drop in signal. In circular roof support coal mine tunnel, circular/gradual curves showed lower attenuation compared to sharp bends similar to mine ventilation loss. The metal lined support infrastructure in MÜZ coal mine enhances the signal propagation. In railway and hard rock mine tunnels, higher frequencies with omni-directional antenna offered better range in straight tunnels. It is observed that in all three tunnels, high gain patch antenna has low attenuation or high coverage both in line-of-sight (LOS) and non-line-of-sight (NLOS) situations compared to omni-directional antenna. Whereas, Rissafi el. al., in an Experimental characterization of an UWB propagation channel in CANMET underground mines [48], found that directional antenna performs better in terms of time dispersion parameters for LOS scenario and omni-directional antenna performs better in terms of path loss for NLOS scenario. Similar attenuation rate and performance has been achieved in railway and hard-rock mine tunnels except for MÜZ coal mine because of the significant cables, pipes and metal equipment. Therefore it is necessary to characterize the underground mining environment instead of generalizing the propagation characteristics based on tunnel geometry.

Figure 4.4 Test locations [47] (a) Ashbourne Railway tunnel (b) CSM (Camborne School of Mines) Hard Rock Mine tunnel (c) Maschinenübungszentrum (MÜZ) Coal Mine – typical European coal mine

4.6 Iron Ore Mine

Ferrer-Coll et al, in a study of characterisation of electromagnetic properties in iron-mine production tunnels [22], did testing in the world's largest iron ore mine situated in Sweden for finding the suitability of wireless technology for this mine. Measurements were performed in narrow (width of 4.4-6.3m) and wide (width of 21m) tunnel with directional antenna of 16 dBi gain for path loss and omni-directional antenna of 6 dBi gain for multipath measurements. It is observed that the operating frequency effect the system performance. Moreover, curved part of the tunnel imposed higher attenuation. The maximum delay spread of 100 nsec in NLOS indicates that the underground tunnel is moderately reflective and MIMO antenna system cannot be fully exploited.

4.7 Lead-Zinc Mine

A Lead-Zinc mine tunnel has been characterized with linearly polarized biconical antenna array in different antenna orientation, antenna separation and polarization [49], as shown in Figure 4.5. It is a rectangular shaped tunnel with width 5-5.7m and height 3.5-4.2m with electric wires, pipes and leaky feeder along the ceiling and the mud on the floor. The result showed that 4-element uniform linear array with 2λ element spacing in horizontal orientation provides the sufficient decorrelation among MIMO elements. Horizontally polarized antennas performed better in horizontal aspect-ratio (i.e. width is greater than height) and vertically polarized antennas perform better in vertical aspect ratio [2, 33, 47, 49, 50]. The radio propagation was also dependent on the antenna placement.

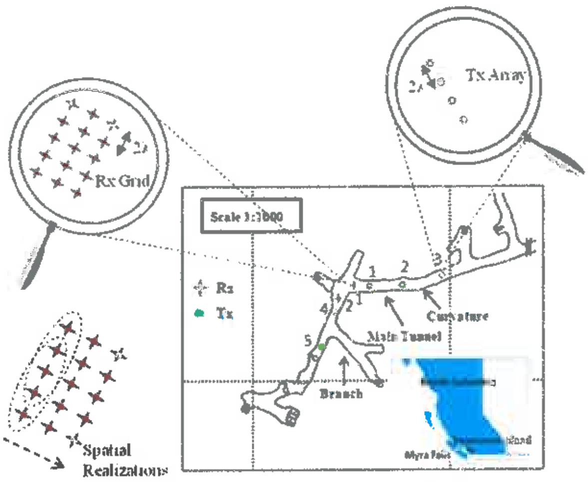

Figure 4.5 Lead-Zinc Mine at Myra Falls [49]

4.8 WITS Digital Mock-mine

The digital-mine mock-up that is being built beneath the School of Mining Engineering at the University of the Witwatersrand includes a mock-tunnel, stope panel and a vertical shaft. The purpose of Digital Mine laboratory is to provide a platform to action the existing strategy of the mining industry to continuously improve working conditions and mine economics [63]. Actual underground mine material has been used to build the 67m long tunnel in order to allow realistic testing [64] and the mock-mine environment (i.e. shape and size of tunnel, tunnel supporting infrastructure and ventilation system) is very similar to what is actually found in South African mines. The following sub-section covers different communication systems tested in this tunnel.

4.8.1 Monitoring and Tracking Systems

Asset management, person tracking, seismographs, weather station, crack meter, stress meter and video analytics systems have been installed at the strategic positions in the mock-mine for testing, integrating and improving the mine working environment. These systems were installed by Schauenburg, Vibra-Tech and EOH vendors that follow the leading mining practices (Figure 4.6 (a)).

The Schauenburg Systems provided asset management system, gas detection instruments (GDI) and person tracking system. The passive RFID tags are used for asset management by installing a turnstile gate and person tracking by installing omni-directional linear polarized antennas in the mock-mine. The hand-held and fixed GDI's are installed for detecting Oxygen (O_2), Carbon Monoxide (CO) and Methane (CH_4). The data collection nodes are connected to the control room by ethernet cable.

Vibra-Tech Engineers, Inc. provided a remote and completely wireless structural monitoring system as part of Digital Mine Project. The purpose of this real time wireless remote monitoring and communication system within the mock-mine was to facilitate real time data collection and analysis within underground mines for the purpose of risk management and decision making at the surface. The theory of operation of this system was to utilize a central PC with a software package to remotely communicate via Wi-Fi with numerous data collection nodes (data loggers) at each remote monitoring location. Data collection nodes were installed within the mock tunnel as well as inside the COM building and on the roof. The use of an actual data logger at each node ensures data is stored and preserved in the event Wi-Fi communication is interrupted. Additionally, if required, each data logger can act as a stand-alone data server within the network and can be remotely communicated with and programmed. The overall function and performance of any of the Wi Fi nodes is dependent on the quality and performance of the network to which it they are connected. This system uses linearly polarized antennas at 2.4GHz operating frequency band for wireless communication.

For the mitigation of illegal miners, the Wits Digital mock-mine is equipped with a system of cameras throughout the mine to monitor the access points and working areas. The IP-cameras are connected to the control room by Ethernet cable. Figure 4.6 (b) shows the installed systems in the WITS mock-mine.

The Vibra-Tech system is providing the connectivity issues that need to be resolved for reliable data transmission. From the above literature survey, it is evident that the system performance (i.e. reliability and capacity) can be improved by using antennas that are more suitable for underground mines. As the system performance is dependent on the underground mining environment (i.e. shape and size of tunnel, tunnel supporting infrastructure and ventilation system) therefore the wireless channel modelling is required for the performance comparison with different antennas parameters in the mock-mine.

The deployment of a wired system is a troublesome task in an underground mine, and it has limited scalability and high maintenance cost. For getting the benefits of wireless system, the mining environment must be modelled for wired systems like Schauenburg and EOH camera system. One of the targets for system optimization is the integration of individual systems for improving working conditions and mine economics, as shown in Figure 4.6 (c). The system integration would also remove the need of duplicate data collection nodes.

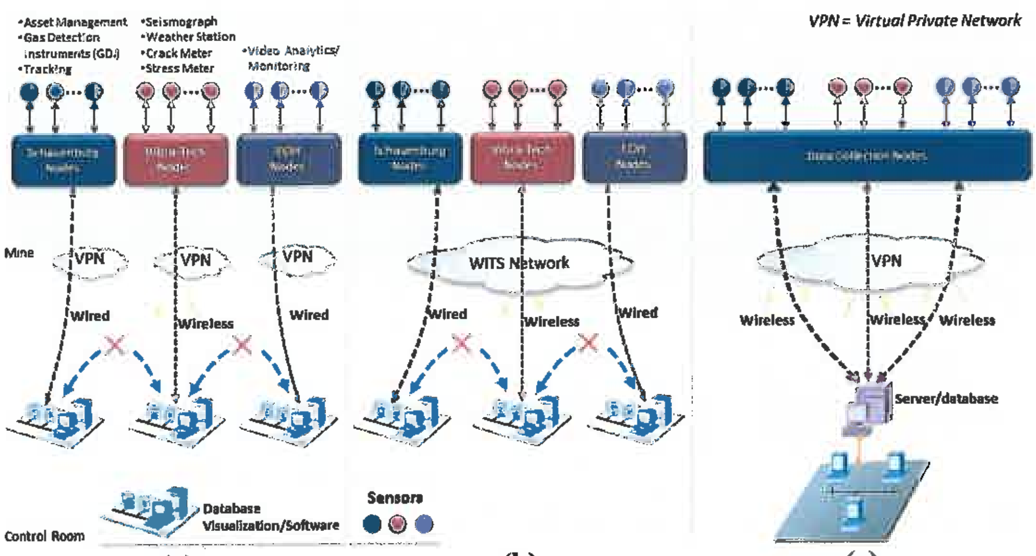

(a) (b) (c)

Figure 4.6 (a) Solution provided by the Vendor Companies, (b) Systems installed in WITS digital mock-mine, (c) Targeted system integration

4.8.2 Emergency Communication System

HUAWEI eLTE Rapid Development Broadband Trunking system [65] was tested in the mock-tunnel (Figure 4.7). Rapid transport and deployment (15 minutes) of this system envision an emergency communication system that is a crucial requirement for emergency response. The kit does not require on-site wireless network planning and configurations. It can improve underground post-accident communication by providing messaging, voice call, video call, push-to-talk and video monitoring functionalities. The kit supports 2x2 omni-directional linearly polarized MIMO antennas (i.e. KBT TQC-1800A mobile antenna and EP680 Handset) in 1785-1805 MHz frequency band. Due the health and safety issues in the confined areas, the kit was tested with a power level of less than 1 Watts (30 dBm). To date, there is no open published result available on the testing of this kit in underground mining environment. Table 4.1 shows the test results of eLTE kit at different positions in WITS mock-tunnel with radio power of 29.5 dBm. The messaging, voice call, and video monitoring and video call were operational in 105 m and 63m transmitter-receiver distance, respectively.

Table 4.1 Test Results of LTE Kit at Different Positions in the Wits Tunnel with Radio Power = 31.2 dBm

Function	Scenario	Observation
SMS	UE A to UE B	Successful
MMS	UE A to UE B	Successful
Voice Call	UE A to UE B	Successful
	UE to Dconsole with headphone	Understandable but echoes
Video Monitoring*	UE to Dconsole	Successful
Video Call*	UE A to UE B	Video Successful; Voice Breaking
	UE to Dconsole with headphone	Video Successful; Voice Breaking and Echoes**
PTT	UE A to UE B	Successful

SMS = Short Message Service; MMS = Multimedia Messaging Service; UE = User Equipment; PTT = Push-to-Talk; DSonsole = Dispatch Console Software on Laptop; *No video in rescue room due to the darkness; **Understandable voice but has echoes.

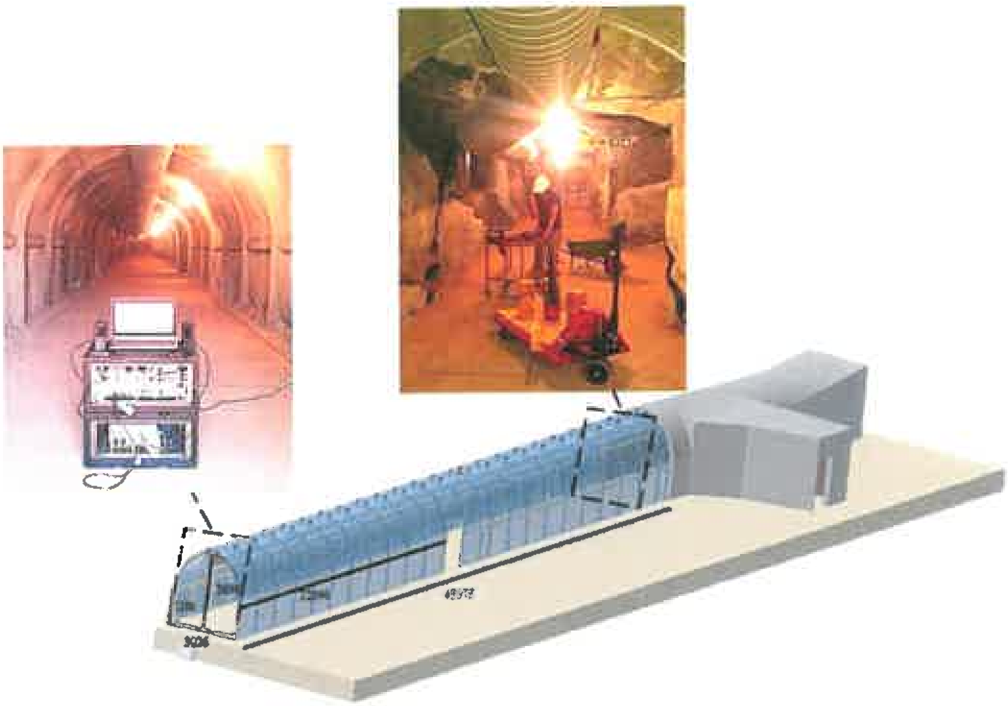

Figure 4.7 HUAWEI eLTE Rapid Development Broadband Trunking System testing in WITS mock-tunnel (all the dimensions are in mm)

4.9 Analytical Model – Multi-mode Waveguide

The Multi-Mode Waveguide model was developed for underground tunnels and claims to be applicable for underground mining tunnels [26]. The key implications of this model are:

- The signals of higher transmission frequency attenuate slower.
- In near region, the signal power attenuates faster and fluctuates rapidly than the far region. This is due to the fact that higher order modes attenuate faster as the distance increases.
- In large tunnels, the modes attenuation is smaller. Moreover, the delay spread of signal is large.
- The horizontally polarized antenna has slower attenuation and larger delay spread in horizontal aspect-ratio (i.e. width is greater than height).
- The antennas placed at the center of the tunnel present the lowest signal attenuation and fluctuation, and has larger delay spread.
- If the transmitted antenna placed near wall (1/8 of width or height), the attenuation and fluctuation of received signal is significant.

The theoretical waveguide models agreed well with the real non-circular and non-rectangular shape with smooth walls and smaller longitudinal non-uniformities [51]. This is in contrast to the cases of caves or mining tunnels, which often have larger wall roughness and significant change of shape in longitudinal direction.

4.10 Conclusions and Open Research Areas

The studies reveal that reliable communication has always been a challenge in underground mines due to dynamic topologies and the harsh environment. Unlike conventional underground mines where the most common communication systems are based on voice application, digital mines require wireless communication systems for two-way real-time voice, video and data communications, video surveillance, tracking miners and equipments, sensing and remote control. The radio channel characterization is required for efficient designing and deploying the wireless communication system. The underground mine geometry is diverse, vast and complex; therefore more measurement campaigns are required to confirm previous findings and reveal new trends. To the best of our knowledge, no open literature is available on the radio propagation of 1) deep underground mining tunnels, 2) mine vertical shaft and 3) underground mining tunnels with circularly polarized antennas. The circular polarized antennas have low signal loss due to polarization miss-match and these are immune to signal-fading effects due to reflected waves. The experimental work on the performance comparison of different antennas in the underground mines is also sparse. The characterization of arch-shaped hard-rock mine tunnels are also required as most of the deep underground hard rock mines (i.e. gold and platinum) are steel supported arch-shaped. Open research areas include the performance study of deep underground mines with antennas having different polarization and directivity. The performance improvement of SISO/MIMO antenna systems by using antenna beam-width equal to the angular spread of underground mine tunnel is also required. Due to the health and safety issues, the transmitting radio power levels must also be considered.

The next chapter explains the methodology adopted for the study. It covers test environment description, experimental protocol, channel sounder and data acquisition procedure for the wideband measurements.

5 Research Methodology

5.1 General

Underground wireless communication systems are more than just sending radio signals. A reliable communication in the underground galleries require radio propagation characterization. The literature showed significant work on the empirical channel characterization approaches for avoiding the unfortunate accidents. The underground mine geometry is diverse, vast and complex; therefore more measurement campaigns are required to confirm previous findings and reveal new trends. The objective of this work is to study the performance of through-the-air communication systems with different antennas at different frequencies in an underground mine.

This chapter describes the test environment and methodology that is used for the statistical radio channel modelling (i.e. wideband measurements). The measurement hardware and software used for the data collection and analysis are also discussed. The wideband measurement setup can characterize the radio channel in 2.4-2.5 GHz and 5.8-5.9 GHz frequency bands.

5.2 Description of the Environment

The measurements were taken in the University of Witwatersrand mock-mine (i.e. mock-mine and vertical shaft). The shape, size, supporting infrastructure and ventilation system of mock-tunnel environment are very similar to what is actually found in the deep hard-rock mines. Actual underground mine material has been used to build the 66.2m[4] long tunnel in order to allow realistic testing [64]. The arch-shaped mock-tunnel is equipped with steel ventilation duct of 0.5m diameter as shown in Figure 5.1. The mock-tunnel walls are supported with sprayed-cement, steel mesh and steel arches. Figure 5.2 shows that vertical shaft inside the Chamber of Mines (CoM) building. The steel vertical shaft has dimensions 1.45m x 1.45m x 6m.

[4] Tunnel dimensions: $x = 66.2\ m$, $y = 3.026\ m$, $[z_{min}, z_{max}] = [1.2\ m, 2.69\ m]$. The position ($x = 0\ m$, $y = 0\ m$, $z = 0\ m$) corresponds to the right bottom corner of the tunnel entrance.

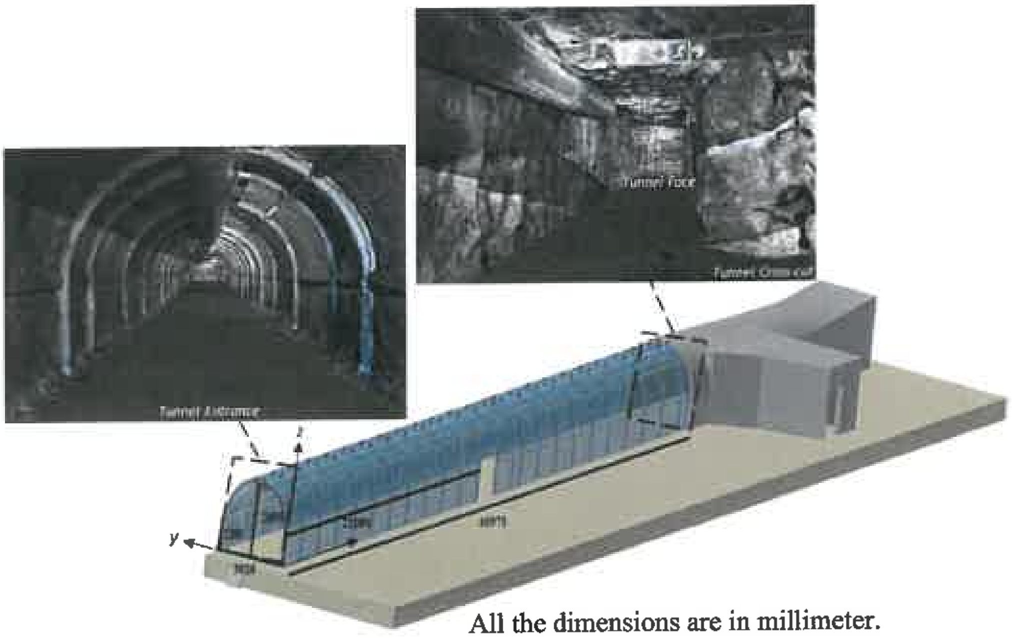

Figure 5.1 Lego-style CADD image of WITS mock-mine [64]

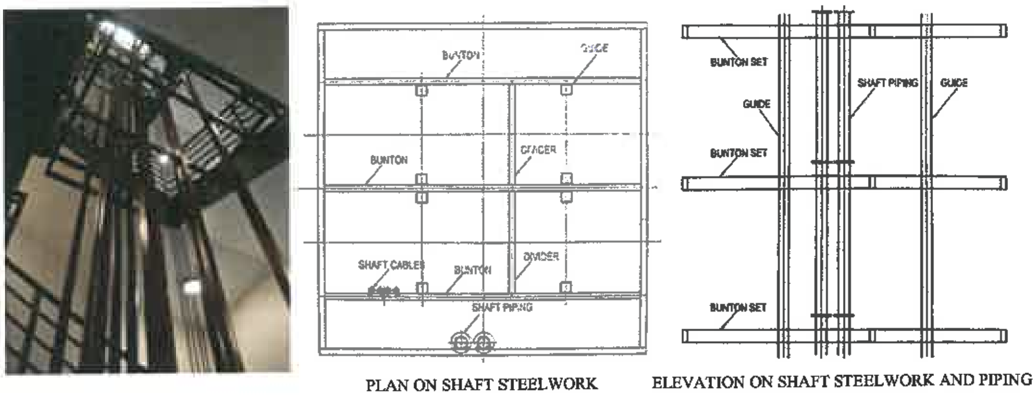

Figure 5.2 The vertical Shaft inside the CoM building

5.3 Methodology

To investigate the statistical behaviour of radio channel, experiments are conducted in the mock-mine. Before the measurement campaign, the system calibration (i.e. noise floor and equipment calibration, appendix B-J) is done in order to remove the effect of environment and measuring equipment [30]. The equipment calibration includes the measurements of antennas, RF cables, RF connectors, high gain amplifier and supper low noise amplifier. The wideband measurements are used to obtain path-loss exponent, shadow fading statistics, channel transfer function, channel impulse response, power delay profile, time dispersion parameters (i.e. mean excess delay, RMS delay spread and maximum delay spread) and coherent bandwidth parameters for the performance study. The path-loss exponent and shadow fading statistics can be deduced from narrowband measurements at any measurement location [28, 30, 34 and 48]. Figure 5.3 shows the flow diagram of the research methodology for measuring statistical radio propagation parameters. The following sub-sections explain the channel sounder and data acquisition procedure.

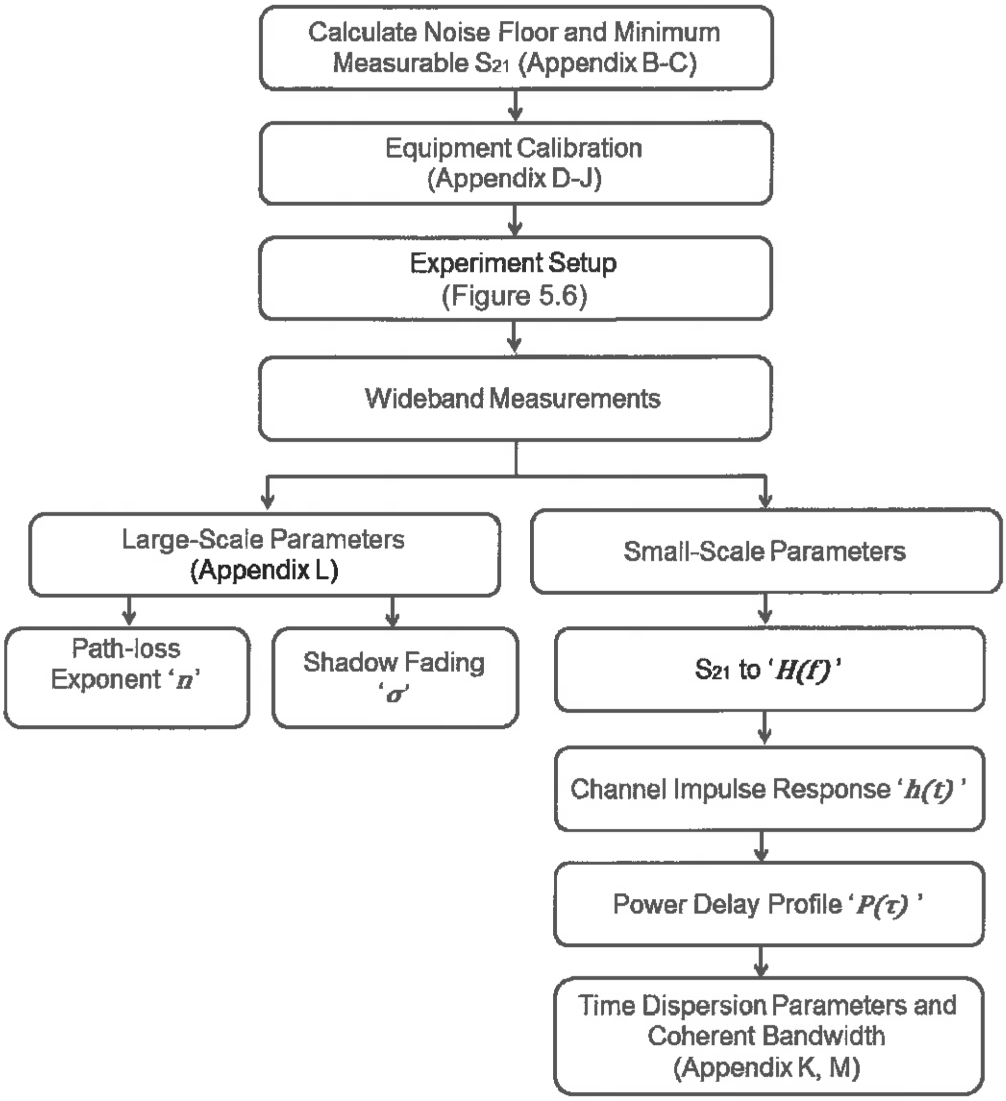

Figure 5.3 Research Methodology for Measuring Statistical Radio Propagation Parameters

The large-scale parameters (i.e. path-loss exponent and shadow fading statistics) are obtained from the transmission co-efficient of the wideband measurements. Figure 5.4 shows the pictorial representation of scattered plot of received power over transmitted power, path-loss exponent and shadow fading statistics. Typically, the local average received power is measured at a track of 5λ - 40λ[5] for large-scale measurements. It is important for link budget calculation and system design because it determines the coverage area and average signal-to-noise ratio (SNR) at the receiver [73].

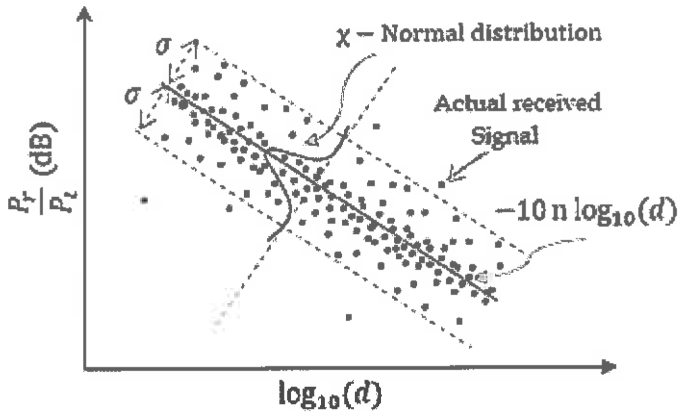

Figure 5.4 Path-loss Exponent and Shadow Fading Statistics [76]

The small-scale fading parameters (i.e. time dispersion parameters) can be obtained from the channel impulse response which is the inverse fast Fourier transform (IFFT) of channel transfer function at a particular distance [57, 73]. The channel impulse response [6] is the characteristics of the channel which is independent of the operational frequency band, as shown in Figure 5.5. If the transmitter, receiver and scatterers are fixed then the channel impulse response is fixed. The frequency band determines the width of the discrete impulse time response bins, i.e. $\Delta\tau = \tau_N - \tau_{N-1}$. The time dispersion parameters are determined from the relative amplitudes of the multipath components power delay

[5] 5λ - 40λ = 0.6122 m - 4.897 m at 2.45 GHz; 5λ - 40λ = 0.256 m - 2.051 m at 5.85 GHz.

[6] Channel impulse response is a function of 'τ' (delay spread) and 't' (which depends on the motion of mobile receiver).

profile (PDP), i.e. $P(\tau)$. For small-scale channel modelling, the $P(\tau)$ can be obtained by spatial average of $|h(t,\tau)|^2$ over local area[7] (see appendix K). By finding $P(\tau)$ over many local areas, the $P(\tau)$ over large-area can be obtained. The received $P(\tau)$ in a local area is given by [12]:-

$$P(\tau) \approx \overline{k\,|h(t,\tau)|^2} \tag{11}$$

where, $h(t,\tau)$ is the channel impulse response, k is the gain which relates the transmitted power to the total received and the bar represents the spatial average over local area. The received power does not fluctuate significantly over local area when the measurements are done with bandwidth greater than the coherent bandwidth [12].

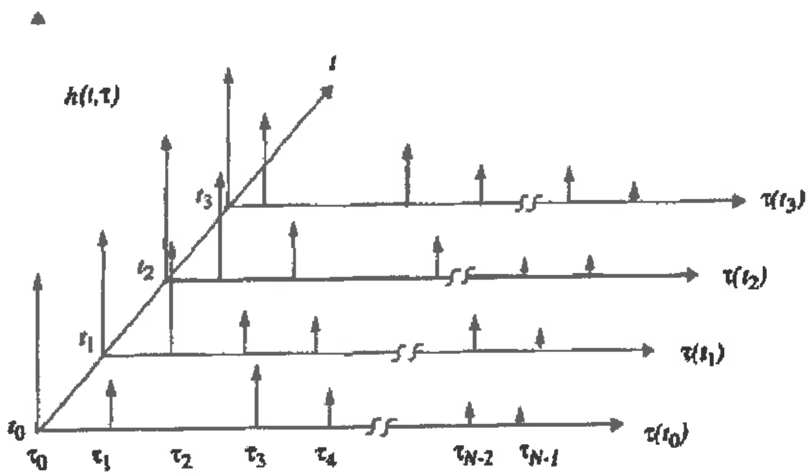

Figure 5.5 Example of Discrete-time Impulse Response [12]

5.3.1 Channel Sounder

The frequency-domain channel sounding (i.e. vector network analyser) is used for extracting the large-scale and small-scale parameters form wideband measurements [12, 28, 48, 73]. The fast sweep time is necessary to keep total sweep frequency measurement in short interval for time-varying channels [12]. The vector network analyser (VNA, ANRITSU MS 2036A), high gain amplifier

[7] Local area means a spatial distance of one quarter of a wavelength over a receiver moment of 2m in the indoor channel for 450 MHz - 6 GHz range [12].

(HGA, MINI-CIRCUITS ZX60-V63+), super low noise amplifier (SLNA; WENTEQ ALN0230-26-4007, ALN0560-11-2709), RF cables (L-COM 400-series low loss ultra-flex and 195-series low loss cables), attenuators and antennas are used for these measurements, as shown in Figure 5.6. The channel sounder can characterize radio channel in 2.4-2.5 GHz (SLNA, WENTEQ ALN0230-26-4007) and 5.8-5.9 GHz (SLNA, WENTEQ ALN0560-11-2709) frequency bands. The vector network analyser transmitting power was set to 0dBm (1mW). The quasi-static channel is assumed during the measurement campaign.

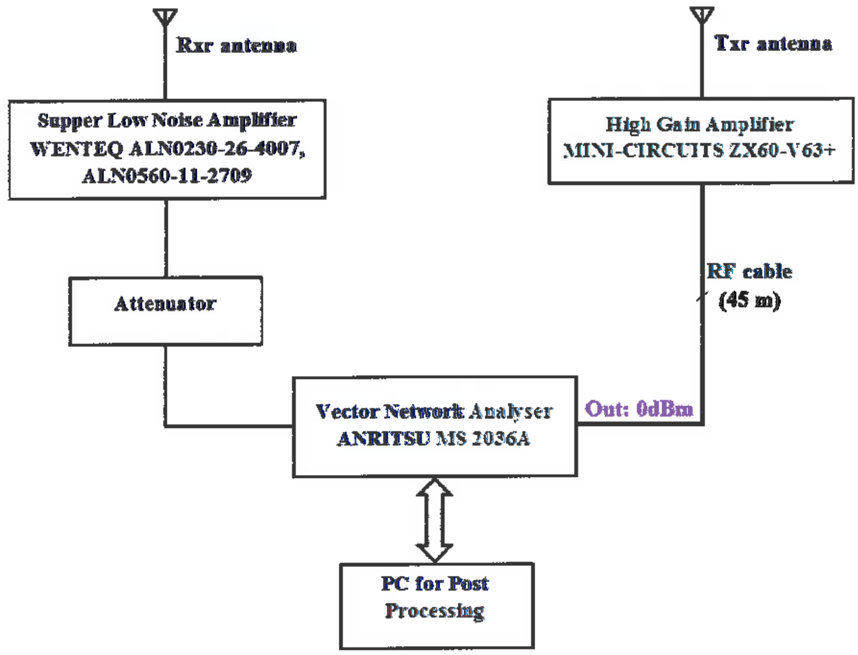

Figure 5.6 Schematic Diagram of Wideband Measurement Setup

5.3.2 Data Acquisition

Matlab files are used for analysing the large-scale and small-scale fading parameters (see appendix L-M). The linear least square regression method [8] is used to evaluate the scatters received power over transmitted power as a function of Tx-Rx distance for path-loss exponent. The value of shadow fading is estimated

[8] Linear least square regression method is a statistical model of linear curve fitting which minimizes the sum of squared differences between the data values and the corresponding estimated values.

by measuring the deviation of P_r/P_t from the linear regression line. The Kolmogorov-Smirnov (KS) test is used to identify the best fit distribution for the shadow fading [28]. Equation (3) is used to evaluate the large-scale parameters for the entire transfer function. The shadow fading normally follow the normal distribution [12].

The frequency bands ranging from 2.4-2.5 or 5.8-5.9 GHz with 100 MHz bandwidth, which corresponds to the time resolution ($\Delta\tau$) of 10 nsec and frequency step of 0.182 MHz is used for the small-scale parameters. After using the Hanning window function, which is a good compromise between sidelobe suppression and the main peak width during IFFT operation, the time resolution is multiplied by a factor of 2 [74]. The 5.499 μsec temporal range, which is the inverse of frequency step, is quite sufficient when comparing with the maximum excess delay and propagation delays of cables [30]. Hence, the occurrence of aliasing is minimized. The time dispersion and coherent bandwidth are calculated from power delay profile using Equations (K1-5) (see appendix K).

5.4 Conclusion

This chapter describes the WITS mock-mine test environment and research methodology for the statistical radio propagation measurements as a whole and of the two main components, channel sounder and data acquisition. Details on the methodology adopted for each component of the study is also discussed.

The next chapter presents and analyses the effect of antenna placement, polarization, directivity and configuration, and transmission frequency on the performance of TTA communication system in WITS mock-tunnel by dividing into different case studies. Each scenario in a case study followed the procedure mentioned in the methodology section for measuring the radio propagation parameters. This chapter also evaluates the statistical radio propagation of WITS vertical shaft.

6 CASE STUDIES: RESULTS AND ANALYSIS

6.1 General

This work investigates the wideband radio channel characteristics of WITS mock-mine (i.e. an arch-shaped steel supported underground mining tunnel and vertical shaft) in the form of seven case studies for single-input-single-output antenna system. Statistical parameters related to path-loss and delay spread are extracted to study the effect of antenna placement, polarization, directivity and configuration, and transmission frequency on the performance of TTA communication systems in each case study.

The path-loss is estimated by using the measured channel transfer function, as shown in the following Equation [28]:

$$P_L(d) = -10log_{10}\left[\frac{1}{NM}\sum_{i=1}^{N}\sum_{j=1}^{M}\left|H_j(f_i,d)\right|^2\right] \quad (12)$$

where $H_j(f_i, d)$ is the jth measured channel transfer function at frequency f_i and distance d, N is the number of sweep point in every channel transfer function (551 in our measurements) and M is the number of measurements taken at every point (10 in our measurements). Equation (3) (in chapter 2) is used to evaluate the large-scale parameters for the entire transfer function. The small-scale parameters are obtained from the power delay profile, which is a function channel impulse response as shown in Equation (11) (in chapter 5).

This work is organized into seven case studies as 1) effect of antenna placement on the performance of TTA communication system, 2) performance study of circular and linear polarized, 3) effect of antenna directivity on the performance of TTA communication system, 4) performance comparison of different polarized antennas at the receiver and transmitter, 5) performance comparison of omni-directional and directional antennas in line-of-sight (LOS) and non-line-of-sight (NLOS), 6) performance comparison of 2.4 and 5.8 GHz transmission frequency on TTA communication system, and 7) channel characterization of WITS vertical shaft for TTA communication system. First-six case studies investigate the wideband radio channel characteristics in WITS mock-tunnel. The following sub-sections present and analyse radio channel parameters in each case study.

6.2 Case Study 1: Effect of Antenna Placement on the Performance of TTA Communication System

This case study investigates the effect of antenna placement on the line-of-sight performance of TTA communication system in WITS mock-tunnel. The right-hand circularly polarized (RHCP) directional antennas of beamwidth $(60^{\circ}, 60^{\circ})$ were used at the transmitter and receiver. The tripod stands used for the antenna mounting had no significant impact on the reflection coefficient (i.e. $S_{11} < -10$dB) of the antenna. Figure 6.1 shows the wideband measurement setup in WITS mock-tunnel. The vector network analyser and the receiving antenna with other Rx-components were stationed at fixed location for different scenarios[9], as shown in Table 6.1. These scenarios correspond to access point-to-access point communication. The transmitting antenna and the Tx-components were moved to different locations by varying their position 2m lengthwise for 38m. The measurements include the effect of tunnel cross-cut and tunnel face. The following sub-sections show the large-scale and small-scale parameters for investigating the effect of antenna placement on the line-of-sight performance of TTA communication system. These parameters are obtained from the complex channel transfer function of the radio propagation.

[9] The position (y = 1.5m, z = 1.22m) corresponds to center of the tunnel. The positions (y = 1.41m, z = 1.8m) and (y = 1.5m, z = 1.8m) correspond to roof-center antenna placement. The positions (y = 0.5m, z = 1.8m) and (y = 2.5m, z = 1.8m) correspond to close-to-side-wall antenna placement.

Table 6.1 Scenarios for Case Study1: Effect of Antenna Placement

Scenario	Transmitter Position	Receiver Position
Case 1	$y = 1.5\,\text{m}, z = 1.22\,\text{m}$	$x = 18\text{m}, y = 1.5\text{m}, z = 1.22\text{m}$
Case 2	$y = 0.5\,\text{m}, z = 1.8\,\text{m}$	$x = 62.2\text{m}, y = 1.41\text{m}, z = 1.8\text{m}$
Case 3	$y = 1.5\,\text{m}, z = 1.8\,\text{m}$	
Case 4	$y = 2.5\,\text{m}, z = 1.8\text{m}$	
Case 5	$y = 0.5\,\text{m}, z = 1.8\text{m}$	$x = 62.2\text{m}, y = 0.5\text{m}, z = 1.8\text{m}$
Case 6	$y = 1.5\text{m}, z = 1.8\text{m}$	
Case 7	$y = 2.5\text{m}, z = 1.8\text{m}$	

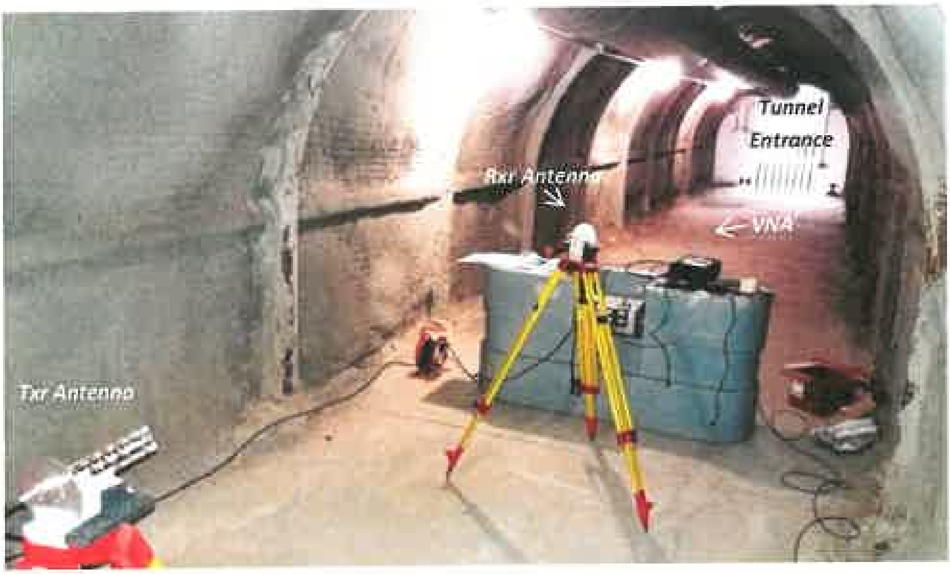

Figure 6.1 Wideband Measurement Test Setup in WITS mock-tunnel

6.2.1 Path Loss Exponent and Shadow Fading

The scattered received power over transmitted power as a function of Tx-Rx distance and the estimated path-loss exponent values are shown in Figure 6.2. It is observed that the path-loss exponent values are less than the free space, i.e. $n < 2$, except in case 5. This can be explained by the waveguide effect [28]. The results show that the antennas placement at the center of tunnel offer the lowest attenuation, i.e. $n = 1.34$. It becomes impractical to place the antennas at the center of the tunnel when the mine is in operation. Therefore, the measurements are performed at different antenna positions to study the effect of antenna placements (i.e. close to the sidewalls and roof) on TTA communication system performance. Table 6.1 shows different antenna positions in the tunnel. The results reveal that antenna placement in diagonal configuration has the lowest attenuation rate (i.e. the lowest value of path-loss exponent), as in case 7.

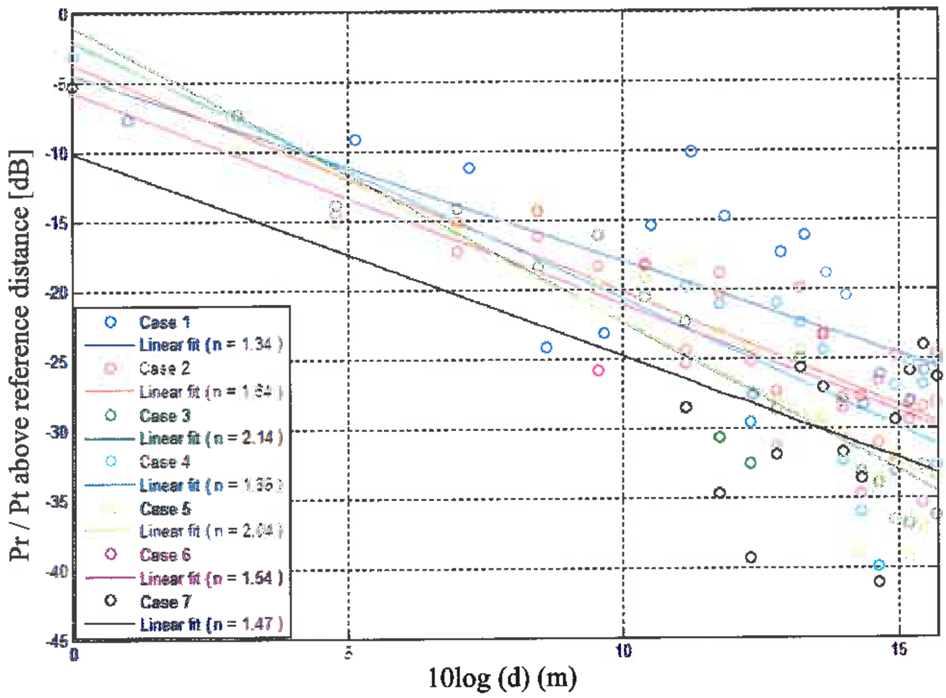

Figure 6.2 Received power over transmitted power at 2.45 GHz; *n* = path-loss exponent

The CDF[10] of shadow fading that fits with normal distribution, KS-test k[11] values and shadow fading statistics are shown in Figure 6.3. The results reveal that a higher value of shadow fading standard deviation means the higher variation of received signal from the estimated value. Therefore, antenna placement with higher standard deviation has lesser coverage reliability. It is observed that lowest path-loss exponent (i.e. attenuation rate) does not correspond to the highest coverage reliability. It is concluded that the antennas placed close to roof-center present the lowest value of shadow fading statistics, i.e. $\sigma = 3.15$ dB. The shadow fading value obtained from other antenna placements are 3.76 dB, i.e. roof-center to side-wall: average (2.91, 3.55, 4.82), and 4.85 dB, i.e. side-wall to side-wall: average (3.67, 6.025).

[10] Cumulative Distribution Function

[11] The KS-test *k* value represents the maximum difference between the data values and the corresponding estimated values.

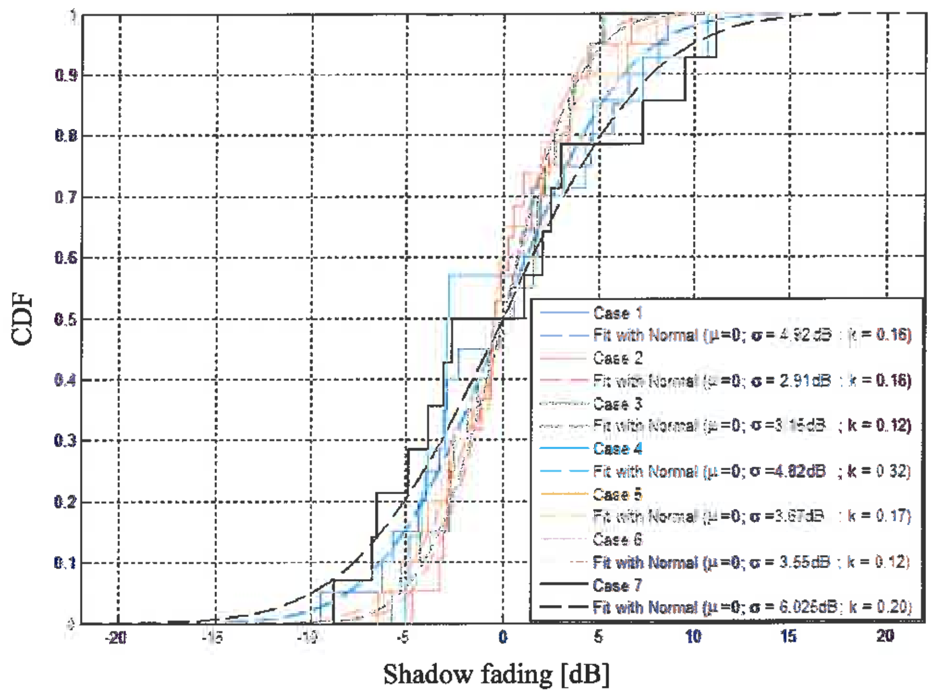

Figure 6.3 Kolmogorov-Smirnov test for the shadow fading at 2.45 GHz; μ = mean, σ = standard deviation of shadow fading, k = KS-test value

6.2.2 Time Dispersion Parameters

The magnitude and phase of channel frequency response, magnitude of channel impulse response and normalized power delay profile of RHCP directional antenna are shown in Figure 6.4. The notches in the magnitude of complex channel transfer function illustrate the frequency-selective nature of the propagation channel. The channel impulse response shows the first arriving component along with other multipath components. The mean excess delay, the RMS excess delay and maximum delay spread are computed at all the measurement location at predefined threshold. Table 6.2 summarizes the mean, standard deviation, and maximum value of time dispersion parameters and coherent bandwidth for 20 dB and 40 dB thresholds. The transmitted signal experienced frequency-selective fading when the transmission signal has higher bandwidth than the coherent bandwidth. The results also illustrate that the antennas placed at the center of the tunnel perform better in terms of time dispersion parameters and have the highest coherent bandwidth. It becomes impractical to place the antennas at the center of the tunnel when the mine is in operation. Therefore, the measurements are performed at different antenna positions to study the effect of antenna placements. The results also shows that the antennas placed close-to-side-wall perform worse in terms of time dispersion parameters and have the lowest coherent bandwidth. The other antennas placements have no significant on the time dispersion parameters and coherent bandwidth.

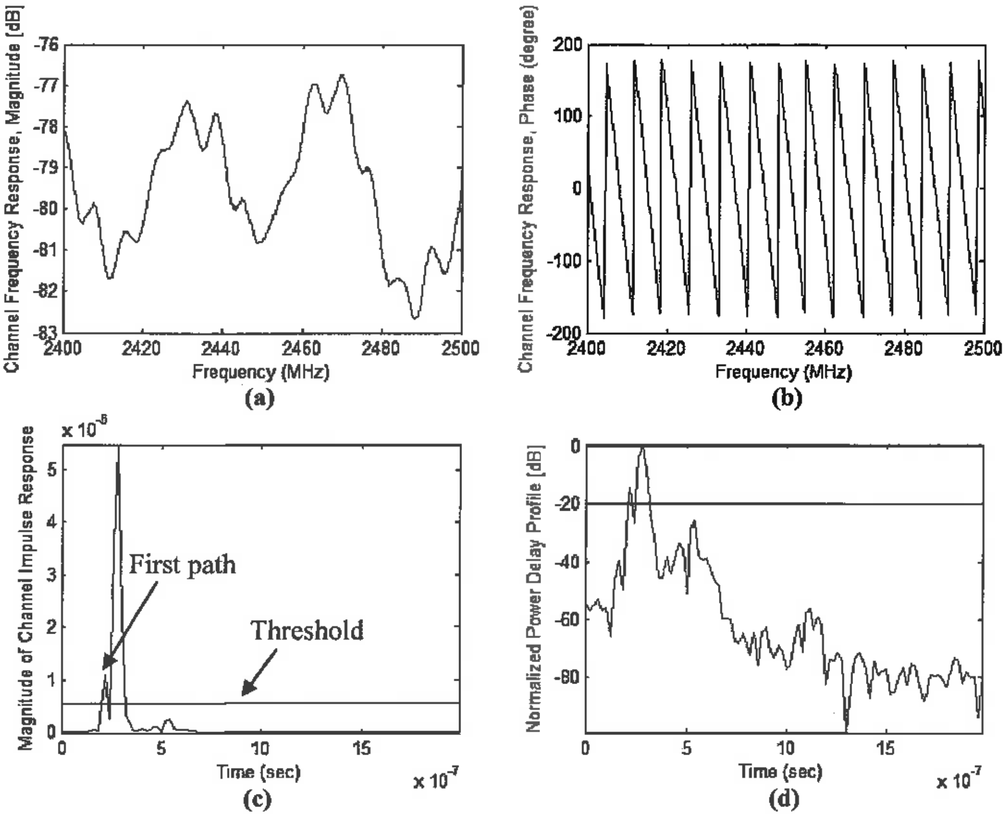

Figure 6.4 (a) Channel Frequency Response, Magnitude [dB] (b) Channel Frequency Response, Phase (degree) (c) Magnitude of Impulse Response (d) Normalized Power Delay Profile [dB] of RHCP Directional Antenna at a Tx-Rx distance of 38 meter; Case 1

6.2.3 Conclusion

In this case study, the RHCP directional antenna is tested for the radio propagation characterization of WITS mock-tunnel in 2.4 - 2.5 GHz frequency band. The results reveal that RHCP directional antenna performs better in terms of path-loss exponent as compared to omni-directional linearly polarized antenna (see appendix A). In a wide tunnel, RHCP directional antenna performs better in terms of RMS-delay spread as compared to omni-directional linearly polarized antenna (see appendix A).

This case study also reveals that antenna placement has significant effect on performance of TTA communication system. The antennas placed at the center of the tunnel have the best performance in terms of path-loss exponent and time dispersion parameters. However, it becomes impractical to place the antennas at the center of the tunnel when the mine is in operation. Therefore, the wideband measurements are performed for different antenna placements. It is observed that antenna placement in diagonal configuration offers the lowest attenuation rate. However, the antennas placed close to the roof-center perform better in terms of shadow fading statistics and time dispersion parameters. This case study concludes that there is no single antenna placement for the best performance in terms of attenuation rate, coverage reliability and time dispersion parameters.

Table 6.2 Mean, Standard Deviation, and Maximum of Mean Excess Delay ($\bar{\tau}$), RMS Delay Spread (σ_t), Maximum Delay Spread (τ_{max}) and Coherent Bandwidth (B_c)

		$\bar{\tau}$ (nanosecond)			σ_t (nanosecond)			τ_{max} (nanosecond)			Coherent Bandwidth (MHz)
	Threshold (decibel)	Mean	Standard Deviation	Maximum	Mean	Standard Deviation	Maximum	Mean	Standard Deviation	Maximum	$B_C \approx \frac{1}{5 \cdot \sigma_t}$
Case 1	- 20	157.84	76.37	280.0	11.94	1.50	16.8	55.0	21.40	120.0	16.75
	- 40	158.48	76.75	280.9	15.42	4.76	27.3	281.0	134.94	440.0	12.97
Case 2	- 20	157.64	73.67	275.4	14.88	0.99	15.7	89.47	16.82	120.0	13.44
	- 40	157.79	73.67	275.1	16.01	1.23	17.4	254.74	72.68	500.0	12.49
Case 3	- 20	152.19	76.78	273.8	15.30	1.57	18.4	95.0	25.03	140.0	13.07
	- 40	152.90	77.42	276.6	19.99	7.06	33.8	383.0	214.55	700.0	10.01
Case 4	- 20	186.04	65.32	274.1	15.47	1.95	20.6	95.71	27.38	160.0	12.93
	- 40	186.30	65.41	273.8	17.18	3.85	27.6	294.29	166.49	660.0	11.64
Case 5	- 20	152.55	76.83	275.9	18.43	11.98	66.5	122.0	125.81	640.0	10.85
	- 40	153.27	77.53	275.9	22.62	16.32	80.5	388.0	226.68	840.0	8.84
Case 6	- 20	157.950	73.84	275.6	14.887	70.93	15.7	86.32	16.40	120.0	13.43
	- 40	158.36	74.17	275.8	18.232	25.44	35.6	345.26	187.48	720.0	10.97
Case 7	- 20	187.61	64.07	275.4	19.557	712.83	62.2	117.14	70.10	320.0	10.23
	- 40	188.24	63.89	275.0	22.41	14.96	71.6	405.71	189.81	680.0	8.92

6.3 Case Study 2: Performance Study of Circularly and Linearly Polarized Antennas

This case study investigates the line-of-sight performance of circularly, vertically and horizontally polarized antennas at RF front-end of TTA communication system. It is organized into three scenarios, each representing the wideband measurements with different antennas. These scenarios correspond to the access point-to-access point TTA communication. Table 6.3 summarizes the antenna's specifications used for wideband measurement campaign in 2.4 - 2.5 GHz frequency band. The tripod stands used for the antenna mounting had no significant impact on the reflection coefficient (i.e. S_{11} < -10dB) of the antenna. The measurements were taken in WITS mock-tunnel.

Table 6.3 Antennas used for Polarization Comparison Antennas for TTA Communication System

Scenario	Transmitter and Receiver Antennas
Case 1	(60°, 60°), Right-hand circularly polarized, 2.37-2.51 GHz
Case 2	(64°, 72°), Vertically polarized, 0.68-2.90 GHz
Case 3	(64°, 72°), Horizontally polarized, 0.68-2.90 GHz

During the measurement campaign, the vector network analyser and the receiving antenna with other Rx-components were stationed at (x = 56.2m, y = 1.5m, z = 1.22m). The transmitting antenna with the Tx-components was moved to different locations by varying their position 1m lengthwise for 40m. The transmitter antenna was placed at the center of the tunnel with a fixed antenna height, i.e. (y = 1.5m, z = 1.22m). The measurements include the effect of tunnel cross-cut and tunnel face. The following sub-sections show the large-scale and small-scale parameters for investigating the effect of circular and linear polarized antennas on the line-of-sight performance of TTA communication system. These parameters are obtained from the complex channel transfer function of the radio propagation.

6.3.1 Path Loss Exponent and Shadow Fading

The scattered received power over transmitted power as a function of Tx-Rx distance and the estimated path-loss exponent values are shown in Figure 6.5. It is observed that the path-loss exponent values are less than the free space, i.e. $n < 2$, except in case 3. This can be explained by the waveguide effect [28]. The smallest value of path-loss exponent reveals that the circularly polarized directional antenna has the highest coverage area. This study demonstrates that the horizontally polarized antennas perform better in terms of path-loss exponent and time dispersion parameters in horizontal aspect-ratio tunnel as compared to vertically polarized antenna.

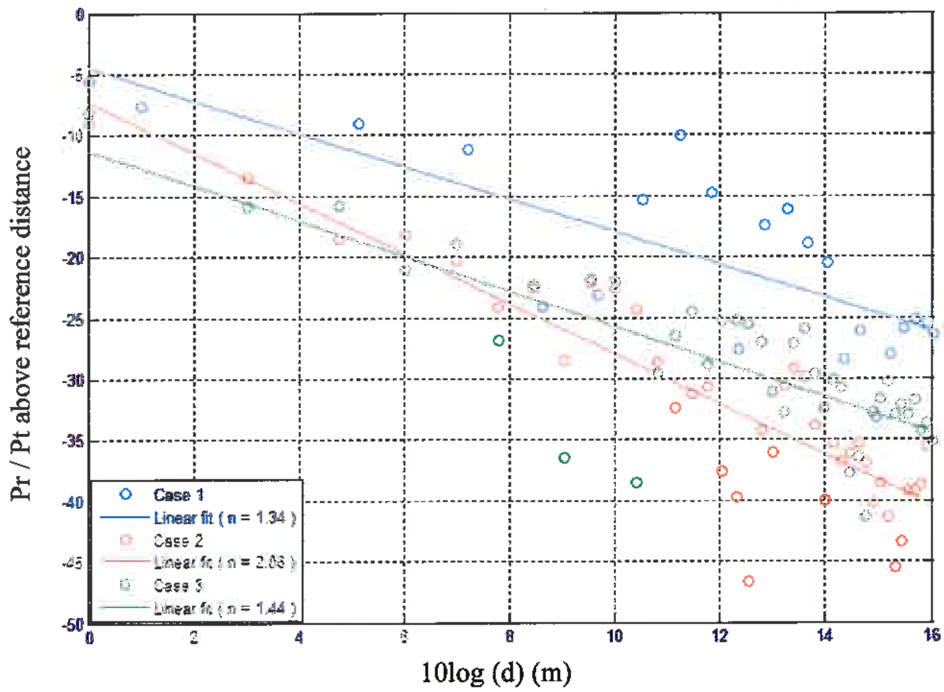

Figure 6.5 Received power over transmitted power at 2.45 GHz; *n* = path-loss exponent

The CDF of shadow fading that fits with normal distribution, KS-test k-values and shadow fading statistics are shown in Figure 6.6. The results reveal that a higher value of shadow fading standard deviation means the higher variation of received signal from the estimated value, i.e. lesser coverage reliability. It is observed that lowest path-loss exponent (i.e. attenuation rate) does not correspond to the highest coverage reliability. It is concluded that the horizontally polarized antenna performs better in terms of shadow fading in horizontal aspect-ratio tunnel as compared to the vertical and circularly polarized antenna.

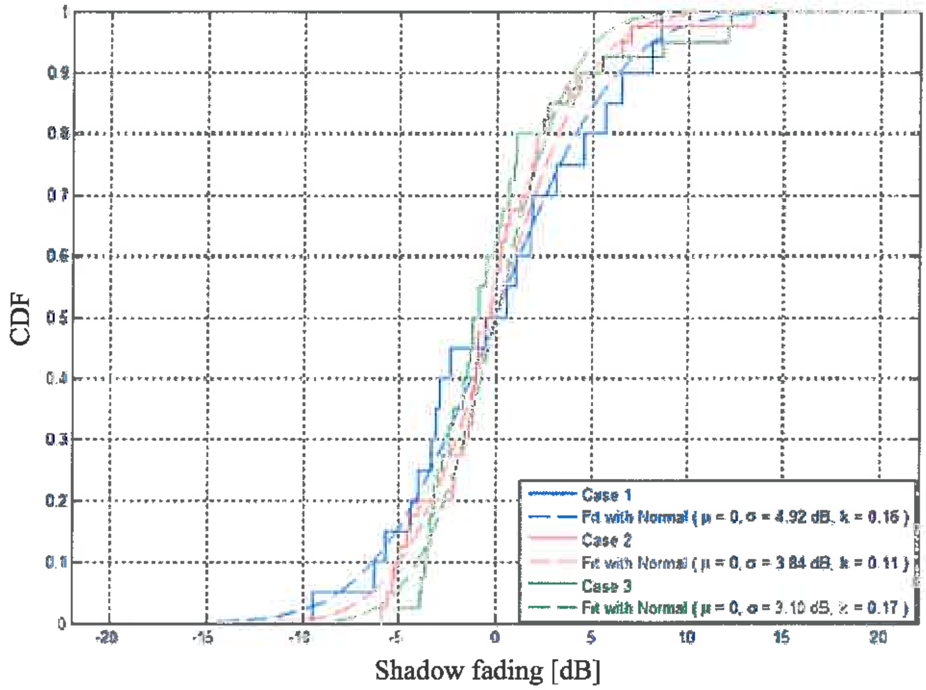

Figure 6.6 Kolmogorov-Smirnov test for the shadow fading at 2.45 GHz; μ = mean, σ = standard deviation, k = KS-test value

6.3.2 Time Dispersion Parameters

The magnitude and phase of channel frequency response, magnitude of channel impulse response and normalized power delay profile of vertical polarized directional antenna are shown in Figure 6.7. The notches in the magnitude of complex channel transfer function illustrate the frequency-selective nature of the propagation channel. The channel impulse response shows the first arriving component along with other multipath components. The mean excess delay, the RMS excess delay and maximum delay spread are computed at all the measurement location at predefined threshold. Table 6.4 summarizes the mean, standard deviation, and maximum value of time dispersion parameters and coherent bandwidth for 20 dB and 40 dB thresholds. The transmitted signal experienced frequency-selective fading when the transmission signal has higher bandwidth than the coherent bandwidth. It is also observed that the circularly polarized antenna offers the highest coherent bandwidth. Moreover, the horizontally polarized antenna performs better in terms of time dispersion parameters in horizontal aspect-ratio tunnel than the vertically polarized antenna.

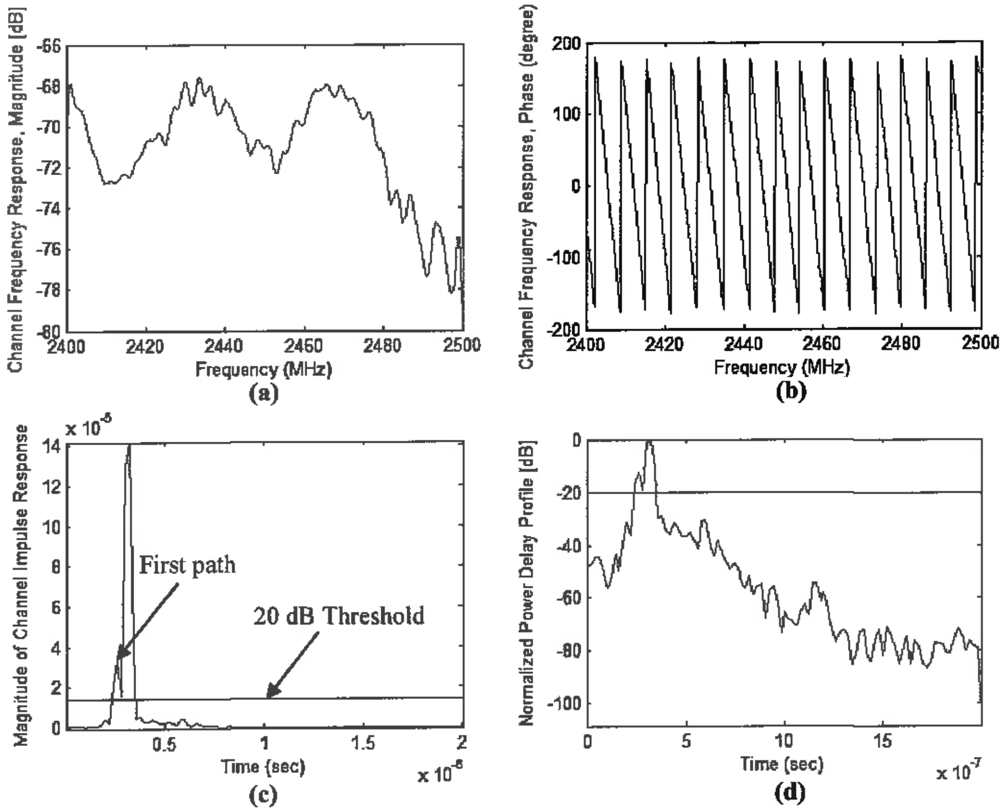

Figure 6.7 (a) Channel Frequency Response, Magnitude [dB] (b) Channel Frequency Response, Phase (degree) (c) Magnitude of Impulse Response (d) Normalized Power Delay Profile [dB] of Vertically Polarizes Directional Antenna at a distance of 40 meter; Case 2

Table 6.4 Mean, Standard Deviation (STDEV), and Maximum (MAX) of Mean Excess Delay ($\bar{\tau}$), RMS Delay Spread (σ_t), Maximum Delay Spread (τ_{max}) and Coherent Bandwidth (B_c)

		$\bar{\tau}$ (nanosecond)			σ_t (nanosecond)			τ_{max} (nanosecond)			Coherent Bandwidth (MHz)
	Threshold (decibel)	Mean	STDEV	MAX	Mean	STDEV	MAX	Mean	STDEV	MAX	$B_C \approx \frac{1}{5 \cdot \sigma_t}$
Case 1	- 20	157.8	76.37	280.0	11.94	1.50	16.8	55.0	21.40	120.0	16.75
	- 40	158.5	76.75	280.9	15.42	4.76	27.3	281.0	134.94	440.0	12.97
Case 2	- 20	175.9	79.64	309.7	17.54	6.62	53.7	119.0	57.99	400.0	11.40
	- 40	176.5	79.94	310.2	21.77	9.71	64.0	413.0	181.76	900.0	9.19
Case 3	- 20	177.4	78.53	307.8	16.17	4.03	38.7	101.5	35.77	240.0	12.37
	- 40	177.2	78.72	309.0	19.01	5.20	42.5	373.0	113.46	700.0	10.52

6.3.3 Conclusion

In this case study, the circularly and linearly polarized antennas are tested for the line-of-sight performance study of TTA communication system in WITS mock-tunnel. The experimental results show that antenna polarization has significant effect on path-loss exponent, shadow fading and time dispersion parameters. This study concludes the following in horizontal aspect-ratio (i.e. width is greater than height) tunnel:

- The RHCP directional antennas offer the highest coverage area and coherent bandwidth.
- The horizontally polarized directional antenna presents the highest coverage reliability.
- The horizontally polarized antennas perform better in terms of path-loss, shadow fading and coherent bandwidth than the vertically polarized antenna.

6.4 Case Study 3: Effect of Antenna Directivity on the Performance of TTA Communication System

This case study investigates the line-of-sight performance of antenna directivity at TTA communication system RF front-end in WITS mock-tunnel. It is organized into two scenarios, each representing the wideband measurements with antennas of different directivity. These scenarios correspond to the access point-to-access point wireless communication. Table 6.5 summarizes the antenna's specifications used for wideband measurements in the 2.4 - 2.5 GHz frequency band. The tripod stands used for the antenna mounting had no significant impact on the reflection coefficient (i.e. $S_{11} < -10$dB) of the antenna.

Table 6.5 Antennas used for Case Study 3

Scenario	Transmitter and Receiver Antennas
Case 1	(64°, 72°), Horizontally polarized, 0.68-2.90 GHz
Case 2	(13°, 17.5°), Horizontally polarized, 2.4-2.5 GHz

During the measurement campaign, the vector network analyser and the receiving antenna with other Rx-components were stationed at (x = 56.2m, y = 1.5m, z =

1.22m). The transmitting antenna with the Tx-components was moved to different locations by varying their position 1m lengthwise for 40m. The transmitter antenna was placed at the center of the tunnel with a fixed antenna height, i.e. (y = 1.5m, z = 1.22m). The measurements also include the effect of tunnel cross-cut and tunnel face. The following sub-sections show the large-scale and small-scale parameters for investigating the effect of antenna directivity on the line-of-sight performance of TTA communication system. These parameters are obtained from the complex channel transfer function of the radio propagation.

6.4.1 Path Loss Exponent and Shadow Fading

The scattered received power over transmitted power as a function of Tx-Rx distance and the estimated path-loss exponent values are shown in Figure 6.8. It is observed that the path-loss exponent values are less than the free space, i.e. $n < 2$. This can be explained by the waveguide effect [28]. The path-loss exponent values reveal that the antenna directivity has no significant effect on the coverage area.

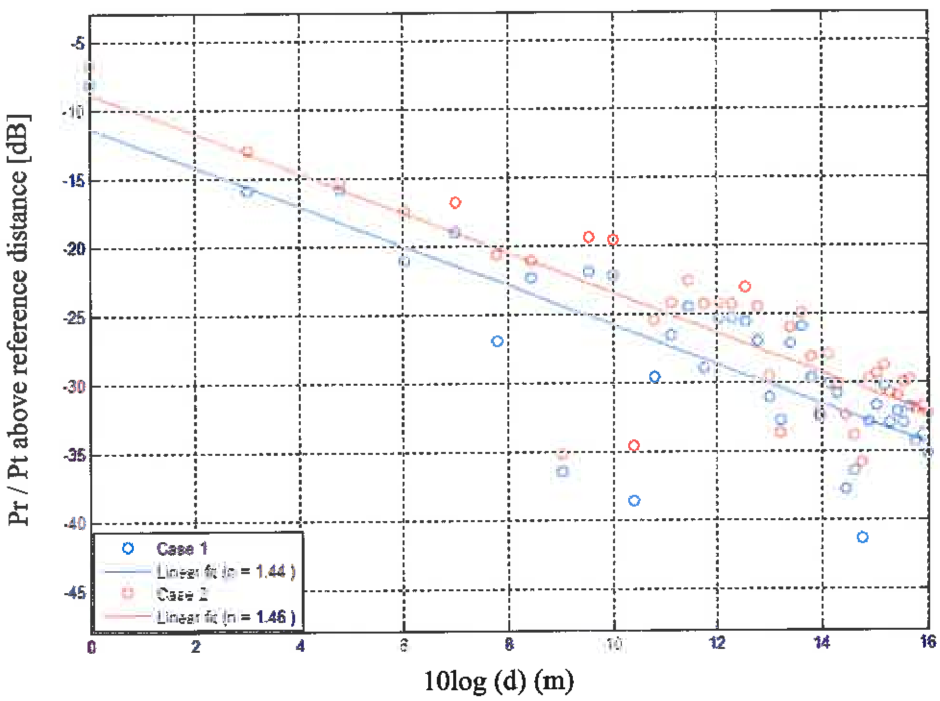

Figure 6.8 Received power over power transmitted at 2.45 GHz; n = path-loss exponent

The CDF of shadow fading that fits with normal distribution, KS-test k values and shadow fading statistics are shown in Figure 6.9. The results reveal that a higher value of shadow fading standard deviation means the higher variation of received signal from the estimated value, i.e. lesser coverage reliability. It is observed that lowest path-loss exponent (i.e. attenuation rate) does not correspond to the highest coverage reliability. The shadow fading standard deviation values show the antenna directivity improves coverage reliability of TTA communication system.

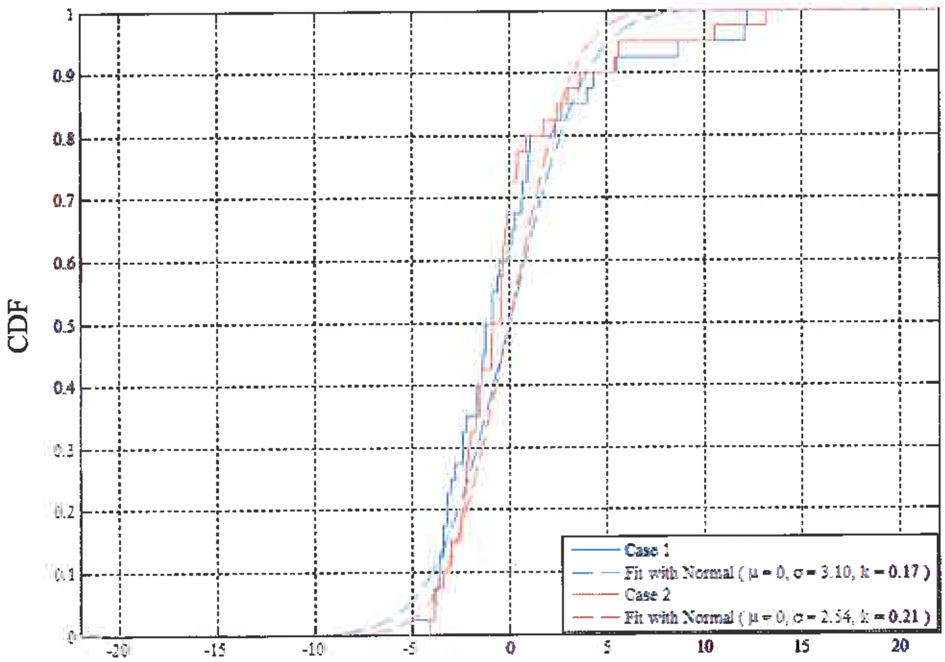

Figure 6.9 Kolmogorov-Smirnov test for the shadow fading at 2.45 GHz; μ = mean, σ = standard deviation, k = KS-test value

6.4.2 Time Dispersion Parameters

The magnitude and phase of channel frequency response, magnitude of channel impulse response and normalized power delay profile of (13°, 17.5°) horizontally polarized antenna are shown in Figure 6.10. The notches in the magnitude of complex channel transfer function illustrate the frequency-selective nature of the propagation channel. The channel impulse response shows the first arriving component along with other multipath components. The mean excess delay, the RMS excess delay and maximum delay spread are computed at all the measurement location at predefined threshold. Table 6.6 summarizes the mean, standard deviation, and maximum value of time dispersion parameters and coherent bandwidth for 20 dB and 40 dB thresholds (most commonly used for radio propagation characterisation). The transmitted signal experienced frequency-selective fading when the transmission signal has higher bandwidth than the coherent bandwidth. It concludes that there is no significant effect of antenna directivity on the time dispersion parameters and coherent bandwidth.

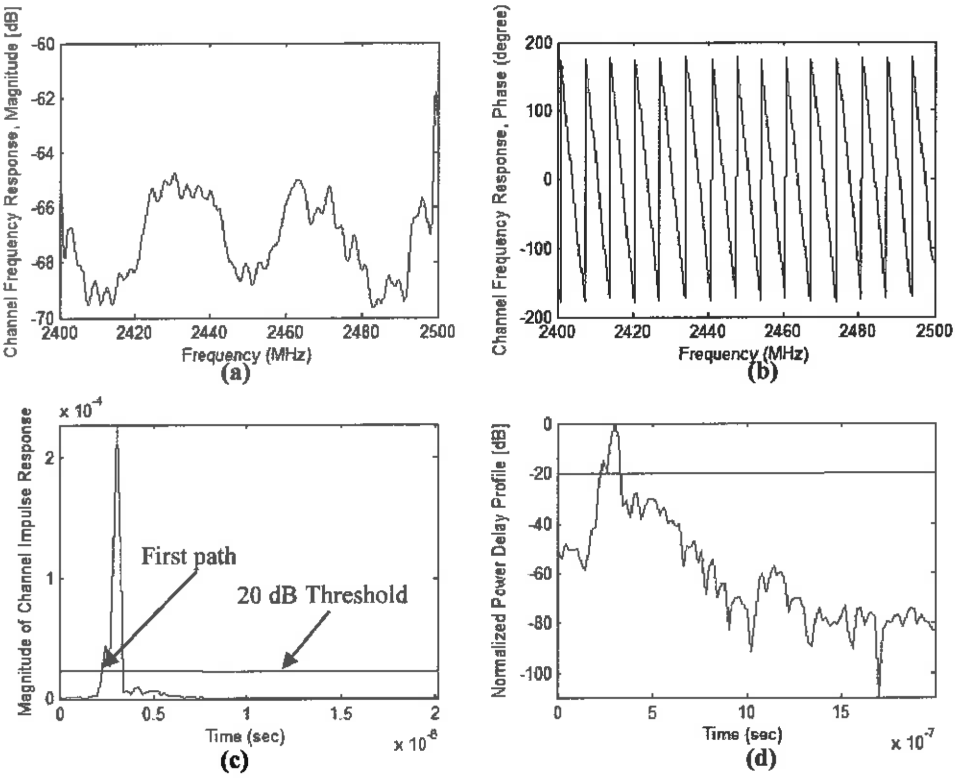

Figure 6.10 (a) Channel Frequency Response, Magnitude [dB] (b) Channel Frequency Response, Phase (degree) (c) Magnitude of Impulse Response (d) Normalized Power Delay Profile [dB] of Horizontally Polarized Directional Antenna at a distance of 40 meter; Case 2

6.4.3 Conclusion

In this study, the effect of antenna directivity on the line-of-sight performance of TTA communication is studied in WITS mock-tunnel. The horizontally polarized antennas of (64°, 72°) and (13°, 17.5°) beam-widths are used for wideband measurements. The experimental results show that antenna directivity has no significant effect on the path-loss exponent and time dispersion parameters. This study concludes that a high directive antenna improves the coverage/link reliability.

Table 6.6 Mean, Standard Deviation (STDEV), and Maximum Value of Mean Excess Delay ($\bar{\tau}$), RMS Delay Spread (σ_t), Maximum Delay Spread (τ_{max}) and Coherent Bandwidth (B_c)

		$\bar{\tau}$ (nanosecond)			σ_t (nanosecond)			τ_{max} (nanosecond)			Coherent Bandwidth (MHz)
	Threshold (decibel)	Mean	STDEV	MAX	Mean	STDEV	MAX	Mean	STDEV	MAX	$B_C \approx \frac{1}{5 \cdot \sigma_t}$
Case 1	- 20	177.4	78.53	307.8	16.17	4.03	38.7	101.5	35.77	240.0	12.37
	- 40	177.2	78.72	309.0	19.01	5.20	42.5	373.0	113.46	700.0	10.52
Case 2	- 20	166.1	78.56	298.3	15.68	2.92	31.7	94.0	22.74	180.0	12.76
	- 40	166.6	78.65	298.9	18.29	4.27	37.2	369.5	117.49	620.0	10.93

6.5 Case Study 4: Performance Study of Different Antennas in RF front-end of TTA Communication System

This case study investigates the effect of different antennas on the line-of-sight performance of TTA communication system. It is organized into four scenarios, each representing the wideband measurements with different antennas. These scenarios correspond to the access point-to-mobile wireless communication. Table 6.7 summarizes the antennas used for the wideband measurement campaign in 2.4 - 2.5 GHz frequency band. The tripod stands used for the antenna mounting had no significant impact on the reflection coefficient (i.e. S_{11} < -10dB) of the antenna. The measurements were taken in WITS mock-tunnel.

Table 6.7 Antennas used for Case Study 4

Scenario	Receiver Antenna	Transmitter Antenna
Case 1	(60°, 60°), Right-hand circularly polarized, 2.37-2.51 GHz	Omni-Directional, Right-hand circularly polarized, 2.4-2.5 GHz
Case 2		Omni-Directional, Horizontal polarized, 2.4-2.5 GHz
Case 3		Omni-Directional, Vertical polarized, 2.4-2.5 GHz
Case 4	(64°, 72°), Horizontal polarized, 0.68-2.90 GHz	Omni-Directional, Horizontal polarized, 2.4-2.5 GHz

During the measurement campaign, the vector network analyser and the receiving antenna with other Rx-components were stationed at (x = 56.2m, y = 1.5m, z = 1m). The transmitting antenna with the Tx-components was moved to different locations by varying their position 1m lengthwise for 40m. The transmitter antenna was placed at the center of the tunnel with a fixed antenna height, i.e. (y = 1.5m, z = 1m). The measurements also include the effect of tunnel cross-cut and tunnel face. The following sub-sections show the large-scale and small-scale parameters for investigating the effect of different antennas on the line-of-sight performance of TTA communication system. These parameters are obtained from the complex channel transfer function of the radio propagation.

6.5.1 Path Loss Exponent and Shadow Fading

The scattered received power over transmitted power as a function of Tx-Rx distance and the estimated path-loss exponent values are shown in Figure 6.11. It is observed that the path-loss exponent values are less than the free space, i.e. $n < 2$. This can be explained by the waveguide effect [28]. The path-loss exponent values reveal that the combination of RHCP directional antenna and horizontally polarized omni-directional antenna in RF front-end of TTA communication system has the lowest attenuation rate, i.e. $n = 1.07$. It is also observed that the combination of horizontally polarized antennas present the highest attenuation rate.

The CDF of shadow fading that fits with normal distribution, the KS-test k values and the shadow fading statistics are shown in Figure 6.12. The results reveal that a higher value of shadow fading standard deviation means the higher variation of received signal from the estimated value, i.e. lesser coverage reliability. It is observed that lowest path-loss exponent (i.e. attenuation rate) does not correspond to the highest coverage reliability. The shadow fading standard deviation values reveal that circularly polarized antennas performs better in terms of coverage reliability, i.e. $\sigma = 2.96$ dB. It is also observed that horizontally polarized antennas offer the lowest coverage/link reliability.

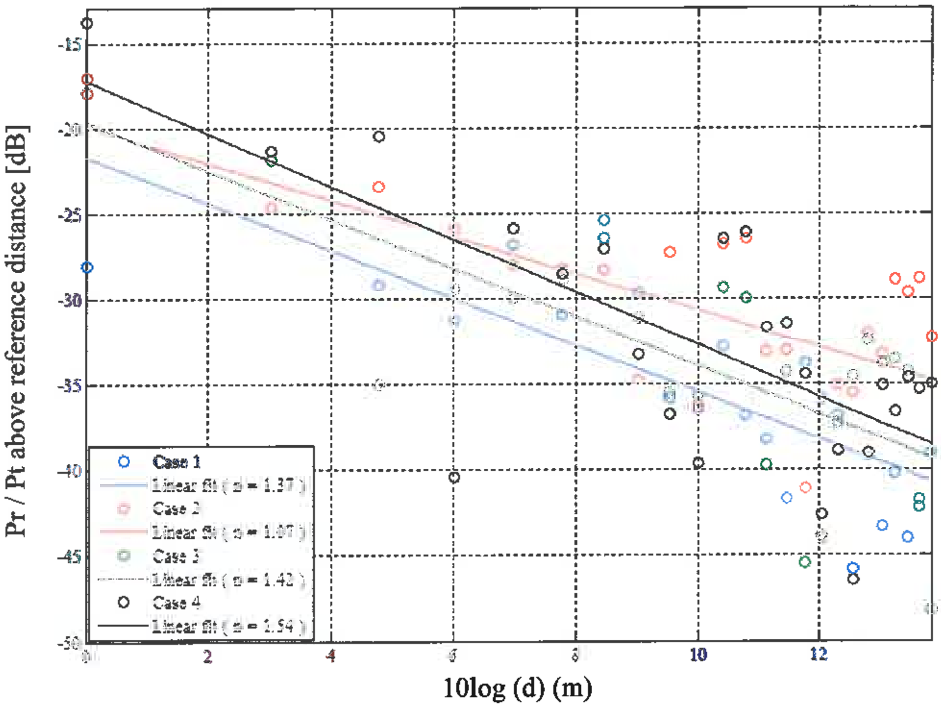

Figure 6.11 Received Power as a function of Tx-Rx distance at 2.45 GHz; n = path-loss exponent

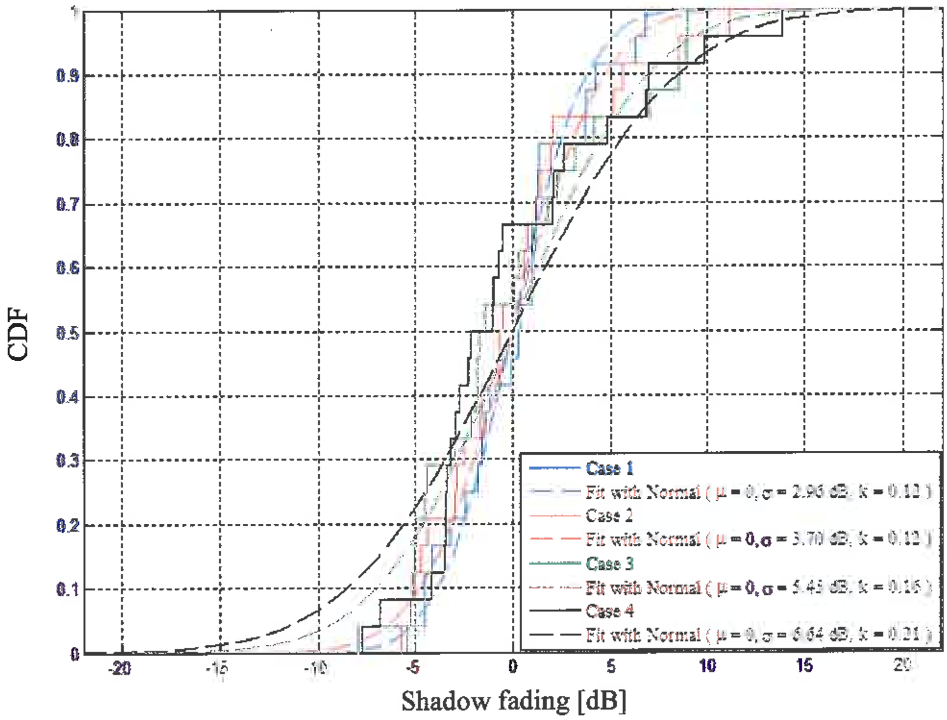

Figure 6.12 Kolmogorov-Smirnov test for the shadow fading at 2.45 GHz; μ = mean, σ = standard deviation, k = KS-test value

6.5.2 Time Dispersion Parameters

The magnitude and phase of channel frequency response, magnitude of channel impulse response and normalized power delay profile of horizontally polarized antennas at 20 meter Tx-Rx distance are shown in Figure 6.13. The notches in the magnitude of complex channel transfer function illustrate the frequency-selective nature of the propagation channel. The channel impulse response shows the first arriving component along with other multipath components. The mean excess delay, the RMS excess delay and maximum delay spread are computed at all the measurement location at predefined threshold. Table 6.8 summarizes the mean, standard deviation, and maximum value of time dispersion parameters and coherent bandwidth for 20 dB and 40 dB thresholds. The transmitted signal experienced frequency-selective fading when the transmission signal has higher bandwidth than the coherent bandwidth. The time dispersion parameters reveal that the combination of RHCP directional antenna and horizontally polarized omni-directional antenna offers the highest coherent bandwidth. It is also observed that the combination of circularly polarized antennas offer worse coherent bandwidth.

Table 6.8 Mean, Standard Deviation (STDEV), and Maximum (MAX) of Mean Excess Delay ($\bar{\tau}$), RMS Delay Spread (σ_t), Maximum Delay Spread (τ_{max}) and Coherent Bandwidth (B_c)

		$\bar{\tau}$ (nanosecond)			σ_t (nanosecond)			τ_{max} (nanosecond)			Coherent Bandwidth (MHz)
	Threshold (decibel)	Mean	STDEV	MAX	Mean	STDEV	MAX	Mean	STDEV	MAX	$B_C \approx \frac{1}{5 \cdot \sigma_t}$
Case 1	- 20	122.8	49.24	202.2	34.5	23.26	114.0	272.5	201.89	660.0	5.80
Case 1	- 40	125.5	50.48	206.9	47.3	24.52	122.9	655.0	220.45	1080.0	4.23
Case 2	- 20	118.1	50.92	195.9	18.9	11.88	71.0	138.3	126.68	660.0	10.58
Case 2	- 40	119.5	51.55	198.3	26.9	14.56	81.1	577.3	219.80	940.0	7.43
Case 3	- 20	117.3	50.93	223.0	25.5	20.37	103.0	175.2	152.01	640.0	7.84
Case 3	- 40	119.4	52.36	228.3	35.3	24.53	112.9	604.8	230.21	1020.0	5.67
Case 4	- 20	122.0	49.48	201.0	29.2	20.34	94.1	245.8	195.18	700.0	6.85
Case 4	- 40	124.0	50.16	201.6	37.8	24.71	104.2	596.3	226.48	980.0	5.29

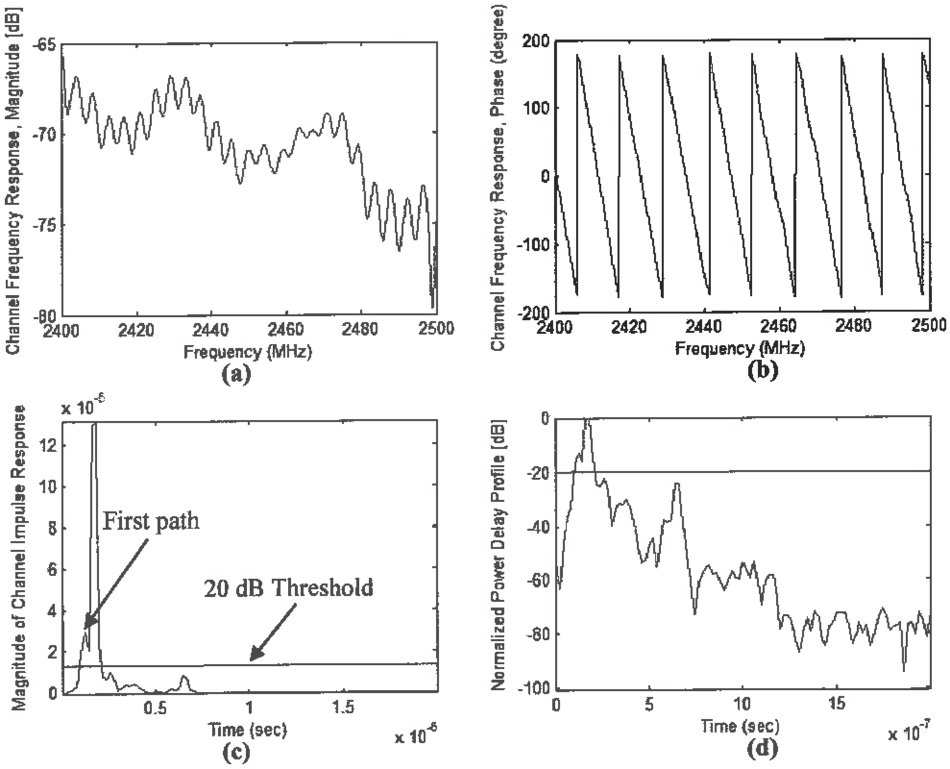

Figure 6.13 (a) Channel Frequency Response, Magnitude [dB] (b) Channel Frequency Response, Phase (degree) (c) Magnitude of Impulse Response (d) Normalized Power Delay Profile [dB]; Case 4

6.5.3 Conclusion

In this case study, the effect of different antennas on the line-of-sight performance of through-the-air (TTA) communication is analysed in the WITS mock-tunnel. The experimental results reveal that Tx- Rx antennas combination in the RF front-end has significant effect on path-loss exponent, shadow fading and time dispersion parameters. This study concludes the following:

- The combination of RHCP directional antenna and horizontally polarized omni-directional antenna offers the lowest attenuation rate and the highest coherent bandwidth. However, the circularly polarized antennas combination presents the highest coverage/link reliability.

6.6 Case Study 5: Performance Study of Omni-Directional and Directional Antennas in LOS and NLOS

This case study compares the performance of omni-directional and directional antennas in line-of-sight (LOS) and non-line-of-sight (NLOS) situations. It is organized into four scenarios, each representing the wideband measurements with antennas in different situations. Table 6.9 summarizes the antennas used for the wideband measurement campaign in 2.4 - 2.5 GHz frequency band. These scenarios correspond to the access point-to-access point, access point-to-mobile and mobile-to-mobile wireless communication. The tripod stands used for the antenna mounting had no significant impact on the reflection coefficient (i.e. $S_{11} <$ -10dB) of the antenna. The measurements are taken in WITS mock-tunnel.

Table 6.9 Antennas used for Case Study 5

Scenario	Receiver and Transmitter Antennas
Case 1 **(LOS)**	(13°, 17.5°), Horizontally polarized, 2.4-2.5 GHz
Case 2 **(NLOS)**	
Case 3 **(LOS)**	Omni-Directional, Horizontally polarized, 2.4-2.5 GHz
Case 4 **(NLOS)**	

During the measurement campaign, the vector network analyser and the receiving antenna with other Rx-components were stationed at (x = 48.6m, y = 1.5m, z = 1.22m). The transmitting antenna with the Tx-components was moved to different locations by varying their position 1m lengthwise for 40m. The transmitter antenna was placed at the center of the tunnel with a fixed antenna height, i.e. (y = 1.5m, z = 1.22m). The measurements also include the effect of tunnel cross-cut and tunnel face. The following sub-sections show the large-scale and small-scale parameters for investigating the effect of circular and linear polarized antennas on the line-of-sight performance of TTA communication system. These parameters are obtained from the complex channel transfer function of the radio propagation.

6.6.1 Path Loss Exponent and Shadow Fading

The scattered received power over transmitted power as a function of Tx-Rx distance and the estimated path-loss exponent values are shown in Figure 6.14. It is observed that the path-loss exponent values are less than the free space, i.e. $n < 2$. This can be explained by the waveguide effect [28]. The CDF of shadow fading that fits with normal distribution, the KS-test k values and the shadow fading statistics are shown in Figure 6.15. The results reveal that a higher value of shadow fading standard deviation means the higher variation of received signal from the estimated value, i.e. lesser coverage reliability. The path-loss exponent and shadow fading standard deviation values reveal that the omni-directional antenna has lower attenuation rate and higher coverage reliability in line-of-sight situation. However, the directional antenna has lower attenuation rate and higher coverage reliability in the non-line-of-sight situation. It is also observed that there is no significant difference in the attenuation rate of omni-directional antenna in all the situations.

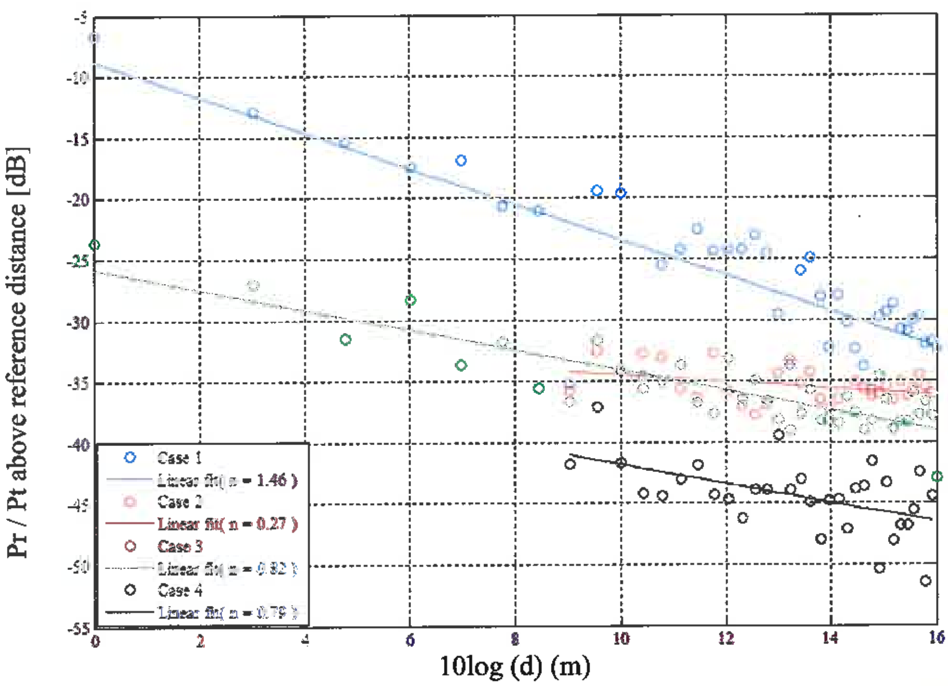

Figure 6.14 Received Power as a function of Tx-Rx distance at 2.45 GHz; n = path-loss exponent

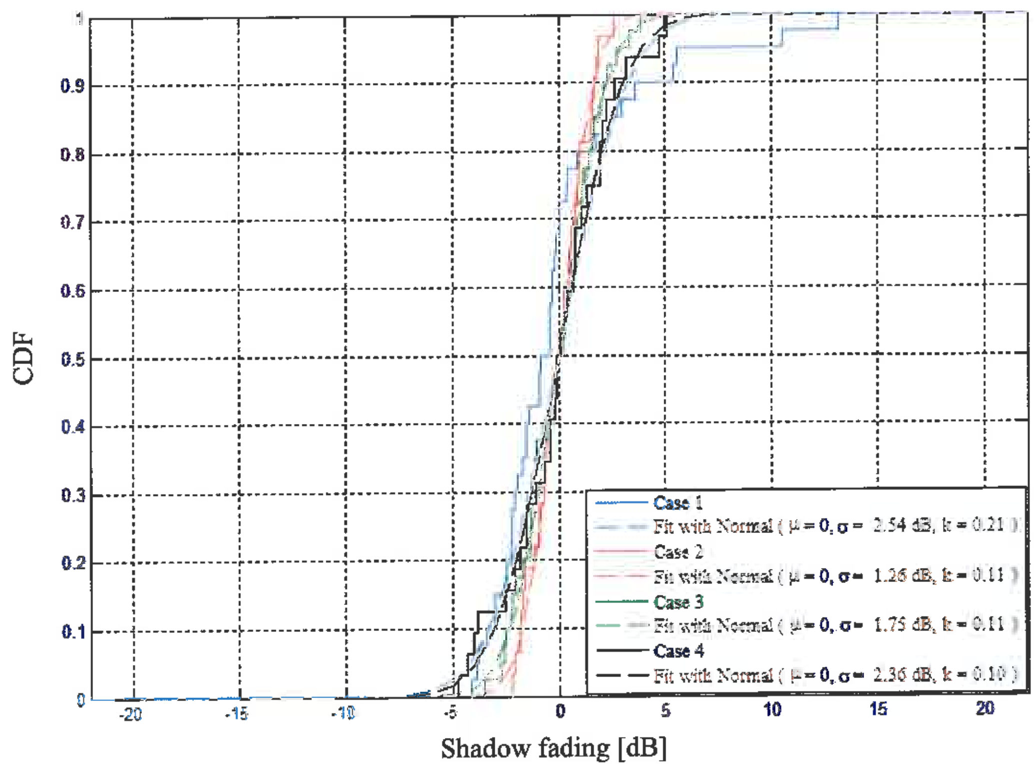

Figure 6.15 Kolmogorov-Smirnov test for the shadow fading at 2.45 GHz; μ = mean, σ = standard deviation, k = KS-test value

Table 6.10 summarises the path-loss at reference distance, path-loss exponent and shadow fading statistics. The experimental results reveal that the omni-directional antenna has higher path-loss at reference distance, the smaller attenuation rate and higher coverage reliability in line-of-sight situation. This indicates the presence of high relative power of low-order electromagnetics modes. It is also evident that the omni-directional antenna presents higher path-loss, i.e. $P_L(d_o)$, compared to directional antenna.

Table 6.10 Summary of Path-loss at Reference Distance, Path-loss Exponent and Shadow Fading at 2.45 GHz

Scenarios	$P_L(d_o)$ [dB]	n	σ [dB]
Case 1 ($d_o = 1m$)	-39.56	1.46	2.54
Case 2 ($d_o = 8m$)	-70.14	0.27	1.26
Case 3 ($d_o = 1m$)	-56.5	0.82	1.75
Case 4 ($d_o = 8m$)	-75.25	0.79	2.36

6.6.2 Time Dispersion Parameters

The magnitude and phase of channel frequency response, magnitude of channel impulse response and normalized power delay profile of omni-directional antenna in non-line-of-sight are shown in Figure 6.16. The notches in the magnitude of complex channel transfer function illustrate the frequency-selective nature of the propagation channel. The channel impulse response shows the first arriving component along with other multipath components. The mean excess delay, the RMS excess delay and maximum delay spread are computed at all the measurement location at predefined threshold. Table 6.11 summarizes the mean, standard deviation, and maximum value of time dispersion parameters and coherent bandwidth for 20 dB threshold. The transmitted signal experienced frequency-selective fading when the transmission signal has higher bandwidth than the coherent bandwidth. The time dispersion parameters reveal that the directional antennas offer the highest coherent bandwidth in line-of-sight situation. It is also observed that there is no significant difference in the time dispersion parameters of directional antenna in NLOS and omni-directional antennas in LOS/NLOS situation.

Table 6.11 Mean, Standard Deviation (STDEV), and Maximum (MAX) of Mean Excess Delay ($\bar{\tau}$), RMS Delay Spread (σ_t), Maximum Delay Spread (τ_{max}) and Coherent Bandwidth (B_c) at 20 dB Threshold

	$\bar{\tau}$ (nanosecond)			σ_t (nanosecond)			τ_{max} (nanosecond)			Coherent Bandwidth (MHz)
	Mean	STDEV	MAX	Mean	STDEV	MAX	Mean	STDEV	MAX	$B_C \approx \frac{1}{5 \cdot \sigma_t}$
Case 1	166.1	78.56	298.3	15.68	2.92	31.7	94.0	22.74	180.0	12.76
Case 2	169.5	35.06	225.5	65.2	30.90	121.1	360.3	148.29	620.0	3.07
Case 3	168.8	80.94	324.5	62.8	44.19	154.4	392.5	237.25	780.0	3.18
Case 4	204.7	63.78	339.9	57.9	69.37	292.8	451.5	602.24	2280.0	3.45

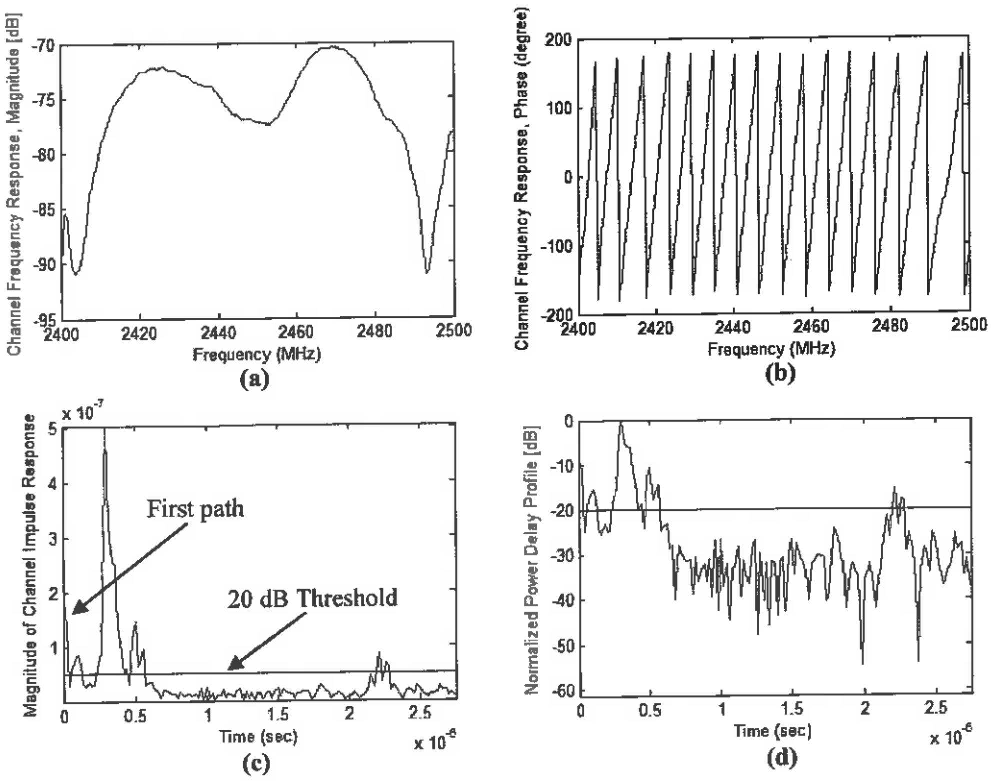

Figure 6.16 (a) Channel Frequency Response, Magnitude [dB] (b) Channel Frequency Response, Phase (degree) (c) Magnitude of Impulse Response (d) Normalized Power Delay Profile [dB] at a Tx-Rx distance of 32 meter; Case 4

6.6.3 Conclusion

In this case study, the line-of-sight and non-line-of-sight performance of omni-directional and directional antennas is investigated in WITS mock-tunnel. The wideband measurements were performed at 2.4 - 2.5 GHz frequency band. The study concludes the following:

- There is no significant difference in the performance of omni-directional antennas in line-of-sight and non-line-of-sight.
- The directional antenna offers the highest coherent bandwidth in the line-of-sight but has lowest coverage/link reliability.
- The attenuation rate in non-line-of-sight is lower than the line-of-sight. However, the path loss in non-line-of-sight is higher than the line-of-sight.

6.7 Case Study 6: Performance Comparison of 2.4 GHz and 5.8 GHz on TTA Communication System

This case study investigates the effect of transmission frequency on the line-of-sight performance of TTA communication system in WITS mock-tunnel. It is organized into two scenarios, each representing the wideband measurements with different antennas at 2.4 GHz and 5.8 GHz frequency. Table 6.12 summarizes the antennas used for the wideband measurement campaign. These scenarios correspond to the access point-to-access point wireless communication. The tripod stands used for the antenna mounting had no significant impact on the reflection coefficient (i.e. $S_{11} < -10$dB) of the antenna.

Table 6.12 Antennas used for Case Study 6

Scenario	Receiver and Transmitter Antennas
Case 1	(13°, 17.5°), Horizontally polarized, 2.4-2.5 GHz
Case 2	(35°, 40°), Horizontally polarized, 5.6-5.95 GHz

During the measurement campaign, the vector network analyser and the receiving antenna with other Rx-components were stationed at (x = 56.2m, y = 1.5m, z = 1.22m). The transmitting antenna with the Tx-components was moved to different locations by varying their position 1m lengthwise for 40m. The transmitter antenna was placed at the center of the tunnel with a fixed antenna height, i.e. (y = 1.5m, z = 1.22m). The measurements also include the effect of tunnel cross-cut and tunnel face. The following sub-sections show the large-scale and small-scale parameters for investigating the effect of transmission frequency on the line-of-sight performance of TTA communication system. These parameters are obtained from the complex channel transfer function of the radio propagation.

6.7.1 Path Loss Exponent and Shadow Fading

The scattered received power over transmitted power as a function of Tx-Rx distance and the estimated path-loss exponent values are shown in Figure 6.17. It is observed that the path-loss exponent values are less than the free space, i.e. $n < 2$. This can be explained by the waveguide effect [28]. The path-loss exponent values reveal that the higher operating frequency has lower attenuation rate. The CDF of shadow fading that fits with normal distribution, the KS-test k values and the shadow fading statistics are shown in Figure 6.18. The results reveal that a higher value of shadow fading standard deviation means the higher variation of received signal from the estimated value, i.e. lesser coverage/link reliability. It is observed that lowest path-loss exponent (i.e. attenuation rate) does not correspond to the highest coverage reliability. The shadow fading standard deviation values show that there is no significant effect of transmission frequency on the shadow fading. The experimental results reveal that the higher transmission frequency has higher path-loss and lower attenuation rate.

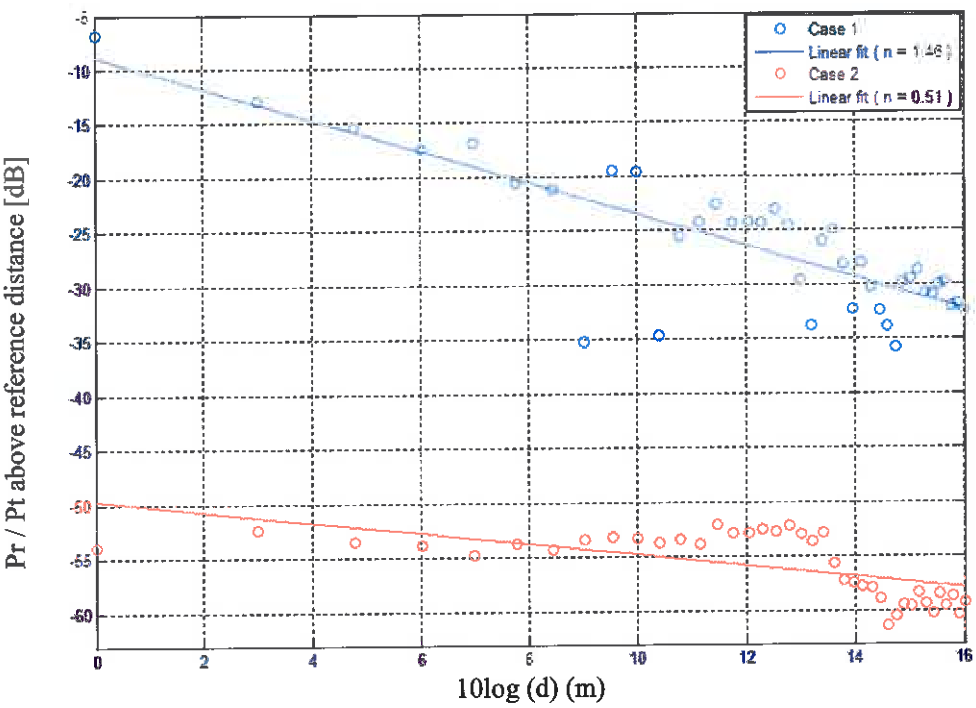

Figure 6.17 Received Power as a function of Tx-Rx distance; *n* = path-loss exponent

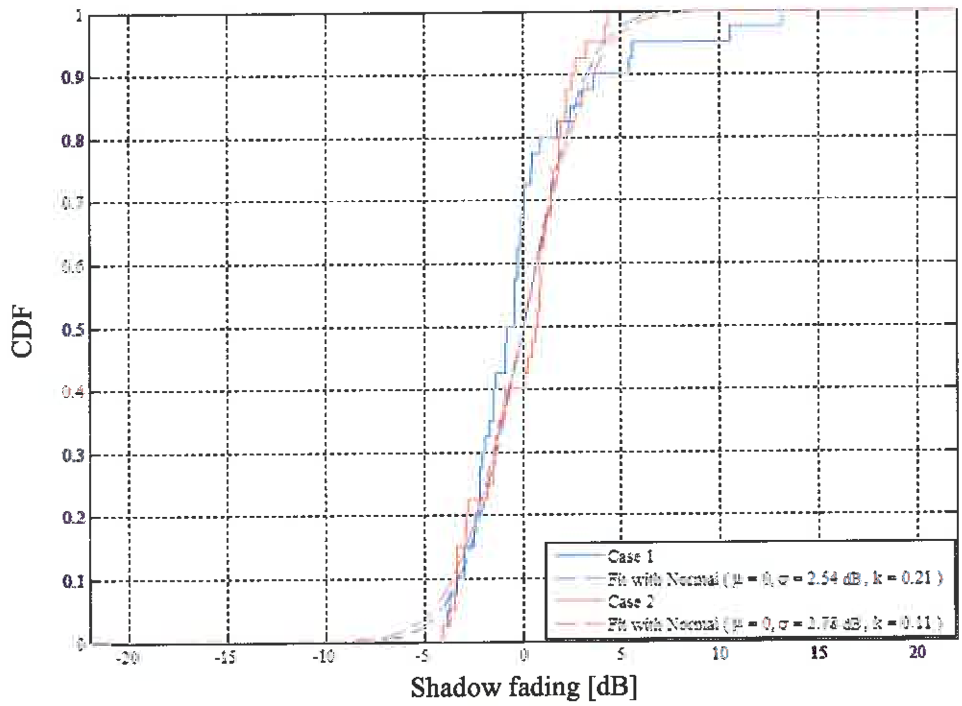

Figure 6.18 Kolmogorov-Smirnov test for the shadow fading; μ = mean, σ = standard deviation, k = KS-test value

6.7.2 Time Dispersion Parameters

The magnitude and phase of channel frequency response, magnitude of channel impulse response and normalized power delay profile at 30 meter Tx-Rx distance for case 2 are shown in Figure 6.19. The notches in the magnitude of complex channel transfer function illustrate the frequency-selective nature of the propagation channel. The channel impulse response shows the first arriving component along with other multipath components. The mean excess delay, the RMS excess delay and maximum delay spread are computed at all the measurement location at predefined threshold. Table 6.13 summarizes the mean, standard deviation, and maximum value of time dispersion parameters and coherent bandwidth for 20 dB threshold. The transmitted signal experienced frequency-selective fading when the transmission signal has higher bandwidth than the coherent bandwidth. The time dispersion parameters reveal that transmission frequency has significant effect on the coherent bandwidth of TTA communication system. It is concluded that 2.4 GHz transmission frequency has higher coherent bandwidth than 5.8 GHz transmission frequency.

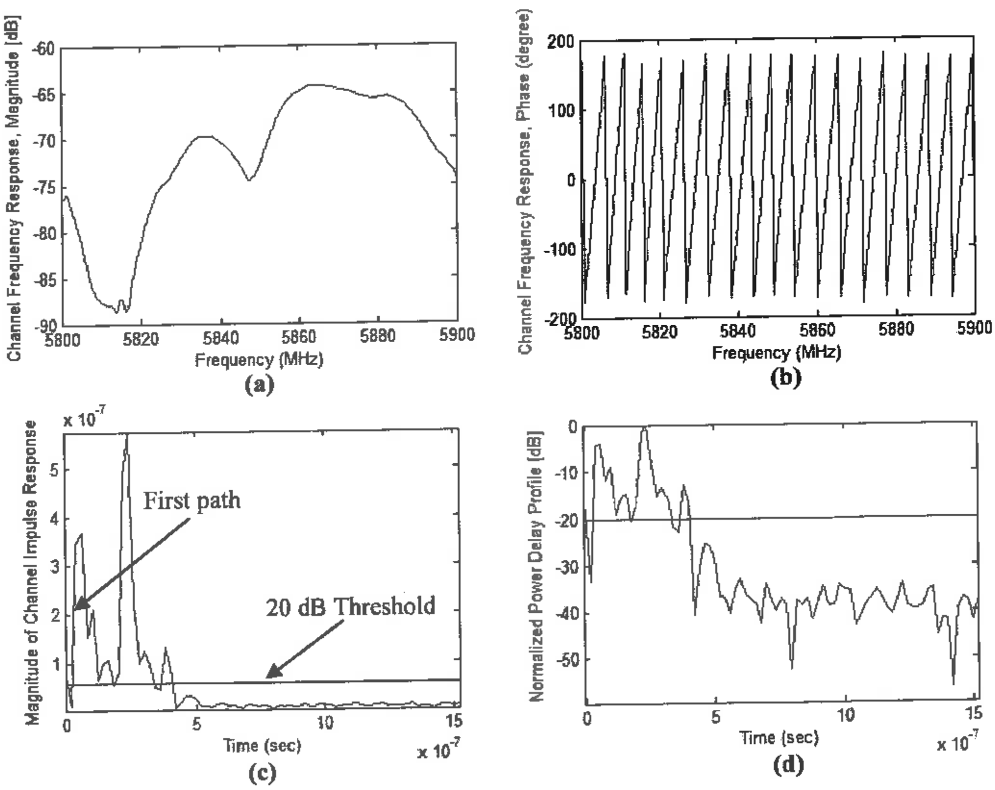

Figure 6.19 (a) Channel Frequency Response, Magnitude [dB] (b) Channel Frequency Response, Phase (degree) (c) Magnitude of Impulse Response (d) Normalized Power Delay Profile [dB] at a Tx-Rx distance of 30 meter; Case 2

Table 6.13 Mean, Standard Deviation (STDEV), and Maximum (MAX) of Mean Excess Delay ($\bar{\tau}$), RMS Delay Spread (σ_t), Maximum Delay Spread (τ_{max}) and Coherent Bandwidth (B_c) at 20 dB Threshold

	$\bar{\tau}$ (nanosecond)			σ_t (nanosecond)			τ_{max} (nanosecond)			Coherent Bandwidth (MHz)
	Mean	STDEV	MAX	Mean	STDEV	MAX	Mean	STDEV	MAX	$B_c \approx \frac{1}{5 \cdot \sigma_t}$
Case 1	166.1	78.56	298.3	15.68	2.92	31.7	94.0	22.74	180.0	12.76
Case 2	132.5	43.57	206.1	61.52	36.66	119.8	306.0	131.98	540.0	3.25

6.7.3 Conclusion

In this case study, the effect of transmission frequency on the line-of-sight performance of TTA communication system is analysed in WITS mock-tunnel. The wideband measurements were performed at 2.4 - 2.5 GHz and 5.8 - 5.9 GHz frequency bands. The study concludes the following:

- 5.8 GHz frequency band has higher path loss at the reference distance and lower attenuation rate than 2.4 GHz frequency band.
- There is no significant effect of 2.5 GHz and 5.8 GHz frequency bands on the coverage reliability.
- 2.4 GHz transmission frequency has higher coherent bandwidth than 5.8 GHz transmission frequency. This indicates that the higher transmission frequency electromagnetic modes attenuate slower and cause in high multipath fading.

6.8 Case Study 7: Radio Propagation of CoM Vertical Shaft

This case study statistically characterises the Chamber of Mines vertical shaft for the line-of-sight performance analyses of through-the-air communication system. The right-hand circularly polarized (RHCP) directional antennas of beamwidth (60°, 60°) were used for the wideband measurements in the 2.4 - 2.5 GHz frequency band. This study corresponds to the access point-to-access point TTA communication. Figure 6.20 shows the test antenna in Chamber of Mines (CoM) vertical shaft.

During the measurement campaign, the vector network analyser and the receiving antenna with other Rx-components were stationed at the bottom of the vertical shaft. The transmitting antenna with the Tx-components was moved to different locations by varying their position 1m lengthwise for 12m. The transmitter and receiver antennas were placed close to the vertical shaft boundary. The following sub-sections show the large-scale and small-scale parameters for studying the line-of-sight performance of RHCP directional antenna in CoM vertical shaft. These parameters are obtained from the complex channel transfer function of the radio propagation.

Figure 6.20 Test Antenna in CoM Vertical Shaft

6.8.1 Path Loss Exponent and Shadow Fading

The scattered received power over transmitted power as a function of Tx-Rx distance and the estimated path-loss exponent values are shown in Figure 6.21. It is observed that the path-loss exponent value is less than the free space, i.e. $n < 2$. This can be explained by the waveguide effect [28]. The CDF of shadow fading that fits with normal distribution, the KS-test k values and the shadow fading statistics are shown in Figure 6.22. The CDF reveal that a higher value of shadow fading standard deviation means the higher variation of received signal from the estimated value, i.e. lesser coverage/link reliability. The obtained values of path-loss exponent and shadow fading standard deviation in the vertical shaft are 0.88 and 3.65 dB, respectively.

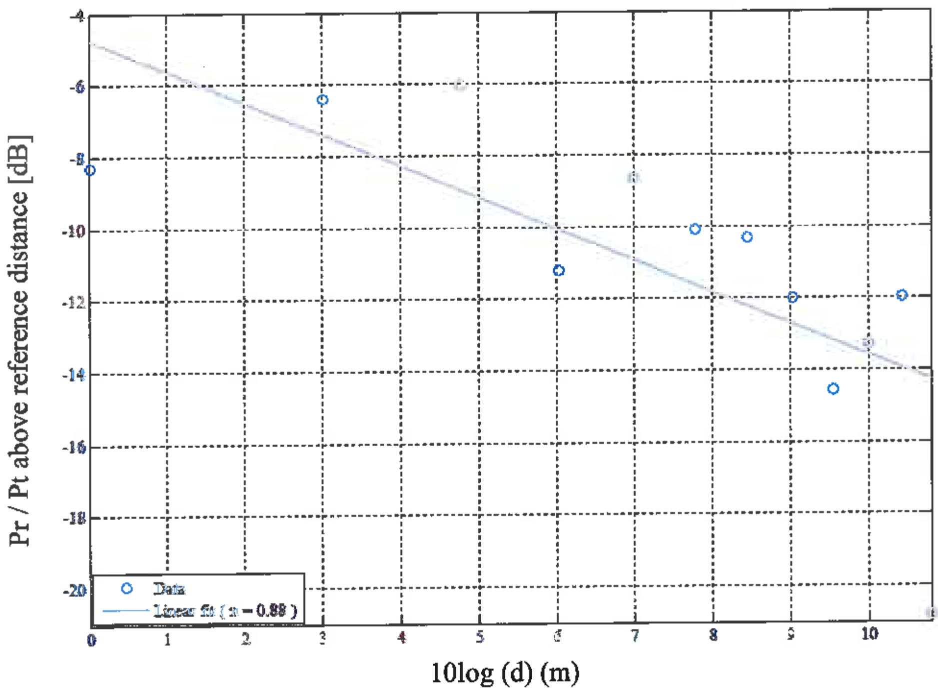

Figure 6.21 Received Power as a function of Tx-Rx distance;
n = path-loss exponent

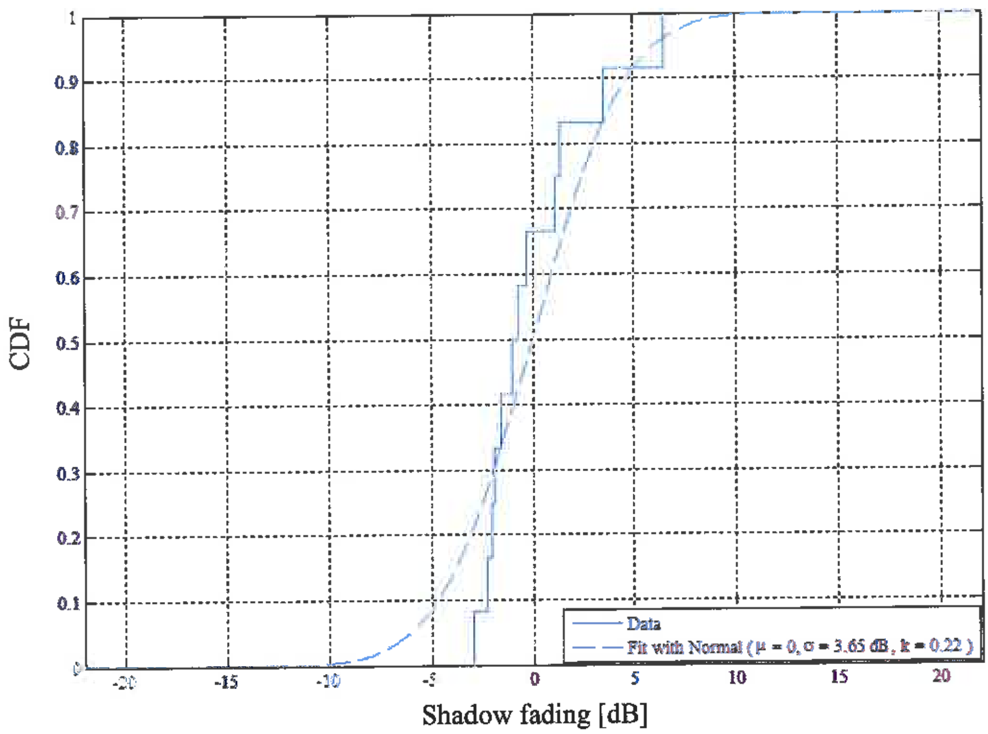

Figure 6.22 Kolmogorov-Smirnov test for the shadow fading;
μ = mean, σ = standard deviation, k = KS-test value

6.8.2 Time Dispersion Parameters

The magnitude and phase of channel frequency response, magnitude of channel impulse response and normalized power delay profile at 12 meter Tx-Rx distance are shown in Figure 6.23. The notches in the magnitude of complex channel transfer function illustrate the frequency-selective nature of the propagation channel. The channel impulse response shows the first arriving component along with other multipath components. The mean excess delay, the RMS excess delay and maximum delay spread are computed at all the measurement location at predefined threshold. Table 6.14 summarizes the mean, standard deviation, and maximum value of time dispersion parameters and coherent bandwidth for 20 dB and 40 dB thresholds. The transmitted signal experienced frequency-selective fading when the transmission signal has higher bandwidth than the coherent bandwidth. The obtained value of mean RMS delay spread and coherent bandwidth are 14.4 nanosecond and 13.89 MHz at 20dB threshold, respectively.

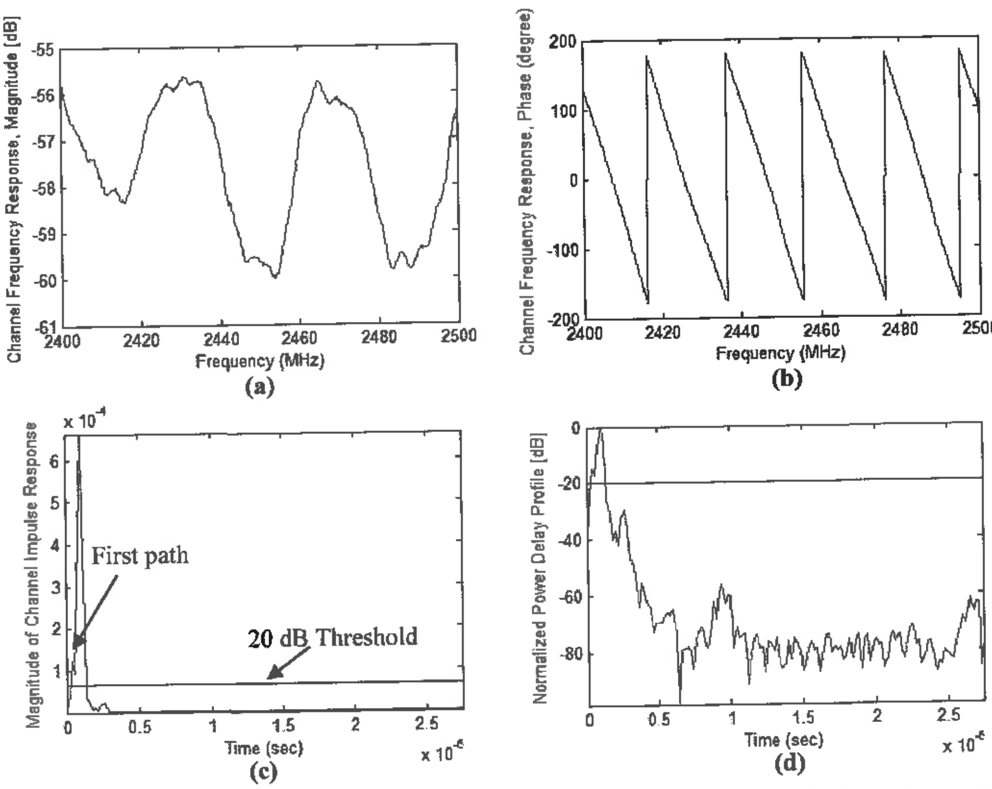

Figure 6.23 (a) Channel Frequency Response, Magnitude [dB] (b) Channel Frequency Response, Phase (degree) (c) Magnitude of Impulse Response (d) Normalized Power Delay Profile [dB] at a Tx-Rx distance of 12 meter

Table 6.14 Mean, Standard Deviation (STDEV), and Maximum (MAX) of Mean Excess Delay ($\bar{\tau}$), RMS Delay Spread (σ_t), Maximum Delay Spread (τ_{max}) and Coherent Bandwidth (B_c)

	$\bar{\tau}$ (nanosecond)			σ_t (nanosecond)			τ_{max} (nanosecond)			Coherent Bandwidth (MHz)
Threshold (decibel)	Mean	STDEV	MAX	Mean	STDEV	MAX	Mean	STDEV	MAX	$B_C \approx \frac{1}{5 \cdot \sigma_t}$
- 20	69.7	21.0	98.9	14.4	1.12	15.6	85.2	19.3	110.5	13.89
- 40	69.9	21.1	99.0	15.6	1.75	18.0	199.7	46.29	268.2	12.82

6.8.3 Conclusion

In this case study, radio propagation of Chamber of Mines (CoM) vertical shaft is investigated for the line-of-sight performance of TTA communication system. The RHCP directional antenna is used for the wideband measurements. This study concludes the following:

- The path-loss exponent is less than the free-space, i.e. $n < 2$.
- The path-loss exponent and shadow fading standard deviation in CoM vertical shaft are 0.88 and 3.65 dB, respectively.
- The right-hand circular polarized directional antenna offers 13.89 MHz coherent bandwidth at 20 dB threshold in CoM vertical shaft.

6.9 Conclusion of the Chapter

This chapter investigated the wideband characterization of radio propagation channel for WITS mock-mine. This work is organized into seven case studies for analysing the effect of antenna placement, antenna polarization, antenna directivity and transmission frequency on the performance of TTA communication systems. The statistical parameters related to path-loss and delay spread are extracted from wideband measurements for the performance study. Each case study presents and analyses in-detail the obtained large-scale and small-scale parameters with a conclusion.

The next chapter; Summary and Conclusion, covers the findings and conclusion of the research. The future work is also discussed for performance enhancement of TTA communication systems.

7 SUMMARY AND CONCLUSION

7.1 Summary

Communication systems play an important role to improve safety and enhance productivity in the mining operations. The underground mine communication systems are broadly classified as through-the-earth (TTE), through-the-wire (TTW) and through-the-air (TTA) communication systems. TTE communication systems operational concept envisions mine emergency, which offers several hundred of meters signal propagation through solid rock with limited transmission rates. Whereas, TTW and TTA communication systems offers higher transmission rates for two-way real-time voice, video and data communication, video surveillance, tracking miners and equipment, sensing and remote control. TTA communication systems can benefit from its ease of deployment with an increased scalability, self-adaptive nature and low maintenance cost.

Radio Propagation in the underground mining environment is highly dynamic due to the complex tunnel geometry, roughness of walls and mine infrastructure. In recent years, significant work has been done on empirical radio channel characteristics of different underground mining tunnels. To the best of our knowledge, no open literature is available on the radio propagation of 1) deep underground mining tunnels, 2) mine vertical shaft and 3) underground mining tunnels with circularly polarized antennas. The experimental work on the performance comparison of different antennas in the underground mining tunnels is also sparse.

This work presents the statistical radio propagation of WITS mock-mine (i.e. steel-supported arch-shaped mock-tunnel and vertical shaft). It also analyses the effect of antenna placement, polarization, directivity and configuration, and transmission frequency on the performance of TTA communication system. The wideband measurements are used to extract the statistical parameters related to path-loss and delay spread for performance study.

The experimental radio propagation in the complex underground mining environment gives more accurate results than the theoretical models [49].

However, the measurements do not give the physical insight of the radio propagation. Before the wideband measurements for the radio propagation, WITS mock-tunnel model was simulated in the CST[12], an Electromagnetics Simulation Software, on 64 GB RAM PC for quick performance study. The model could not run due to 21.5 billion required mesh cells. It is concluded that the EM software requires significant computational resources for large and complex problems[13].

7.2 Key Findings of the Research

The key findings of WITS mock-mine radio propagation with omni-directional/directional linearly and circularly polarized antennas at different antenna placements and transmission frequencies are summarized as follows:

- Antenna placement, antenna polarization, antenna directivity and transmission frequency have significant impact on the performance of TTA communication system.
    - Antennas placed at the center of the mining tunnel provide the highest coverage area and coherent bandwidth (shown in Figure 6.2 and table 6.2). However, it is impractical to place antennas at the center of the tunnel when the mine is in operation.

---

[12] Computer Simulation Software simulates the electromagnetic (EM) fields in the arbitrary three-dimensional structures.

[13] Matthew Miller, president of Delcross Technologies: *As the electrical size (as measured in wavelengths) of an object increases, memory requirements and run time for full-wave techniques—such as method of moments (MoM), finite-difference time domain (FDTD), finite element method (FEM), finite integral technique (FIT), etc.—increase rapidly. At some point, it is no longer practical to use a full-wave solver. It is at this point that users typically switch to an asymptotic, ray-based solution, such as geometric theory of diffraction (GTD) or physical theory of diffraction (PTD)* [77]. The ray tracing simulations fail to provide the consistent accuracy in different scenarios [49].

- Different antenna placements, i.e. close-to tunnel side-wall and roof, show that antennas placement in diagonal configuration offers the highest coverage range. However, antennas placement close-to roof center have better coverage/link reliability and coherent bandwidth (shown in case study 1; Figure 6.2-6.3 and table 6.2).
- In a wide tunnel, RHCP directional antenna has the highest coverage range and coherent bandwidth. Whereas, horizontally polarized antenna presents the highest coverage/link reliability. The horizontal polarized antenna performs better in terms of range, link reliability and coherent bandwidth than the vertically polarized antenna (shown in case study 2; Figure 6.5-6.6 and table 6.4).
- Antenna directivity has no significant effect on the coverage range and coherent bandwidth. However, antenna directivity improves the coverage reliability (shown in case study 3).
- For access point-to-mobile TTA communication, the combination of RHCP directional antenna and horizontally polarized omni-directional antenna in RF front-end offers the highest coverage area and coherent bandwidth. However, the circularly polarized antennas combination presents the highest coverage/link reliability (shown in case study 4; Figure 6.11-6.12 and table 6.8).
- There is no significant difference in the performance of omni-directional antennas in line-of-sight and non-line-of-sight situations (shown in table 6.10-6.11).
- Directional antenna offers the highest coherent bandwidth in the line-of-sight but has lowest coverage/link reliability (shown in table 6.11 and Figure 6.15).
- 5.8 GHz frequency band has higher path loss at the reference distance and lower attenuation rate than the 2.4 GHz frequency band. However, 2.4 GHz transmission frequency has higher coherent bandwidth than 5.8 GHz transmission frequency (shown in Figure 6.17 and table 6.13).
- 2.4 GHz and 5.8 GHz transmission frequencies have no significant impact on the coverage/link reliability (shown in Figure 6.18).

- The path-loss exponent, shadow fading standard deviation and coherent bandwidth (at 20dB threshold) in CoM vertical shaft are 0.88, 3.65 dB and 13.89 MHz respectively (shown in case study 7; Figure 6.21-6.22 and table 6.14).

This work concludes that that the antenna placement, antenna polarization, antenna directivity, antenna configuration and transmission frequency have significant impact on the performance of TTA communication system. The measurement-based study also reveals that a single scenario cannot provide the best performance in terms of attenuation rate, coverage/link reliability, time dispersion parameters and coherent bandwidth.

7.3 Recommendations for the Future Research Work

The performance enhancement of through-the-air (TTA) communication system in the underground mines is recommended by using multiple antenna systems. MIMO is an evolving technology that improves the traditional single antenna communication systems by orders of magnitude. This technology has found application in terrestrial and satellite communication systems. The future work aims to characterise the propagation of radio signals in an underground deep hard-rock mine with MIMO antenna system. It further aims to determine the optimal antenna configuration for MIMO systems and modulation scheme in deep hard-rock mines. For future research the following recommendations are made:

- Propagation channel modelling of deep hard rock mine with omni and directional MIMO antenna systems.
- Performance study of linear and circular polarized MIMO antenna systems.
- Optimal antenna design or configuration and modulation scheme for MIMO antenna system.
- Performance study of MIMO communication system by using antennas having beamwidth equal to angular spread.

References

[1] Saad Qaiser, "Safety Assurance in High Stress Environments" [Online]. Available: http://connekt.seecs.nust.edu.pk/SAHSE.php?&session -id=d68ed1c95a06c690fdb9518ddccb8b33 [Accessed on 19 Feb, 2016]

[2] Forooshani, A.E.; Bashir, S.; Michelson, D.G.; Noghanian, S., "A Survey of Wireless Communications and Propagation Modeling in Underground Mines," *Communications Surveys & Tutorials, IEEE* , vol.15, no.4, pp.1524,1545, Fourth Quarter 2013.

[3] R. S. Nutter and M. D. Aldridge, "Status of mine monitoring and communications," *IEEE Trans. Ind. Appl.*, vol. 24, pp. 820–826, 1988.

[4] J. Murphy and H. E. Parkinson, "Underground mine communications," in *Proc. IEEE*, Jan. 1978, pp. 26–50.

[5] D. J. R. Martin, "Leaky-feeder radio communication: A historical review," in *Proc. IEEE VTC*, May 1984, pp. 25–30.

[6] Underground Coal Mine Monitoring with Wireless Sensor Networks. Li, Mo and YUNHAO, Liu. *ACM Transactions on Sensor Networks*, Vol. 5, March 2009.

[7] Larbi Talbi, Ismail Ben Mabrouk and Mourad Nedil, *Progress Research on Wireless Communication Systems for Underground Mine Sensors*, Available: www.intechopen.com.

[8] S. Yarkan, S. Güzelgöz, H. Arslan and R.R. Murphy, "Underground mine communications: A survey," *IEEE Communications Survey & Tutorials*, vol. 11, no. 3, pp. 125-142, Third Quarter 2009.

[9] Ranjan, A. and Sahu, H.B. 2014. "Communication Challenges in Underground Mines", *Search & Research*, Vol. V, No. (2), pp. 23-29, 2014.

[10] Milda Tamošiūnaitė, Mindaugas Žilinskas, Milda Tamošiūnienė, Kouji Tamošiūnas and Stasys Ara, *"Atmospheric Attenuation due to Humidity"*, Available: http://www.intechopen.com/books/electromagneticwaves/atmosphericattenuation -due-to-humidity

[11] P. Misra, S. Kanhere, D. Ostry and S. Jha, "Safety assurance and rescue communication systems in high-stress environments: A mining case study," in *IEEE Communications Magazine*, vol. 48, no. 4, pp. 66-73, April 2010.

[12] T. S. Rappaport, *Wireless Communications: Principles & Practice*, 2nd Ed., Prentice-Hall: Upper Saddle River, NJ, 2002, ISBN 0-13-042232-0.

[13] School of Electrical and Information Engineering, *Principles of Communication course lecture notes*, University of the Witwatersrand, Johannesburg, 2015.

[14] T. Sarkar, Z. Ji, K. Kim, A. Medouri, and M. Salazar-Palma, "A survey of various propagation models for mobile communication," *IEEE Trans. Antennas Propag.*, vol. 45, pp. 51–82, 2003.

[15] L.K. Bandyopadhyay, S. K. Chaulya, and P. K. Mishra, *Wireless Communication in Underground Mines*, Springer, 2010.

[16] Lincan Yan; Waynert, J.A.; Sunderman, C., "Measurements and Modeling of Through-the-Earth Communications for Coal Mines," *Industry Applications, IEEE Transactions on* , vol.49, no.5, pp.1979,1983, Sept.-Oct. 2013.

[17] W. H. Schiffbauer and J. F. Brune, "Coal mine communications," *American Longwall Mag.*, 2006.

[18] Bandyopadhyay, L. K., Chaulya, S. K., and Mishra, P. K., "*Wireless Communication in Underground Mines: RFID-based Sensor Networking*", Boston, MA, USA: Springer, 2010.

[19] Michael R. Yenchek, *"Through-the Earth Mine Communication Systems"*, Pittsburgh Research Laboratory, 2009. Available: http://www.cdc.gov/niosh/mining/UserFiles/workshops/commtrack2009/ThroughTheEarth-Yenchek.pdf

[20] Lockheed Martin, "MagneLink™ Magnetic Communication System (MCS) Through-The-Earth Two-Way Emergency Wireless Communications for Mine Industry Safety", 2010. Available: www.lockheedmartin.com

[21] P. Delogne, "EM propagation in tunnels," *IEEE Trans. Antennas Propag.*, vol. 39, pp. 401–406, 1991.

[22] J. Ferrer-Coll, P. Angskog, J. Chilo and P. Stenumgaard, "Characterisation of electromagnetic properties in iron-mine production tunnels," in *Electronics Letters*, vol. 48, no. 2, pp. 62-63, January 19 2012.

[23] National Institute for Occupational Safety and Health (NIOSH), Mining Program, "Advanced Tutorial on Wireless Communication and Electronic Tracking: Communication System Performance", Available: http://www.cdc.gov/niosh/mining/content/emergencymanagementandresponse/commtracking/advcommtrackingtutorial2.html [Accessed on 16 Feb, 2016]

[24] Tian Hongxian; Yang Wei, "Research on emergency rescue communication and exploration system underground," Service Operations, Logistics, and Informatics (SOLI), *2011 IEEE International Conference on* , vol., no., pp.443,446, 10-12 July 2011.

[25] Yarkan, S.; Arslan, H., "Statistical Wireless Channel Propagation Characteristics in Underground Mines at 900MHz," *Military Communications Conference, 2007. MILCOM 2007. IEEE* , vol., no., pp.1,7, 29-31 Oct. 2007.

[26] Zhi Sun and Ian F. Akyildiz, "Channel Modeling and Analysis for Wireless Networks in Underground Mines and Road Tunnels," *IEEE Transactions On Communications*, Vol. 58, No. 6, June 2010.

[27] M. Lienard and P. Degauque, "Natural wave propagation in mine environments," *IEEE Trans. Antenna Propag.*, vol. 48, no. 9, pp. 1326-1339, Sep. 2000.

[28] El Khaled, M.; Fortier, P.; Ammari, M.L., "A Performance Study of Line-of-Sight Millimeter-Wave Underground Mine Channel," *Antennas and Wireless Propagation Letters, IEEE* , vol.13, no., pp.1148,1151, 2014.

[29] Emslie, A.; Lagace, R.; Strong, P., "Theory of the propagation of UHF radio waves in coal mine tunnels," in *Antennas and Propagation, IEEE Transactions on* , vol.23, no.2, pp.192-205, Mar 1975.

[30] Chahé Nerguizian, Charles L. Despins, Sofiène Affès, and Mourad Djadel." Radio-Channel Characterization of an Underground Mine at 2.4 GHz,"

IEEE Transactions On Wireless Communications, Vol. 4, No. 5, September 2005.

[31] Pierre Laliberte, *Summary Study of Underground Communications Technologies*, CANMET Mining and Mineral Sciences Laboratory, Final project report 603478-0-0, May 2009.

[32] P. Tao, "Technology Study of Wireless Communication System under the Coal Mine Tunnel," *Intelligent System Design and Engineering Application (ISDEA), 2010 International Conference on*, Changsha, 2010, pp. 553-556.

[33] Y. P. Zhang, G. X. Zheng and J. H. Sheng, "Radio propagation at 900 MHz in underground coal mines," in *IEEE Transactions on Antennas and Propagation*, vol. 49, no. 5, pp. 757-762, May 2001.

[34] Mathieu Boutin, Ahmed Benzakour, Charles L. Despins and Sofiène Affes, "Radio Wave Characterization and Modeling in Underground Mine Tunnels," *IEEE Transactions On Antennas And Propagation*, Vol. 56, No. 2, February 2008.

[35] I. Ben Mabrouk, J. Hautcoeur, L. Talbi, M. Nedil and K. Hettak, "Feasibility of a Millimeter-Wave MIMO System for Short-Range Wireless Communications in an Underground Gold Mine," in *IEEE Transactions on Antennas and Propagation*, vol. 61, no. 8, pp. 4296-4305, Aug. 2013.

[36] B. Mnasri, M. Nedil, N. Kandil, L. Talbi, and I. Ben Mabrouk, "Experimental characterization of wireless MIMO channel at 5.8 GHz in underground gold mine," *Progress In Electromagnetics Research C*, Vol. 36, 169-180, 2013.

[37] Ben Mabrouk, I.; Talbi, L.; Nedil, M.; Hettak, K., "MIMO-UWB Channel Characterization Within an Underground Mine Gallery," in *Antennas and Propagation, IEEE Transactions on* , vol.60, no.10, pp.4866-4874, Oct. 2012.

[38] I. Ben Mabrouk, L. Talbi, M. Nedil and K. Hettak, "Experimental characterization of MIMO-UWB multipath underground mine radio channels," *Antennas and Propagation Society International Symposium (APSURSI), 2012 IEEE*, Chicago, IL, 2012, pp. 1-2.

[39] Ben Mabrouk, I.; Reyes-Guerrero, J.C.; Nedil, M.; Talbi, L., "Line of sight MIMO-UWB short range communication in underground mine tunnel," in *Antennas and Propagation (EuCAP), 2015 9th European Conference on* , vol., no., pp.1-4, 13-17 April 2015.

[40] I. Ben Mabrouk , L. Talbi , M. Nedil & K. Hettak, "The Effect of the Human Body on MIMO-UWB Signal Propagation in an Underground Mine Gallery", *Journal of Electromagnetic Waves and Applications*, 26:4, 560-569, DOI: 10.1163/156939312800030695, 2012.

[41] Ismail Ben Mabrouk, Larbi Talbi, Rachid Ait Jilal, Mourad Nedil, Yacouba Coulibaly, Tayeb A. Denidni, "MIMO Channel Characterization at 2.4 GHz in Underground Gold Mines," in *Antennas and Propagation (APSURSI), 2011 IEEE International Symposium on*, 2011.

[42] R. Ait Jilal, M. Nedil, Y. Coulibaly, T. A. Denidni, I. Ben Mabrouk and L. Talbi, "Characterization of the MIMO channel for LTE standard in underground mine," *Antennas and Propagation (APSURSI), 2011 IEEE International Symposium on*, Spokane, WA, pp. 2777-2780, 2011.

[43] Ben Mabrouk, I.; Talbi, L.; Nedil, M., "Performance Evaluation of a MIMO System in Underground Mine Gallery," in *Antennas and Wireless Propagation Letters, IEEE* , vol.11, no., pp.830-833, 2012.

[44] Ghaddar, M.; Nedil, M.; Ben Mabrouk, I.; Talbi, L., "Multiple-input multiple-output beam-space for high-speed wireless communication in underground mine," in *Microwaves, Antennas & Propagation, IET* , vol.10, no.1, pp.8-15, 1 9 2015.

[45] I. B. Mabrouk, L. Talbi and M. Nedil, "Enhancement of wireless channel performance using MIMO system in underground mine gallery," *Wireless Communications in Unusual and Confined Areas (ICWCUCA), 2012 International Conference on*, Clermont Ferrand, pp. 1-5, 2012.

[46] I. B. Mabrouk, L. Talbi, M. Nedil, Y. Coulibaly and T. A. Denidni, "Effect of antenna directivity on performance of multiple input multiple output systems in an underground gold mine," in *IET Microwaves, Antennas & Propagation*, vol. 6, no. 5, pp. 555-561, April 12 2012.

[47] Gareth Allan Kennedy, *High resilience wireless mesh networking characteristics and safety applications within underground mines*, PhD thesis, University of Exeter, September 2006.

[48] Y. Rissafi, L. Talbi, and M. Ghaddar, "Experimental characterization of an UWB propagation channel in underground mines," *IEEE Trans. Antennas Propagat.*, vol. 60, no. 1, pp. 240–246, 2012.

[49] A. E. Forooshani, *Configuration of Multiple Input Multiple Output Antenna Arrays for Wireless Communications in Underground Mines*, PhD thesis, The University of British Columbia, August 2013.

[50] Chenming Zhou, Timothy Plass, Ronald Jacksha, and Joseph A. Waynert, "RF Propagation in Mines and Tunnels: Extensive measurements for vertically, horizontally, and cross-polarized signals in mines and tunnels," *IEEE Antennas & Propagation Magazine*, August 2015.

[51] Dudley, D.G.; Lienard, M.; Mahmoud, S.F.; Degauque, P., "Wireless propagation in tunnels," in *Antennas and Propagation Magazine, IEEE*, vol.49, no.2, pp.11-26, April 2007.

[52] Y. Kim, M. Jung, and B. Lee, "Analysis of radio wave propagation characteristics in rectangular road tunnel at 800 MHz and 2.4 GHz," in *Antennas and Propagation Society International Symposium, 2003. IEEE*, vol. 3, pp. 1016–1019, 2003.

[53] Andrej Hrovat, Gorazd Kandus, Toma˘z Javornik, "A Survey of Radio Propagation Modeling for Tunnels," *IEEE Communications Surveys & Tutorials*, VOL. 16, NO. 2, Second Quarter 2014.

[54] Z. Changsen and M. Yan, "Effects of cross section of mine tunnel on the propagation characteristics of UHF radio wave," in *Antennas, Propagation EM Theory, 2006. ISAPE '06. 7th International Symposium on*, 2006, pp. 1–5.

[55] S. Wang, "Radio wave attenuation character in the confined environments of rectangular mine tunnel," *Modern Applied Science*, vol. 4, no. 2, pp. 65–70, 2010.

[56] Y. Huo, Z. Xu, H. dang Zheng, and X. Zhou, "Effect of antenna on propagation characteristics of electromagnetic waves in tunnel

environments," in *Microelectronics Electronics, 2009. PrimeAsia 2009. Asia Pacific Conference on Postgraduate Research in*, pp. 268-271, 2009.

[57] Benzakour, A.; Affes, S.; Despins, C.; Tardif, P.-M., "Wideband measurements of channel characteristics at 2.4 and 5.8 GHz in underground mining environments," in *IEEE Vehicular Technology Conference, 2004*.

[58] Boutin, M.; Affes, S.; Despins, C.; Denidni, T., "Statistical modelling of a radio propagation channel in an underground mine at 2.4 and 5.8 GHz," in *Vehicular Technology Conference, 2005. VTC 2005-Spring. 2005 IEEE 61st*, vol.1, no., pp.78-81 Vol. 1, 30 May-1 June 2005.

[59] M. Linard, P. Degauque, J. Baudet, and D. Degardin, "Investigation on MIMO channels in subway tunnels," *IEEE J. Sel. Areas Commun.*, vol. 21, pp. 332–339, 2003.

[60] Emami Forooshani, A.; Noghanian, S.; Michelson, D.G., "Characterization of Angular Spread in Underground Tunnels Based on the Multimode Waveguide Model," in *Communications, IEEE Transactions on*, vol.62, no.11, pp.4126-4133, Nov. 2014.

[61] C. Briso-Rodriguez, J. M. Cruz and J. I. Alonso, "Measurements and Modeling of Distributed Antenna Systems in Railway Tunnels," in *IEEE Transactions on Vehicular Technology*, vol. 56, no. 5, pp. 2870-2879, Sept. 2007.

[62] K. Guan, Z. Zhong, J. I. Alonso and C. Briso-Rodriguez, "Measurement of Distributed Antenna Systems at 2.4 GHz in a Realistic Subway Tunnel Environment," in *IEEE Transactions on Vehicular Technology*, vol. 61, no. 2, pp. 834-837, Feb. 2012.

[63] Cawood F., "Digital Mine laboratory prepared for digital mining," Available: http://www.ee.co.za/wp-content/uploads/2015/03/positionit-march15-p26-30.pdf

[64] Cawood F., "Wits 'digital mine' taking satellite communication underground," Available: http://www.miningweekly.com/article/wits-digital-mine-bringing -satellite-communication-to-underground-mining-2014-03-12 [Accessed on 20 Mar., 2016]

[65] HUAWEI, "eLTE Rapid Deployment Broadband Trunking System," Available: http://e.huawei.com/za/products/wireless/elte-trunking/rapid-deployment/elte-rapid [Accessed on 20 Apr., 2016]

[66] Y. P. Zhang and Y. Hwang, "Characterization of UHF radio propagation channels in tunnel environments for microcellular and personal communications," in *IEEE Transactions on Vehicular Technology*, vol. 47, no. 1, pp. 283-296, Feb 1998.

[67] I. B. Mabrouk, L. Talbi, B. Mnasri, M. Nedil, and N. Kandil, "Experimental characterization of a wireless MIMO channel at 2.4 GHz in underground mine gallery," *Progress In Electromagnetics Research Letters*, Vol. 29, 97-106, 2012.

[68] T. Klemenschits and E. Bonek, "Radio coverage of road tunnels at 900 and 1800 MHz by discrete antennas," *Personal, Indoor and Mobile Radio Communications, 1994. Wireless Networks - Catching the Mobile Future., 5th IEEE International Symposium on*, The Hague, pp. 411-415 vol.2, 1994.

[69] Proxim Wireless Corporation, "Definition & Calculation of Fresnel Clearance Zone," Available http://www.proxim.com/products/knowledge-center/calculations/ calculations-fresnel-clearance-zone [Accessed on 20 Aug., 2016]

[70] Balanis, Constantine. "Antenna Theory: A Review", *Proceedings of the IEEE*, vol. 80, January 1992

[71] Zhang, Y.P.; Hwang, Y.; Kouyoumjian, R.G., "Ray-optical prediction of radio-wave propagation characteristics in tunnel environments. 2. Analysis and measurements," *in Antennas and Propagation, IEEE Transactions on* , vol.46, no.9, pp.1337-1345, Sep 1998.

[72] B. Nkakanou, G. Y. Delisle, and N. Hakem, "Experimental Characterization of Ultra-Wideband Channel Parameter Measurements in an Underground Mine," *Journal of Computer Networks and Communications*, vol. 2011, Article ID 157596, 7 pages, 2011.

[73] C. G. Spiliotopoulos and A. G. Kanatas, "CHANNEL MEASUREMENTS AND MODELLING IN A MILITARY CARGO AIRPLANE," *Progress In Electromagnetics Research* B, Vol. 26, 69-100, 2010.

[74] Alan V. Oppenheim, S. Hamid Nawab, *Signals and Systems*, Second Edition by Prentice Hall, 957 pages, Published August 16th 1996

[75] Lou Frenzel, " What's The Difference Between The Third-Order Intercept And The 1-dB Compression Point?," Available: m.electronicdesign.com [Accessed on 19 Feb, 2016]

[76] Andrea Goldsmith, *Wireless Communications*, Cambridge University Press, September 2005 . ISBN: 9780521837163

[77] Jean-Jacques DeLisle, "How to EM Simulate Large and Complex Objects," Available: http://mwrf.com/software/how-em-simulate-large-and-complex-objects [Accessed on 24 Aug., 2016]

[78] Minicircuits, "Application Notes: AN60-008 Operating precautions for RF Amplifiers," Available: http://www.minicircuits.com/pages/app_notes.html [Accessed on 24 Mar., 2016]

Appendix A PATHLOSS EXPONENT AND MEAN RMS-DELAY SPREAD FOR DIFFERENT TUNNEL GEOMETRIES AND ANTENNA PARAMETERS

Environment/ Tunnel Size (width x height x test length) all in meters	Measurement Frequency	Antenna Polarization	Antenna Configuration*	Antenna Beamwidth	Scenario	Path Loss Exponent	Mean RMS-delay Spread (nsec)	Reference
Free Space	----	----	----	----	----	2	----	[12]
In Building Line-of-Sight						1.6-1.8		
Obstructed in building						4-6		
Straight Long Tunnel ** (7.5x4x2000)	900MHz	Linear	SISO	Omni-directional	LOS	3.87-4.44	< 103	[66]
Straight Long Tunnel ***(7x3.7x120)						2.96-3.71		
Straight Long Tunnel ***(4.2x3x10000)						1.87-2.37		
**Straight Long Tunnel (3.34x2.6x259)	900MHz	Linear	SISO	Omni-directional	LOS	4.2-4.49	< 58.65	
	1.8GHz					2.12-2.46		
**CANMET Level 40m (5x5x75)	2.3-2.5GHz	Linear	SISO	Omni-directional (360°, 65°)	LOS, NLOS	2.13-2.33	< 60	[30]
**CANMET Level 70m (2.5x4x70)	2.3-2.5GHz	Linear	SISO	Omni-directional	LOS	2.03	6.49	[34, 57]
					NLOS	4.62		
	5.7-5.9GHz				LOS	2.22	5.11	
					NLOS	3.52		
**CANMET Level 70m (2.5x4x10)	3-10 GHz	Linear	SISO	Omni-directional	LOS	2.11	9.74	[48]
					NLOS	3.00	21.05	
				Directional	LOS	2.01	2.09	
					NLOS	6.16	8.24	
**CANMET Level 40m (4x5x8)	57.24-59.4 GHz	Linear	SISO Horn-Horn	Omni-directional and horn (no information on antenna beamwidth)	LOS	1.82	N.I.	[28]
			SISO Omni-Horn			1.28		
**CANMET Level 70m (2.5x4x8)			SISO Horn-Horn			1.45		
			SISO Omni-Horn			1.41		
**CANMET Level 40m (5x5x25)	2.3-2.5 GHz	Linear	2x2 MIMO	Directional Patch	LOS	1.73	N.I.	[67]
					NLOS	3.03		
**CANMET Level 40m (5x5x25)	2-3 GHz	Linear	2x2 MIMO-Monopole	Omni-directional (360°, 65°),	LOS	1.36	1.73	[45-46]
			2x2 MIMO-Patch	Directional (92.4°, 71.3°)		1.34	1.33	

**CANMET Level 70m (2.5x4x10)	5.7-5.9 GHz	Linear	2x2 MIMO	Vivaldi (30°, 30°)	LOS	2.1	N.I.	[36]
**CANMET Level 40m (5x5x10)	57-64 GHz	Linear	2x2 MIMO Patch	Directional (N.I.)	LOS	1.48	7.65	[35]
					Human Effect	2.40	15.14	
**CANMET Level 40m (3.4x4.6x30)	2.35-2.55 GHz	Linear	4x4 MIMO PMPA	Directional (92.4°, 71.3°)	LOS	1.29	1.38	[44]
					NLOS	3.8	15.6	
			4x4 MIMO CMPA		LOS	1.18	2.08	
					NLOS	2.56	11.47	

* Antenna height = 1.7-1.9; MIMO antenna's element spacing = $\lambda/2$; N.I. = No Information provided;

**Rectangular Shaped Tunnels; ***Slightly Arched-Shaped Tunnels reinforced with concrete.

Line-of-Sight (LOS): LOS is defined by Fresnel Zones which are ellipse shaped between two radios. The primary Fresnel Zone is required to be at least 60% clear from obstruction for LOS condition.

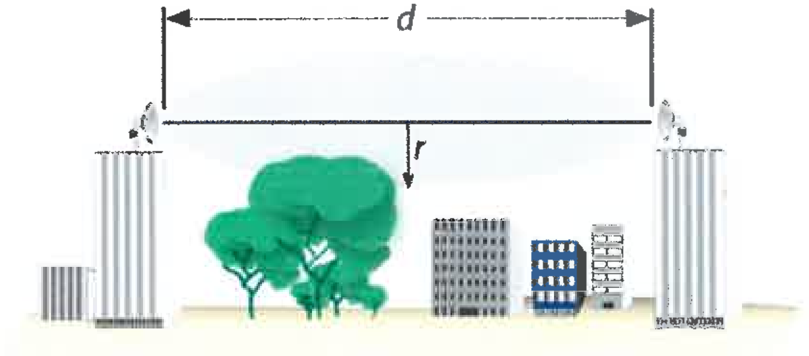

$$r_{(\text{In mts})} = 17.32 \times \sqrt{\frac{d_{(\text{In Km})}}{4f_{(\text{In GHz})}}} \qquad r_{(\text{In ft})} = 72.05 \times \sqrt{\frac{d_{(\text{In miles})}}{4f_{(\text{In GHz})}}}$$

Figure A1 Radius of first Fresnel Zone for LOS condition [69]

Appendix B Calculating Power Received [dBm] from S_{21} [dB]

According to the Friss Tranmission Equation[14] [70], the received power is given by:

$$P_R = \frac{P_T}{L} \cdot G_T \cdot G_R \qquad \text{Equation B1}$$

Where,

P_R	= Received power in watts
P_T	= Transmitted power in watts
L	= Loss
$G_T \cdot G_R$	= Antenna Gains at the transmitter and receiver

Friss Equation in log domain is given by:

$$P_R[dBm] = P_T[dBm] + G_T[dB] + G_R[dB] - L[dB] \qquad \text{Equation B2}$$

The S-parameter S_{21}, forward transmission coefficient (gain) for the following schematic diagram is given by:

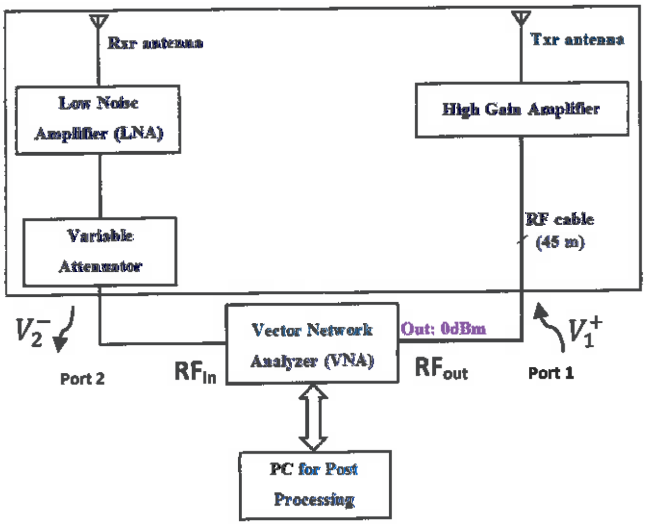

$$S_{21} = \left.\frac{V_2^-}{V_1^+}\right|_{V_2^+=0} = \frac{RF_{in}}{RF_{out}} \qquad \text{Equation B3}$$

[14] Friss Equation is only valid in the far-field region of the transmitted antenna

Where,

V_2^- = Outcome wave at Port 2
V_1^+ = Incident wave at Port 1
V_2^+ = Incident wave at Port 2

Equation (B1) for this test setup becomes,

$$P_{RFin} = \frac{P_{RFout}}{L_P} \cdot \frac{G_T \cdot G_R}{L_{Cables} \cdot L_{Attenuator}}$$

Where,

$G_T \cdot G_R$ = Gain at the transmitter and receiver; includes antenna and amplifier gains
L_P = Path Loss
$L_{Cables} \cdot L_{Attenuator}$ = Loss at the transmitter and receiver; includes cable and attenuator losses

Using equation (B3),

$$\frac{P_{RFin}}{P_{RFout}} = \frac{G_T \cdot G_R}{L_{Cables} \cdot L_{Attenuator} \cdot L_P} = S_{21}$$ Equation B4

$$\frac{G_T \cdot G_R}{L_{Cables} \cdot L_{Attenuator} \cdot S_{21}} = L_P$$ Equation B5

In general,

$$S_{21}\,[dB] = 20 \cdot \log\frac{V_1}{V_2} = 10 \cdot \log\frac{P_1}{P_2}$$

Equation (B3) becomes,

$$\boldsymbol{P_{RFin}\,[dBm] = P_{RFout}\,[dBm] + S_{21}\,[dB]}$$ Equation B6

Appendix C Calculating S_{21} [dB] range from Noise Floor [dBm]

The noise floor (NF) has been measured by the spectrum analyser in the 2.4-2.5 GHz frequency band at WITS mock-mine, as shown in figure C1. The NF is at -120 dBm but there is a spike of -99.43dBm at 2.45 GHz. To avoid the spurious measurements, the received power must be above -99.43 dBm.

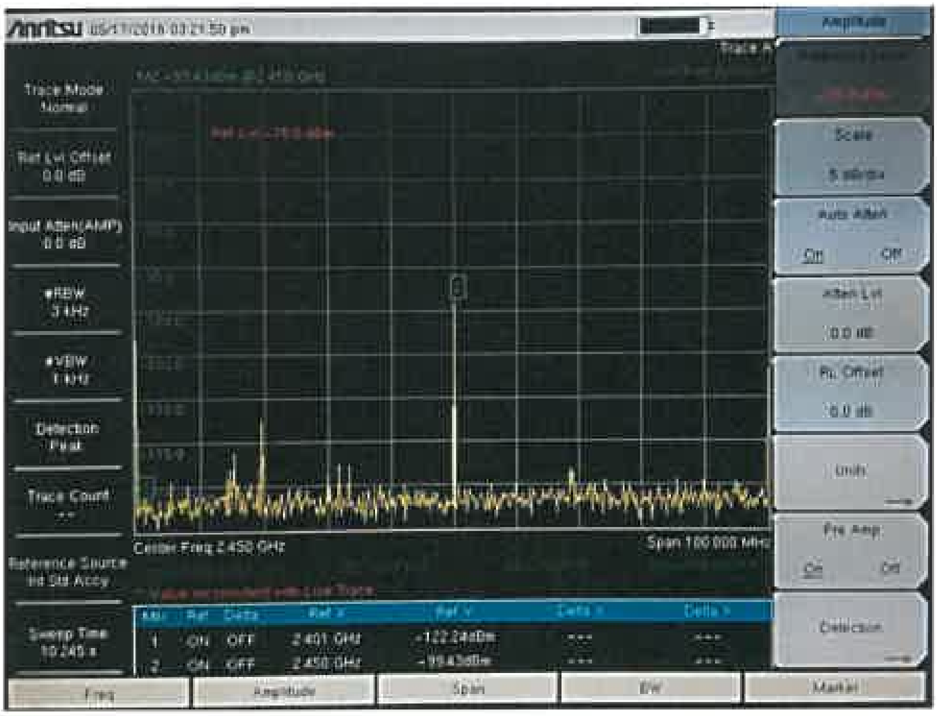

Figure C1 Noise Floor in the 2.4-2.5 GHz frequency band at WITS mock-tunnel

Figure C2 shows the schematic diagram of the wideband measurement system. Table C1 shows the minimum measurable S_{21} calculations in the 2.4-2.5GHz frequency band at WITS mock-tunnel with different antennas.

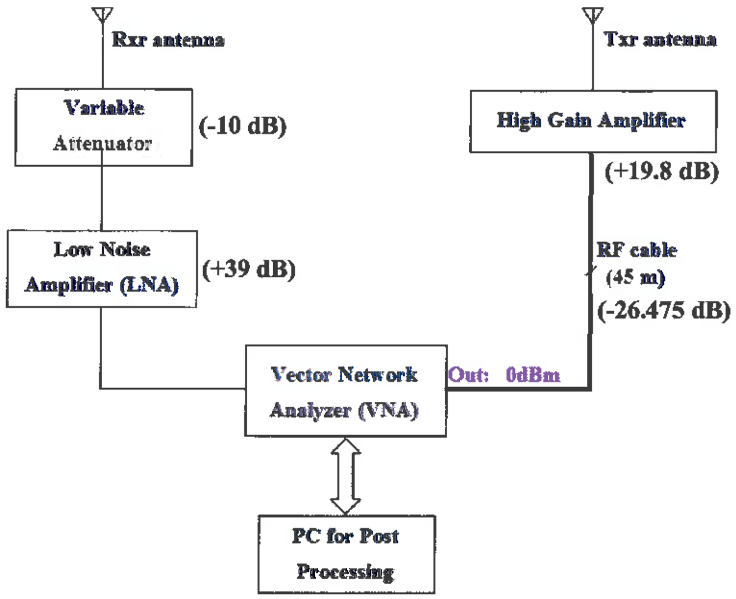

Figure C2 Schematic diagram of the wideband measurement system for 2.4-2.5 GHz frequency band

Table C1 Minimum Measurable S_{21} for 2.4-2.5 GHz frequency band in the WITS mock-tunnel with different antennas (NF = -99dBm)[15] using Equation (B6)

Antenna Gain [dB]	Minimum S_{21} [dB]
11	-99 dBm + 11 dB + 39 dB – 10 dB = **-59dB**
2	-99 dBm + 2 dB + 39 dB – 10 dB = **-68dB**
0	-99 dBm + 0 dB + 39 dB – 10 dB = **-70dB**

[15] S_{21} minimum for 5.8-5.9 GHz frequency band (NF = -11dBm) = -115 dBm + 14 dB + 27 dB – 10 dB = -84dB

Appendix D Calibration of Antennas

Parameters	Description	Appearance
Frequency (GHz)	**2.4-2.5, 5.1-5.85**	
Band Width	100 700	
Gain	8	
SWR	≤1.8 (S_{11} ≤ - 10.88dB)	
Impedance	50ohm	
Rating Power	50W	
Connector	SMA male	
Radiation Pattern	**Omni-directional**	
Polarization	**Linear**	
Measured S_{11}	**< -10 dB**	
Frequency (GHz)	**2.4-2.5**	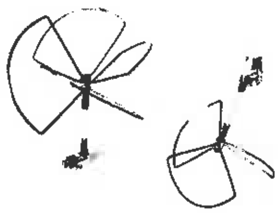
Impedance	50 Ohm	
VSWR	<1.5 (S_{11} < - 13.98dB)	
Gain	2 dBi	
Polarization	**RHCP**	
Radiation Pattern	**Omni-Directional**	
Power Rating	20 W	
Measured S_{11}	**< -8 dB**	
Frequency (GHz)	**2.4-2.5**	
Gain	8dBi	
Input Impedance	50 Ohm	
VSWR	≤1.5 (S_{11} ≤- 13.98dB)	
Polarization	**Vertical, Linear**	
Max. Input Power	50 W	
Connector	Standard N Female	
H-plane Beamwidth[16]	**13 degree**	
E-plane Beamwidth[17]	**17.5 degree**	
Measured S_{11}	**< -10 dB**	E-plane
Frequency (GHz)	**5.600-5.950**	
Gain	14dBi	
3db vertical Beamwidth	**40 degree**	
3db horizontal Beamwidth	**35 degree**	
Impedance	50ohm	
Polarization	**Vertical**	
Side lobe suppression	> = 13dB	
VSWR:	≤1.5 (S_{11} ≤ - 13.98dB)	
Front-to-back ratio	**> = 25dB**	Back-lobe is
Maximum power	50W	out_of_the_page
Connector	SMA /RP-SMA	
Measured S_{11}	**< -10 dB**	

[16] H-plane pattern = Azimuthal/Horizontal plane pattern = Top view
[17] E-plane pattern = Elevation/Vertical plane pattern = Side view

Parameters	Description	Appearance
Frequency (GHz) Polarization Connector Gain SWR Radiation Pattern Measured S_{11}	**5.7-5.9** **RHCP** SMA Male 3dBi <1.5 (S_{11} < - 13.98dB) **Omnidirectional** **< -10 dB**	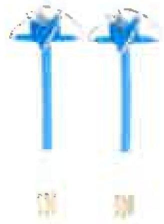
Frequency (GHz) Input Impedance VSWR Gain Horizontal Beamwidth Vertical Beamwidth Polarization Measured S_{11}	**2.370-2.510** 50Ω ≤1.5 (S_{11} ≤ - 13.98dB) 11dBi **60°** **60°** **RHCP** **< -10 dB**	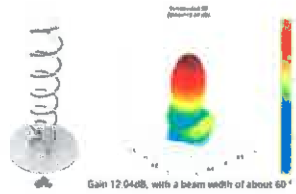
Frequency (GHz) Input Impedance VSWR Gain E-Plane 3 dB Beamwidth H-Plane 3 dB Beamwidth Polarization Front to Back Measured S_{11}	**0.680-2.900** 50Ω < 2 (S_{11} < - 9.54dB) 9dBi **64° (± 2°)** **72° (± 2°)** **Linear** > 20 dB (± 0.5 dB) **< -10 dB**	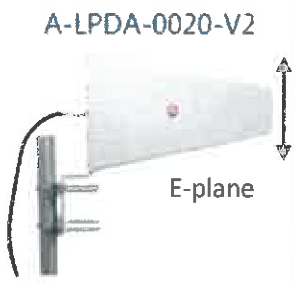

Appendix E Calibration of RF Attenuators/Adaptors/Cables

RF Attenuators	Measured attenuation	Appearance
1dB	0.907dB ± 0.1 @ 2.4 GHz 1.340dB ± 0.02 @ 5.8 GHz	
3dB	3.010dB ± 0.1 @ 2.4 GHz 3.921dB ± 0.02 @ 5.8 GHz	
10dB	9.89dB ± 0.1 @ 2.4 GHz 10.40dB ± 0.02 @ 5.8 GHz	
15dB	14.84dB ± 0.1 @ 2.4 GHz 14.79dB ± 0.02 @ 5.8 GHz	
20dB	19.55dB ± 0.1 @ 2.4 GHz 19.52dB ± 0.02 @ 5.8 GHz	

RF Adaptor Type	Measured transmission co-efficient (S_{21})	Appearance
SMA(F)-SMA(F)	0.15 dB @ 2.4 GHz -0.02dB @ 5.8 GHz	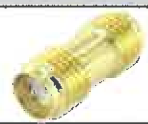
SMA(M)-SMA(M)	0.075dB @ 2.4 GHz 0.18dB @ 5.8 GHz	

RF Cable Type	Length	Measured transmission co-efficient (S_{21})
L-com 400-Series Low Loss Ultra-Flex Cable	2 feet	-0.22 dB @ 2.4 GHz -0.42dB @ 5.8 GHz
	3 feet	-0.175 dB @ 2.4 GHz -0.76dB @ 5.8 GHz
L-com 195R-Series Low Loss Cable	148 feet ~ 45m	-26.29dB @ 2.4 GHz -26.66dB @ 2.5 GHz -42.32dB @ 5.8 GHz -43.37dB @ 5.9 GHz

NOTE:

- dBm + dBm Not Possible;
- dBm = dBm ± dB Possible; dB = dBm - dBm Possible; dB = dB ± dB Possible

Appendix F Electrostatic Discharge (ESD) precautions for Amplifier

E-mail to Professor Alan Clark, Associate Professor WITS EIE

Intikhab Hussain <1024894@students.wits.ac.za> 4 April 2016 at 15:04

To: Alan Clark <AlanRobertClark@gmail.com>, Benjamin Klein <0007862H@students.wits.ac.za>

Cc: Rex Van Olst <rex.vanolst@wits.ac.za>

Dear Prof.

With the connectorized amplifiers (PA and LNA), do I need to have ESD mat during testing? or I can use wood base with proper grounding of the power supplies and VNA with ESD wristband?

Any other ESD precautions that you would recommend.

Regards,

Intikhab

Alan Clark <alanrobertclark@gmail.com> 5 April 2016 at 12:27

To: Intikhab Hussain <1024894@students.wits.ac.za>

Cc: Benjamin Klein <0007862H@students.wits.ac.za>, Rex Van Olst <rex.vanolst@wits.ac.za>

Mini-Circuits and Coax SMA connectors = no ESD requirements whatsoever. It will all just work.

[Quoted text hidden]

--
Alan Robert Clark, Pr.Eng Computational Electromagnetics
Associate Professor Wits University
School of Electrical and Information Engineering

Mini-circuits operating precautions for Amplifiers

The risk of damage due to ESD (Electrostatic discharge) is small in connectorized amplifiers, because a charged object would have to come into contact with the center conductor of the input or output connector. However, other sources of EOS (Electrical Overstress) can enter the amplifiers by way of signal paths in the system [78]. For example, the most frequent causes of user-induced failure in ZHL-series amplifiers are:

a) Excessive power applied to the input

b) Improper sequencing of load connection

NOTE: Do not exceed the specified power in dBm at input.

Table F1 Operating Precautions for Amplifiers

To Connect	To Disconnect
1. Connect output load	1. Remove RF input
2. Apply DC voltage	2. Remove DC voltage
3.Apply RF input	3. Remove load

Appendix G 1dB compression-point of an Amplifier

- At 1dB compression-point, gain reduces 1 dB from the normal expected linear gain plot. It is the point where the amplifier goes into compression and becomes non-linear, as shown in figure G1.
- **Output (dBm) = Input (dBm) + Gain (dB)**

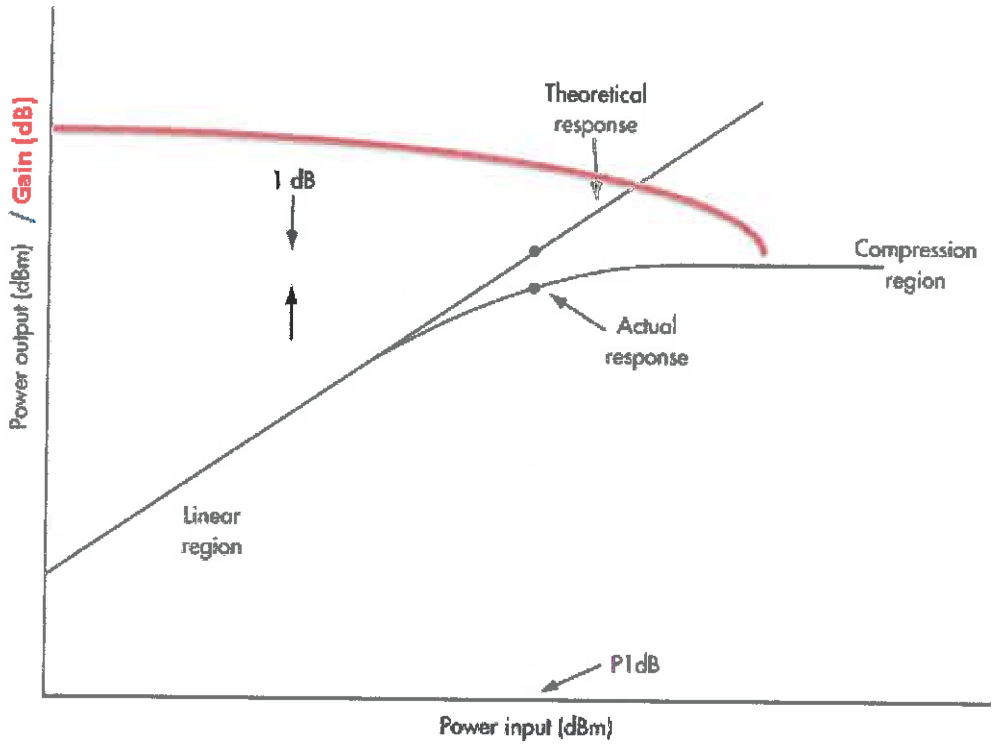

Figure G1 1dB compression point [75]

Appendix H Calibration of Mini-circuits ZX60-V63+ High gain Amplifier

High Gain Wideband (0.05 to 6 GHz) Amplifier

- **From Data Sheet:-**

Pout @ 1dB compression = 17.8 dBm @ 2.0 GHz; 12.1 dBm @ 6GHz

Gain = 20.3dB @ 2.0 GHz; 15.4 dB @ 6GHz

Pin @1dB compression = Pout [dBm] - Gain [dB]

= 17.8-20.3 @2.0 GHz = -2.5 dBm @ 2.0 GHz;

= 12.1-15.4 @6.0 GHz = -3.3 dBm @ 6.0 GHz

- **Test setup:-**

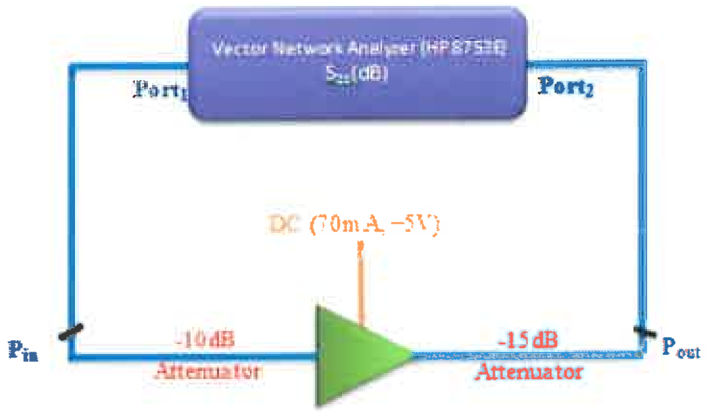

Figure H1 Calibration test setup for HGA

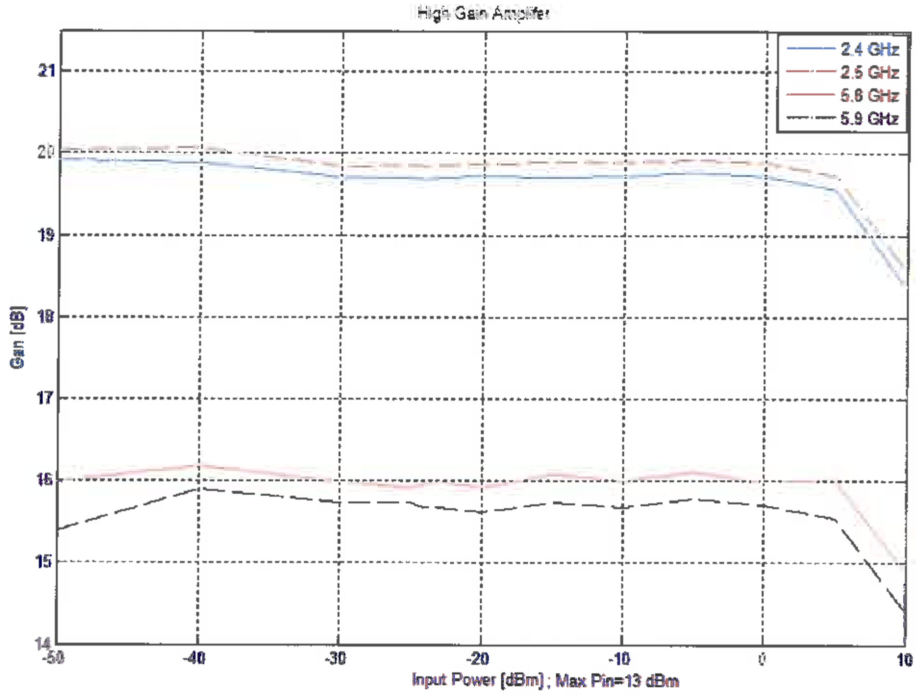

Figure H2 Measured gain of ZX60-V63+ HGA

Appendix I Calibration of WENTEQ ALN0230-26-4007 Super Low Noise Amplifier

2 .0 to 2.6 GHz SLNA

- **From Data Sheet:-**

Pout @ 1dB compression = 12 dBm

Gain = 40 dB

Pin @1dB compression = Pout [dBm] – Gain [dB] = 12 - 40 = -28dBm

- **Test setup:-**

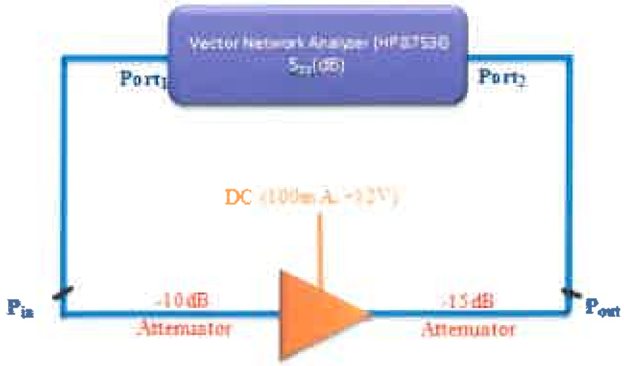

Figure I1 Measurement Test setup

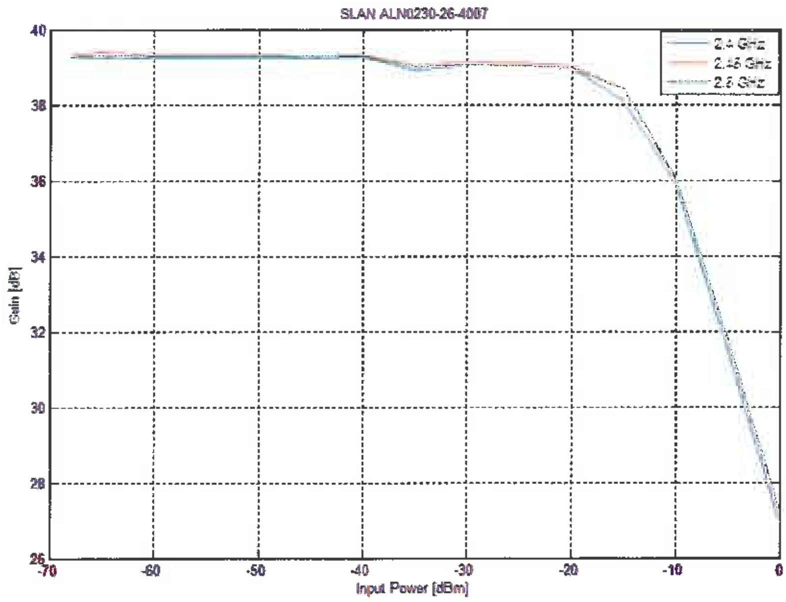

Figure I2 Measured gain of ALN0230-26-4007 SLNA

Appendix J Calibration of WENTEQ ALN0560-11-2709 Super Low Noise Amplifier

5.3 to 5.9 GHz SLNA

- **From Data Sheet:-**

  Pout @ 1dB compression = 13 dBm

  Gain = 27 dB

  Pin @1dB compression = Pout [dBm] – Gain [dB] = 13 - 27 = -14dBm

- **Test setup:-**

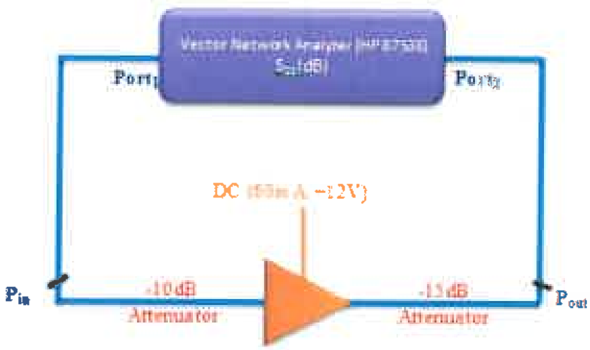

Figure J1 Measurement Test setup

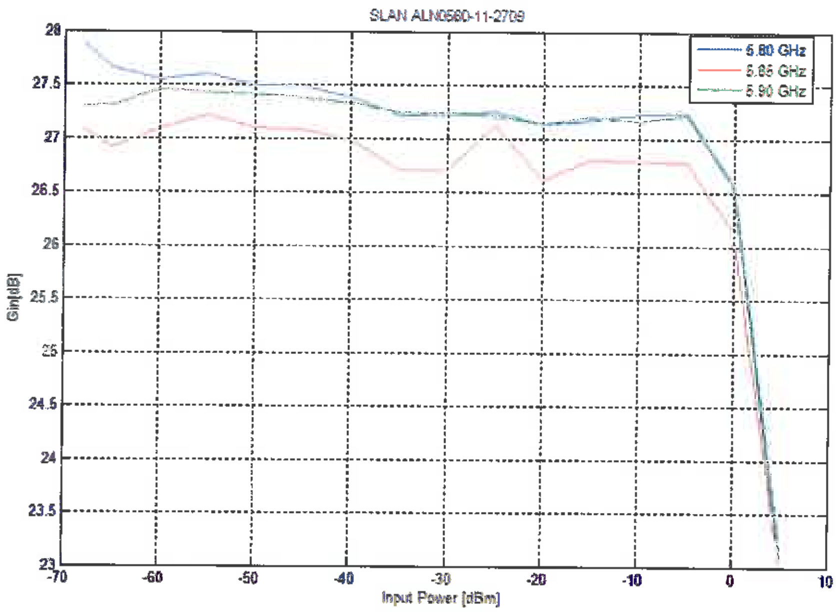

Figure J2 Measured gain of ALN0560-11-2709 SLNA

Appendix K Time Dispersion Parameters

For comparing different multipath channels and developing some general design guidelines for the wireless communication system, time dispersion parameters like mean *excess delay* ($\bar{\tau}$), *RMS delay spread* (σ_t), *and excess delay spread (XdB)* are determined from the power delay profile (PDP), i.e. $P(\tau)$, and that depends on the threshold. These delays do not relay on the absolute power level of $P(\tau)$, but on the relative amplitudes of the multipath components. The *mean excess delay* is the first moment of the power delay profile and is defined as:

$$\bar{\tau} = \frac{\sum_k a_k^2 \cdot \tau_k}{\sum_k a_k^2} = \frac{\sum_k P(\tau_k) \cdot \tau_k}{\sum_k P(\tau_k)} \qquad \text{Equation K1}$$

The *RMS delay spread* is the square root of the second central moment of the power delay profile (PDP) and is defined as:

$$\sigma_t = \sqrt{\overline{\tau^2} - (\bar{\tau})^2} \qquad \text{Equation K2}$$

where,

$$\overline{\tau^2} = \frac{\sum_k a_k^2 \cdot {\tau_k}^2}{\sum_k a_k^2} = \frac{\sum_k P(\tau_k) \cdot {\tau_k}^2}{\sum_k P(\tau_k)} \qquad \text{Equation K3}$$

The *maximum excess delay (X dB)* of the PDP is defined as the time delay during which the multipath energy falls to *X dB* below the maximum, i.e. $(\tau_X - \tau_o)$. The values of these dispersion parameters depend on the choice of noise threshold of $P(\tau)$. This noise threshold should be above the noise floor of the channel in order to differentiate between the received multipath components and the environment/thermal noise. Figure K 1 shows the example of indoor environment for the time dispersion parameters.

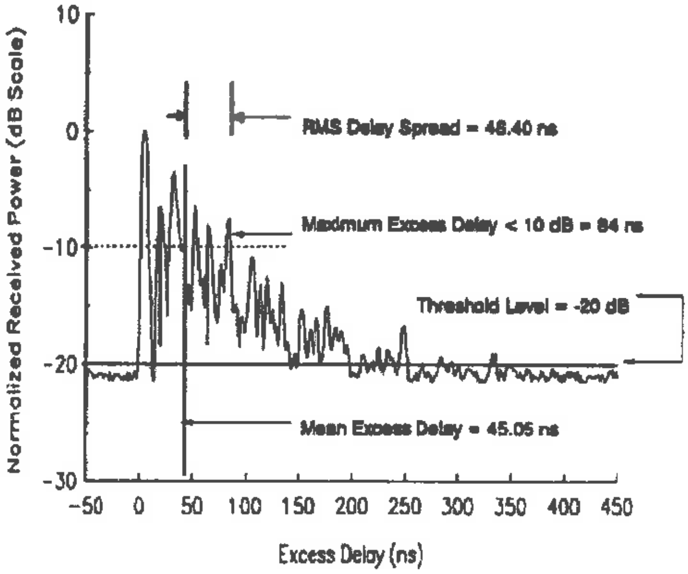

Figure K1 Example of an indoor PDP; Time Dispersion Parameters [12]

The PDP and the frequency response of the radio channel are related by the Fourier Transform. Analogous to the delay spread parameters in the time domain, *coherent bandwidth* is used to characterize the radio channel in frequency domain. The RMS delay spread and coherent bandwidth are inversely proportional to one another, although the exact relation depends on the multipath structure. Coherent bandwidth (B_C) is the statistical measure of the frequencies over which the channel is flat (i.e. the spectral components have approximately equal gain and linear phase). For the frequency correlation of above 0.9, the B_C is approximately given by [12]:-

$$B_C \approx \frac{1}{50 \cdot \sigma_t} \qquad \text{Equation K4}$$

For the frequency correlation of above 0.5, the B_C is approximately given by [12]:-

$$B_C \approx \frac{1}{5 \cdot \sigma_t} \qquad \text{Equation K5}$$

Appendix L MATLAB Code for Calculating and Plotting Path-loss Exponent and Shadow Fading Statistics at Single Frequency

```
%%%%%%%%%%%%%%%%%%%%%%%%%%%%%%%%%%%%%%%%%%%%%%%%%%%%%%%%%%%%%%%%
%%%%%% Path Loss Exponent 'n' and Shadow Fading'sigma' %%%%%%%%%
%%%%%%%%%%%%%%%%%%%% at single frequency %%%%%%%%%%%%%%%%%%%%%%%%
%%%%%%%%%%%%%%%%%%%%%%%%%%%%%%%%%%%%%%%%%%%%%%%%%%%%%%%%%%%%%%%%
clear all
clc
%%%%%%%%%%%%%%%%%%%%%%%%Input Variables %%%%%%%%%%%%%%%%%%%%%%%%
%%%%%%%%%% xData=d (distance in meters)
%%%%%%%%%% s21_real_ and s21_imag_
%ncdf=normcdf(nn,M,s);get idea of standard deviation from 's' then
adjust 's' to get minimum value of KSSTAT
%%%%%%%%%%%%%%%%%%%%%%%%%%%%%%%%%%%%%%%%%%%%%%%%%%%%%%%%%%%%%%%%

d=[1 2 3 4 5 6 7 8 9 10 11 12 13 14 15 16 17 18 19 20 21 22 23 24
25 26 27 28  29 30  31  32 33  34  35   36 37  38 39  40 ];

s21_real_=[46159  43783  -13067  -36566  -17466  7849 996   4567
-18149  -17053  -13868  -5925  -12935 -13843  -5868  -5854  14055
-5751  -9373  -7557  -7261  -4151 -5773  -4868  -4550  -4660 -4429
-2947 -3654 -7646 -4199 -8681 -7048 -6312 -7233 -11887 -4924 -5832
-8935 -5102];

s21_imag_=[46851 7140 -23195 -11551 11240 -24646 -16585 13875
18549 9901 -8840 -16497 -15950 -4231 -11630 -21055 4993 -16891
-11442 -9702 -8410 -12313 -15267 -11231 -11433 -11009 -14491
-12813 -10496 -9467 -18063 -12036 -8731 -10327 -9690 -10596
-11960 -13419 -9047 -5006];


%%%%%%%%%%%%%%%%%%%%%%%%%%%%%%%%%%%%%%%%%%%%%%%%%%%%%%%%%%%%%%%%
for ii=1:40 %%%%% Number of data points for d and s21
s21_real_(ii) = s21_real_(ii)/1000000;
s21_imag_(ii) = s21_imag_(ii)/1000000;
s21_amplitude_(ii) = sqrt( (s21_real_(ii))^2 + (s21_imag_(ii))^2
);
P_(ii)=20*log10(s21_amplitude_(ii));
d1(ii)=10*log10(d(ii));
end
P=P_';
d1=d1';

%%%%%%%%%%%%%%%%%%%%%%%%%%%%%%%%%%%%%%%%%%%%%%%%%%%%%%%%%%%%%%%%
%%%%%%%%%%%%%%%%%%%%%%%%%%%%% for 'n' %%%%%%%%%%%%%%%%%%%%%%%%%%%
%%%%%%%%%%%%%%%%%%%%%%%%%%%%%%%%%%%%%%%%%%%%%%%%%%%%%%%%%%%%%%%%

p = polyfit(d1,P,1) %  it will return slop (m) and y-intercept (c)
.... y = mx + c  P(1) = m and P(2) = c
yfit = polyval(p,d1);  % same as  yfit =  p(1) * x + p(2); LINEAR
REGRESSION --- will get line if plot (yfit)
yresid = P - yfit;
SSresid = sum(yresid.^2);
SStotal = (length(P)-1) * var(P);
rsq = 1 - SSresid/SStotal  % R2 -- R-squared is a statistical
measure of how close the data are to the fitted regression line.
```

```
                                                %-- 0% indicates that the model
explains none of the variability of the response data around its
mean.
                                                %-- 100% indicates that the model
explains all the variability of the response data around its mean.

figure;
plot(d1,P,'o');
hold on
plot(d1,yfit,'r');
xlabel('10log(d)(meter)')
ylabel('Received Power [dBm]')
legend('Data','Curve Fitting','Best');
strn = ['n = ',num2str(abs(p(1))), ', R-square = ',num2str(rsq)];
text(2,-40,strn);                        %%text(1.2,-42,strn);
axis([min(d1) max(d1) min(P) max(P)]);

%%%%%%%%%%%%%%%%%%%%%%%%%%%%%%%%%%%%%%%%%%%%%%%%%%%%%%%%%%%%%%%%%%%%%
%%%%%%%%%%%%%%%%%%%%%%%%%% for 'sigma' %%%%%%%%%%%%%%%%%%%%%%%%%%%%%%
%%%%%%%%%%%%%%%%%%%%%%%%%%%%%%%%%%%%%%%%%%%%%%%%%%%%%%%%%%%%%%%%%%%%%
figure;
df = yfit-P;
M=mean(df)
s=std(df,1)
%x=(x-M)
%S2=std(x1,1)
hold on; hh=cdfplot(df); hold off %%[f,df_values] = ecdf(df);
set(hh,'color','r')
ylabel('CDF')
xlabel('Shadow Fading [dB]')
hold on
[f,df_values] = ecdf(df);
nn=sort(df_values);
nnn=-22:1:25;
%%%%%%%%% nnn for plotting
%%%%%%%%% nn for KS-test
ncdf=normcdf(nn,0,s); %ncdf=normcdf(nn,M,s);get idea of standard
deviation from 's' then adjust 's' to get minimum value of KSSTAT
plot(nn,ncdf);
legend('Shadow Fading','Curve Fitting','Best');
%axis([-10 20 0 1]);
%%%%%%%%%
[H,P,KSSTAT,CV] = kstest(nn,[nn,ncdf],0.1)

strk = ['k = ',num2str(KSSTAT), ', Mean =',num2str(0),', Sigma =
',num2str(s)];
text(-0.8,0.08,strk);
```

Appendix M MATLAB Code for Calculating and Plotting Time Dispersion Parameters for a frequency band at Single Point (or Distance)

```
%%%%%%%%%%%%%%%%%%%%%%%%%%%%%%%%%%%%%%%%%%%%%%%%%%%%%%%%%%%%%%%
%%%%%%%%% Time domain to Frequency domain (IFFT) %%%%%%%%%%%%%%
%%%%%%%%%%%%%%%%% at particular distance %%%%%%%%%%%%%%%%%%%%%%
clear all
%%%%%%%%%%%%%%%%%%%%%%%%%%%%%%%%%%%%%%%%%%%%%%%%%%%%%%%%%%%%%%%
%%%%%%%%%%%%%%%%%%%%%%%%Input Variables %%%%%%%%%%%%%%%%%%%%%%%
%%%%%%%%%%%%%%%%%%%%%%%%%%%%%%%%%%%%%%%%%%%%%%%%%%%%%%%%%%%%%%%
%S21_real
%S21_Imag
                %%% for data, HGA, LNA, Cables, Antennas,
Attenuators
% Antenna Gain
%f=frequency band
%threshold

s21_real1 = xlsread('45m.xlsx','4545m_c','C301:C851'); % 45m cable
files at 2.4-2.5 GHz
s21_imag1 = xlsread('45m.xlsx','4545m_c','D301:D851');


s21_real2 = xlsread('aa1.xlsx','aa1','C301:C851'); % two 1 feet
cables + attenuators( 15+20) files at 2.4-2.5 GHz
s21_imag2 = xlsread('aa1.xlsx','aa1','D301:D851');

s21_real3 = xlsread('amp.xlsx','amp','C301:C851'); % PA +  two 1
feet cables files at 2.4-2.5 GHz
s21_imag3 = xlsread('amp.xlsx','amp','D301:D851');

s21_real4 = xlsread('lna_2.4.xlsx','lna_2.4','C301:C851'); % LNA +
two 1 feet cables + attenuators( 15+20+10)files at 2.4-2.5 GHz
s21_imag4 = xlsread('lna_2.4.xlsx','lna_2.4','D301:D851');

f = xlsread('1_1.xlsx','1_1','E301:E851');

as1='13.40.xlsx';
as_='13.40';
threshold = -40;

s21_real = xlsread(as1,as_,'C301:C851'); % data files
s21_imag = xlsread(as1,as_,'D301:D851');

%%%%%%%%%%%%%%%%%%%%%%%%%%%%%%%%%%%%%%%%%%%%%%%%%%%%%%%%%%%%%%%
%%%%%%%%%%%%%%%%%%%%%%%%%%%% Code %%%%%%%%%%%%%%%%%%%%%%%%%%%%%
%%%%%%%%%%%%%%%%%%%%%%%%%%%%%%%%%%%%%%%%%%%%%%%%%%%%%%%%%%%%%%%

for ii=1:551
s21_real(ii) = s21_real(ii)/1000000;
s21_imag(ii) = s21_imag(ii)/1000000;

s21_real1(ii) = s21_real1(ii)/1000000;
s21_imag1(ii) = s21_imag1(ii)/1000000;

s21_real2(ii) = s21_real2(ii)/1000000;
s21_imag2(ii) = s21_imag2(ii)/1000000;

s21_real3(ii) = s21_real3(ii)/1000000;
```

```
s21_imag3(ii) = s21_imag3(ii)/1000000;

s21_real4(ii) = s21_real4(ii)/1000000;
s21_imag4(ii) = s21_imag4(ii)/1000000;

%Lp(ii)= (( (s21_real(ii)+ i*s21_imag(ii)) *
(s21_real(ii)+i*s21_imag(ii)) ) * 10^(-10/10) ) / (10^(80.8/10));
%10^((19.8+39+11+11)/10)
AA=(s21_real(ii)+ i*s21_imag(ii)); %data
BB=(s21_real1(ii)+ i*s21_imag1(ii)); %cable
CC=(s21_real2(ii)+ i*s21_imag2(ii)); %attenuator
DD=(s21_real3(ii)+ i*s21_imag3(ii)); %HGA
FF=(s21_real4(ii)+ i*s21_imag4(ii)); %LNA
FF=FF/CC;
CC=CC*(10^(35/20));
GG=10^(16/20); %antennas gain 20 is used to represent it in gain
in voltages becasue all other data is in linear-voltage

% Path-loss[dB]= antennas gain + HGA + LNA - S21 + [-Cable loss] +
[-Attenuator]
%H(f)=1/Path-loss=L

L(ii)= ((AA))/(BB*CC*DD*FF*GG);


s21_real_f(ii)=real(L(ii));
s21_imag_f(ii)=imag(L(ii));
s21_amplitude(ii) = sqrt( (s21_real_f(ii))^2 + (s21_imag_f(ii))^2
);
s21_phase(ii) = atan(s21_imag_f(ii)/s21_real_f(ii));

if(s21_real_f(ii) <0 && s21_imag_f(ii) >=0)
    s21_phase(ii)=s21_phase(ii)+pi;
elseif(s21_real_f(ii) <0 && s21_imag_f(ii) <0)
    s21_phase(ii)=s21_phase(ii)-pi;
end

end

S21=s21_amplitude.*exp(1i.*s21_phase);   %S21-complex number
S21=S21.*hann(551)';  %Hanning Window   %%%551 is the number of
data points
c=3e8;              %Speed of light
stepf= 0.181819e    %Frequency Step
dt=1/(stepf*550);  % delta tou (tou=delay spread) %%%551 is the
number of data points
t=2*dt*(0:275);  %%%551 is the number of data points
T_domain=ifft(S21,551, 'nonsymmetric');  %%551 is the number of
data points
for lo=1:276
magnitude(lo)=abs(T_domain(lo));
magnitude_dB(lo)=20*log10(magnitude(lo));    % P(tou)= K average
over local area( abs(h(t))^2); P(tou)[dB]=
10*log(P(tou))=K*10*log( abs(h(t))^2)
end
%%%%%%%%%%%%%%%%%%%%%%%%%%%%%%%%%%%%%%%%%%%%%% Plotting
figure

subplot(2,2,1)
```

```
plot(f,20*log10(s21_amplitude))
xlabel('Frequency (MHz)')
ylabel('Channel Frequency Response, Magnitude [dB]')


subplot(2,2,2)
plot(f,s21_phase*(180/pi))
xlabel('Frequency (MHz)')
ylabel('Channel Frequency Response, Phase (degree)')


subplot(2,2,3)
plot(t,magnitude)
axis([min(t) max(t)/2 min(magnitude) max(magnitude)])
%Plot half the time on axis%%%Plot section of data on existing
axes [xlimitA xlimitB ylimitA ylimitB]
hold on
plot(get(gca,'xlim'), [max(magnitude) max(magnitude)]);
hold on
plot(get(gca,'xlim'), [10^((max(magnitude_dB)+threshold)/20)
10^((max(magnitude_dB)+threshold)/20)]);
xlabel('Time (sec)')
ylabel('Magnitude of Channel Impulse Response')


subplot(2,2,4)
Nomalized_PDP=(magnitude_dB-max(magnitude_dB));
plot(t,Nomalized_PDP)
hold on
plot(get(gca,'xlim'), [max(Nomalized_PDP) max(Nomalized_PDP)]);
hold on
plot(get(gca,'xlim'), [max(Nomalized_PDP)+threshold
max(Nomalized_PDP)+threshold]);
xlabel('Time (sec)')
ylabel('Normalized Power Delay Profile [dB]')
axis([min(t) max(t)/2 min(Nomalized_PDP) max(Nomalized_PDP)])

%%%%%%%%%%%%%%%%%%%%%%%%%%%%%%%%%%%% Delay Spread Calculation
mean_delay_spread_numerator=0;
mean_delay_spread_deniminator=0;
Second_order_delay_spread_numerator=0;
mean_delay_spread=0;
Second_delay_spread=0;
RMS_delay_spread=0;
Maximum_delay_spread=0;
m=0;
for (v=1:551/2)      %%%551 is the number of data points
   if(Nomalized_PDP(v)>=threshold)
       m=t(v);
       break
end
end
for (v=1:551/2)              %%%551 is the number of data points
   if(Nomalized_PDP(v)>=threshold)
    mean_delay_spread_numerator = t(v)*(10^(Nomalized_PDP(v)/10))
+ mean_delay_spread_numerator;
    mean_delay_spread_deniminator = (10^(Nomalized_PDP(v)/10)) +
mean_delay_spread_deniminator;
```

```
    Second_order_delay_spread_numerator =
(t(v)^(2))*(10^(Nomalized_PDP(v)/10)) +
Second_order_delay_spread_numerator;
    Maximum_delay_spread = t(v);
   end
end
mean_delay_spread = mean_delay_spread_numerator /
mean_delay_spread_deniminator
Second_delay_spread = Second_order_delay_spread_numerator /
mean_delay_spread_deniminator;
RMS_delay_spread =  sqrt(Second_delay_spread -
(mean_delay_spread)^2)
Maximum_delay_spread
%%%%%%%%%%%%%%%%%%%%%%%%%%%%%%%%%%%%%%%%%%End
```